DIAGRAMMATIC THEORIES FOR THE VIBRATIONAL MANY-BODY PROBLEM

BY

JACOB A. FAUCHEAUX

DISSERTATION

Submitted in partial fulfillment of the requirements
for the degree of Doctor of Philosophy in Chemistry
in the Graduate College of the
University of Illinois at Urbana-Champaign, 2017

Urbana, Illinois

Doctoral Committee:

Professor So Hirata, Chair
Professor Nancy Makri
Professor Martin Gruebele
Research Assistant Professor Lucas Wagner

Abstract

Anharmonic vibrational many-body methods are developed for and applied to small molecules and extended systems in a bound potential energy surface (PES).

Diagrammatically size-consistent and basis-set-free vibrational coupled-cluster (XVCC) theory for both zero-point energies and transition frequencies, the latter through the equation-of-motion (EOM) formalism, is defined for an nth-order Taylor-series PES. Quantum-field-theoretical tools (the rules of normal-ordered second quantization and Feynman–Goldstone diagrams) for deriving their working equations are established. The equations of XVCC and EOM-XVCC are derived and implemented with the aid of computer algebra. Algorithm optimizations known as strength reduction, intermediate reuse, and factorization are carried out before code generation, producing algorithms with optimal cost scaling.

A similarity-transformed equation-of-motion vibrational coupled-cluster (STEOM-XVCC) method is introduced as a one-mode theory with an effective vibrational Hamiltonian, which is similarity transformed twice so that its lower-order operators are dressed with higher-order anharmonic effects. From diagonalization of this doubly similarity-transformed Hamiltonian in the small one-mode excitation space, the method simultaneously computes accurate anharmonic vibrational frequencies of all fundamentals, which have unique significance in vibrational analyses. We establish a diagrammatic method of deriving the working equations of STEOM-XVCC and prove their connectedness and thus size-consistency as well as the exact equality of its frequencies with the corresponding roots of EOM-XVCC.

An extended STEOM-XVCC (Ext-STEOM-XVCC) method is defined as an mth order configuration interaction method with the doubly similarity-transformed Hamiltonian including up to mth-order excitation operators. Because the doubly transformed Hamiltonian is dressed with higher-order anharmonic effects, the frequencies of overtones and combinations obtained are different and superior to the corresponding EOM-XVCC method. We compare and contrast the Ext-STEOM-XVCC method to its electronic counterpart.

We apply the previously established second-order size-extensive vibrational many-body perturbation (XVMP2) method to the anharmonic phonon dispersion curves of a model two-mass system and the optical phonons of polyethylene. We obtain accurate results despite the presence of multiple Fermi-resonances in the crystalline systems.

To Bobby Faucheaux and Charles "Boo" Faucheaux Jr.

Acknowledgements

First, I must acknowledge my advisor So Hirata for giving me an opportunity to work in his group and his insight and advice along the way. I must also thank Professor Marcel Nooijen for providing the initial inspiration for the STEOM project and assistance along the way. I am also grateful for the funding provided by the National Science Foundation via the NSF graduate research fellowship program.

I am thankful for Professors Nancy Makri, Martin Gruebele, and Lucas Wagner for graciously serving on my committee. I am grateful for the assistance provided by my lab members. Matthew Hermes for providing me with data and numerical results which aided in my method development. Misha and Ryan for always be willing to answer questions and point me in the right direction when I first joined the lab.

I am grateful for friends and family for support along the way. Devin and Avery for always cheering me up. David, Amy, Brigette, and Anthony for their hospitality. Amartya, Luke, and Joe for helping me maintain my sanity, and Jeremy for talking about baseball. Finally, I must thank Khang, Dat, Dustin, and the Calixes for the frequent reminders that the Falcons blew a 25 point lead in the Super Bowl.

Table of Contents

Chapter 1 Introduction **1**
1.1 The vibrational structure problem 1
1.2 Vibrational self-consistent field theory 3
1.3 Vibrational coupled-cluster theory 4
1.4 Similarity transformations with exponential operators 5
1.5 Vibrational structure theory for one-dimensional periodicity 9
1.6 Figure 12

Chapter 2 Higher-order diagrammatic vibrational coupled-cluster theory **13**
2.1 Introduction 13
2.2 Theory 14
2.2.1 XVCC formalism 14
2.2.2 Algebraic derivation of XVCC 16
2.2.3 Diagrammatic derivation of XVCC 22
2.2.4 EOM-XVCC formalism 25
2.2.5 Algebraic derivation of EOM-XVCC 27
2.2.6 Diagrammatic derivation of EOM-XVCC 28
2.3 Automated computer implementation 29
2.3.1 Strength reduction 30
2.3.2 Intermediate reuse 31
2.3.3 Factorization 31
2.4 Numerical tests 33
2.4.1 Water 34
2.4.2 Formaldehyde 36
2.5 Conclusion 37
2.6 Figures 38
2.7 Tables 43

Chapter 3 Similarity-transformed equation-of-motion vibrational coupled cluster theory **50**
3.1 Introduction 50
3.2 XVCC 52
3.3 STEOM-XVCC 55
3.3.1 Ansatz 55
3.3.2 Doubly similarity-transformed Hamiltonian 58
3.3.3 Amplitude and eigenvalue equations 60
3.3.4 Diagrammatic derivation 62
3.4 Comparisons of related theories 65
3.4.1 STEOM-XVCC versus EOM-XVCC 65
3.4.2 Vibrational versus electronic STEOM-CC 67
3.4.3 STEOM-XVCC versus MBGF 69
3.5 Approximate STEOM-XVCC methods 76
3.5.1 Diagonal approximation 77

3.5.2 Perturbation approximation . . . 78
3.5.3 Frequency-independent approximation . . . 80
3.6 Computer implementation . . . 81
3.7 Numerical tests . . . 82
3.7.1 Water . . . 83
3.7.2 Formaldehyde . . . 83
3.7.3 Ethene . . . 84
3.8 Conclusion . . . 85
3.9 Figures . . . 86
3.10 Tables . . . 88

Chapter 4 Extended similarity-transformed equation-of-motion vibrational coupled cluster theory . . . 90
4.1 Introduction . . . 90
4.2 Formalism . . . 91
4.3 Approximations to Ext-STEOM-XVCC . . . 93
4.4 Diagrammatic derivation . . . 94
4.4.1 Diagrammatic form of $\bar{\bar{H}}$ . . . 95
4.5 Comparision to EOM-XVCC . . . 98
4.6 Numerical implementation . . . 99
4.7 Numerical tests . . . 100
4.7.1 Water . . . 101
4.7.2 Formaldehyde . . . 101
4.8 Conclusion . . . 102
4.9 Figures . . . 103
4.10 Tables . . . 104

Chapter 5 XVMP2 for one-dimensional crystalline systems . . . 107
5.1 Introduction . . . 107
5.2 XVMP2 for one-dimensional periodicity . . . 107
5.2.1 Second-order Dyson self-energy . . . 108
5.3 Numerical tests . . . 110
5.3.1 Two-mass system . . . 111
5.3.2 Optical modes of polyethylene . . . 112
5.4 Conclusion . . . 113
5.5 Figures . . . 113
5.6 Table . . . 120

Chapter 6 Conclusion . . . 121

Appendix A XVCC energy and amplitude equations . . . 123

Appendix B EOM-XVCC amplitude equations . . . 130

Appendix C Singly transformed Hamiltonian . . . 133

Appendix D Cost scaling of XVCCm and EOM-XVCCm in an nth-order PES . . . 139

Appendix E Doubly transformed Hamiltonian . . . 142

References . . . 147

Chapter 1

Introduction

1.1 The vibrational structure problem

The calculation of the vibrational motion of nuclei plays an important role in the description of the structure and dynamics of molecules and solids. Such calculations assist in understanding infrared and Raman spectra and enable accurate assignment of vibrational bands to particular vibrational modes. [1] Furthermore, accurate models of the vibrational motion of nuclei are required to predict important bulk material properties.

The description of the electronic and nuclear motion of a molecule is a coupled problem governed by the Schrödinger equation [2]

$$\hat{H}\Psi(\mathbf{r},\mathbf{R}) = E\Psi(\mathbf{r},\mathbf{R}), \tag{1.1}$$

where Ψ is a wave function which depends simultaneously on the electronic coordinates ($\mathbf{r}$) and nuclear coordinates ($\mathbf{R}$), E is the total energy, and the Hamiltonian in atomic units is

$$\hat{H} = -\sum_{I=1}^{N}\frac{1}{2m_I}\nabla_I^2 - \frac{1}{2}\sum_{i=1}^{N}\nabla_i^2 + \sum_{I=1}^{N-1}\sum_{J=I+1}^{N}\frac{Z_I Z_J}{r_{IJ}} + \sum_{i=1}^{n-1}\sum_{j=i+1}^{n}\frac{1}{r_{ij}} - \sum_{i=1}^{n}\sum_{I=1}^{N}\frac{Z_I}{r_{iI}}, \tag{1.2}$$

where I and J label atomic nuclei, i and j label electrons, r_{pq} is the distance between particle p and q, ∇_p^2 is the Laplace operator acting on the particle p, and the atomic number and mass of nucleus I are given by Z_I and m_I. The Schrödinger equation can be solved exactly for hydrogen-like systems, but only approximate solutions are possible for systems of more particles. However, the problem can be greatly simplified by invoking the Born-Oppenheimer approximation. [3] Since the mass of the nuclei are orders of magnitude larger than the mass of the electron, the nuclear positions are effectively frozen with respect to the motion of the electrons. This enables one to break the solution of the Schrödinger equation into two parts. By neglecting the first term of the molecular Hamiltonian (corresponding to the kinetic energy of the nuclei), we obtain the electronic Hamiltonian

$$\hat{H}_e = -\frac{1}{2}\sum_{i=1}^{N}\nabla_i^2 + \sum_{I=1}^{N-1}\sum_{J=I+1}^{N}\frac{Z_I Z_J}{r_{IJ}} + \sum_{i=1}^{n-1}\sum_{j=i+1}^{n}\frac{1}{r_{ij}} - \sum_{i=1}^{n}\sum_{I=1}^{N}\frac{Z_I}{r_{iI}}, \tag{1.3}$$

with the corresponding Schrödinger equation

$$\hat{H}_e \Psi_e(\mathbf{r}; \mathbf{R}) = V(\mathbf{R}) \Psi_e(\mathbf{r}; \mathbf{R}). \tag{1.4}$$

The electronic wave function Ψ_e and the electronic energy $V(\mathbf{R})$ depend parametrically on the nuclear coordinates. The latter is referred to as the potential energy surface (PES) and is used to define the nuclear Hamiltonian

$$\hat{H}_{\mathrm{N}} = -\sum_{i=1}^{N} \frac{1}{2m_I} \nabla_i^2 + V(\mathbf{R}). \tag{1.5}$$

The nuclear Hamiltonian is invariant with respect to overall rotation and translation of the system. Therefore, it can be expressed in a simplified form as originally derived by Watson [4] as

$$\hat{H}_{\mathrm{N}} = -\frac{1}{2} \sum_i \frac{\delta^2}{\delta Q_i^2} + V(\mathbf{Q}) + \frac{1}{2m_{\mathrm{tot}}} \nabla_{\mathrm{CM}}^2 + \sum_{\alpha\beta} \mu_{\alpha\beta} (\Pi_\alpha - \pi_\alpha)(\Pi_\beta - \pi_\beta) - \frac{1}{8} \sum_\alpha \mu_{\alpha\alpha} \tag{1.6}$$

where $\mathbf{Q} = \{Q_1, Q_2, \ldots, Q_M\}$ are orthonormal mass-weighted vibrational coordinates, m_{tot} is the total mass of the system, ∇_{CM}^2 is the Laplace operator for the center of mass of the system, α and β are summed over the three Cartesian coordinates, μ is the reciprocal inertia tensor, and Π and π are angular momentum operators. The translational degrees of freedom, which correspond to the third term, are rigorously separable from rotation and vibration, but the rotational and vibrational degrees of freedom are not separable because μ and π in the fourth and fifth terms depend on the vibrational coordinates $\mathbf{Q}$. However, this rovibrational coupling is usually small and becomes increasingly insignificant for systems of larger size. Therefore, we neglect rotation to obtain a purely vibrational Hamiltonian

$$\hat{H}_{\mathrm{vib}} = -\frac{1}{2} \sum_i \frac{\delta^2}{\delta Q_i^2} + V(\mathbf{Q}). \tag{1.7}$$

The methods described throughout the remainder of this document seek the eigenvalues and eigenvectors of this purely vibrational Hamiltonian, and we drop the subscript "vib" from all further appearances for brevity.

The PES is a high-dimensional function with no general analytical form, but one common representation is to expand $V(\mathbf{Q})$ in a Taylor-series expansion about some reference geometry

$$V(\mathbf{Q}) = V_0 + \sum_i F_i Q_i + \frac{1}{2!} \sum_{i,j} F_{ij} Q_i Q_j + \frac{1}{3!} \sum_{i,j,k} F_{ijk} Q_i Q_j Q_k + \frac{1}{4!} \sum_{i,j,k,l} F_{ijkl} Q_i Q_j Q_k Q_l + \ldots, \tag{1.8}$$

where V_0 is the value of the potential and F's are referred to as force constants. Typical vibrational analysis is carried out at a potential energy minimum obtained by a geometry optimization; therefore, the first-order derivatives of the potential (F_i) vanish. Secondly, a set of normal-coordinates can be found which diagonalize the second-order

derivatives of the potential. Furthermore, neglecting all higher-order terms of the potential defines the harmonic approximation frequently utilized for vibrational problems. The advances in electronic structure theory of the last two decades have enabled the routine calculation of PES's free of empirical parameters, and the vibrational properties of molecules and solids can be routinely calculated within the harmonic approximation.

Unfortunately, the harmonic approximation often fails to produce even qualitatively accurate results. For example, some of the incorrect predictions of the harmonic approximation are:

1. There is no coupling between vibrational modes.
2. Only the fundamental vibrational modes are observable by infrared or Raman spectroscopy.
3. The frequency of overtones and combinations are exact multiples of the harmonic frequencies.
4. There is no thermal expansion of solids.
5. The thermal conductivity of solids is infinite.

1.2 Vibrational self-consistent field theory

To correct the deficiencies of the harmonic approximation requires a rigorous treatment of anharmonic effects. To this end, the toolkit of many-body methods developed for the electronic structure problem can be adapted for vibrations. Bowman and Ratner pioneered the vibrational self-consistent field (VSCF) method which relies on a single reference Hartree product of one-mode functions ("modals") along normal coordinates. These modals are determined so as to minimize the VSCF energy and are numerically defined on a grid or a basis set. [5–7]

We have recently shown that many of the Hamiltonian matrix elements of VSCF end up vanishing in the thermodynamic limit. [8] When these elements are erased from the VSCF equation, we arrive at a far more efficient, rigorously size-consistent, but less accurate variant of VSCF, which we call XVSCF(n) and XVSCF[n], [9–11] depending on whether an anharmonic geometry correction is suppressed (in the former) or not (in the latter). Each modal of XVSCF (or that of VSCF in the thermodynamic limit) is shown to be a harmonic-oscillator wave function with its frequency and center dressed with mean-field anharmonic effects, [8,9] which is consistent with Makri's theorem. [12] Since the Hamiltonian matrix elements in harmonic-oscillator modals are expressed simply with force constants, XVSCF and vibrational correlation theories based on it can be defined compactly with force constants and excitation amplitudes. Grids, basis sets, and quadratures are no longer necessary. This more efficient formulation does restrict the potential to be expressed as a polynomial in terms of normal coordinates. While this is computationally attractive, it is not always sufficient for high accuracy results. Other vibrational methods, such as MCTDH, can use curvilinear coordinates, while MCTDH and methods based on traditional VSCF do not require a polynomial form of the PES.

Furthermore, a normal-ordered second-quantized form of the vibrational Hamiltonian has been introduced recently, [13] and we have shown that the constant term and excitation amplitudes of the normal-ordered second-quantized form of the vibrational Hamiltonian [13] are identified as the energy, gradient, and frequency expressions of XVSCF (not of VSCF). This observation highlights the central place this theory occupies in anharmonic vibrational structure theory and the fact that XVSCF provides an ideal reference wave function for vibrational correlation theories. It further indicates that the algebraic interpretations of vertices in diagrammatic expressions of these theories are the XVSCF amplitudes. In this spirit, a diagrammatically size-extensive vibrationally perturbation (XVMP2) theory which relies on XVSCF as a reference was defined and implemented. [14] A logical next step is the development of a vibrational coupled-cluster (VCC) theory which obtains the efficiency of the underlying reference but recovers high accuracy.

1.3 Vibrational coupled-cluster theory

Coupled-cluster (CC) theory [15] was introduced by Coester and Kümmel [16,17] in nuclear physics and soon adopted by Čížek and coworkers [18, 19] in the field of quantum chemistry, where it was fully developed into the most accurate, versatile, and widely applicable electronic structure theory. [20–22] Being rigorously (i.e., diagrammatically) size consistent, [23,24] it was applied to problems in solid-state physics. [25–31] It also witnessed a revival in nuclear physics, [32, 33] as the Hamiltonian for nucleons became increasingly more accurate. Another area where the applicability of this theory is being explored is quantum nuclear dynamics in a bound potential energy surface (PES), i.e., anharmonic vibrational structure theory. [34, 35]

Following its applications to model PES's, [36–38] vibrational CC (VCC) theory was pioneered and extensively developed by Prasad and coworkers for general molecules with truncated Taylor-series PES's. [39–47] They considered both zero-point energies and transition frequencies using the equation-of-motion (EOM) [40, 45] or multireference [42,47] formalism. They also calculated spectra and band intensities in either the time-dependent [39,41,43,44] or independent [46] framework. These methods are based on a single Hartree product of harmonic-oscillator wave functions as a reference, of which the mode frequencies and coordinate center are varied to minimize its energy. Their working equations are derived using the second-quantized ladder operators, which are valid for harmonic oscillators. The reference wave function adopted can be identified as that of the size-extensive vibrational self-consistent field (XVSCF) method with an anharmonic geometry correction, i.e., XVSCF[n] (n is the rank of the Taylor-series PES). [10]

In the meantime, Christiansen and coworkers [48–54] proposed alternative formulations of VCC theory and its excited-state analog, VCC linear response (VCCLR). They may be viewed as a direct extension of vibrational correlation theories pioneered by Bowman and coworkers and by Ratner and coworkers, such as vibrational configuration-

interaction (VCI) [55] and vibrational Møller–Plesset perturbation (VMP) theories, [56] and share similar design philosophies. They all rely on a single reference Hartree product of one-mode functions ("modals") along normal coordinates furnished by VSCF, and they inherit the terms of VSCF which are not size-consistent.

Insofar as the modern formulation of CC theory is based on normal-ordered second quantization or diagrams, XVSCF should play a key role in the formulation of VCC theory. In Chapter 2, we present a rigorously (i.e., diagrammatically) size-consistent VCC theory for the ground and excited states, the latter through the EOM formalism.

1.4 Similarity transformations with exponential operators

Coupled-cluster (CC) theory [18, 57–61] for electronic structures is one of the most successful examples of an effective Hamiltonian theory, which is an equivalent but often more advantageous approach to solving the Schrödinger equation than the straightforward diagonalization of the bare Hamiltonian matrix. [62–67] Consider the action of a wave operator [64, 68] on a single-Slater-determinant [such as Hartree–Fock (HF)] wave function of the ground state $|\Phi_0\rangle$, which converts it into the exact wave function $|\Psi_0\rangle$,

$$|\Psi_0\rangle = \hat{\Omega}|\Phi_0\rangle. \tag{1.9}$$

The Schrödinger equation is then rewritten as

$$\hat{H}\hat{\Omega}|\Phi_0\rangle = E_0\hat{\Omega}|\Phi_0\rangle. \tag{1.10}$$

By left multiplying with $\hat{\Omega}^{-1}$, one can further recast it into an alternative form:

$$\bar{H}|\Phi_0\rangle = E_0|\Phi_0\rangle, \tag{1.11}$$

where the effective Hamiltonian $\bar{H}$ is defined by the similarity transformation of the bare Hamiltonian $\hat{H}$,

$$\bar{H} = \hat{\Omega}^{-1}\hat{H}\hat{\Omega}. \tag{1.12}$$

Equation (1.11) may be viewed as a trans-correlated Schrödinger equation with the effective Hamiltonian $\bar{H}$. [69,70] It has the HF wave function as an eigenfunction solution, yet the corresponding eigenvalue gives the exact ground-state energy E_0.

Such an approach falls into one of two broad categories. If $\hat{\Omega}^{-1} = \hat{\Omega}^{\dagger}$, the similarity transformation in Eq. (1.12) is also a unitary transformation and $\bar{H}$ is Hermitian. If $\hat{\Omega}^{-1} \neq \hat{\Omega}^{\dagger}$, the transformation is not unitary and $\bar{H}$ is no longer

Hermitian. In either case, the eigenvalue spectrum of the Hamiltonian is unchanged by the transformation.

In CC theory, the wave operator is an exponential excitation operator,

$$\hat{\Omega} = e^{\hat{T}}, \tag{1.13}$$

where $\hat{T}$ is a sum of one- through m-electron excitation operators. The effective Hamiltonian is then given by

$$\bar{H} = e^{-\hat{T}} \hat{H} e^{\hat{T}}. \tag{1.14}$$

The amplitudes of $\hat{T}$ are determined such that $|\Phi_0\rangle$ satisfies the trans-correlated Schrödinger equation of Eq. (1.11) only in the space of all n-electron ($0 \leq n \leq m$) excited determinants. If m is less than the number of electrons, this constitutes an approximation which alters the eigenvalue spectrum. Taking CC with singles and doubles (CCSD) [60] as an example, the equations to solve for $\hat{T}$ read

$$\langle \Phi_i^a | \bar{H} | \Phi_0 \rangle = 0, \tag{1.15}$$

$$\langle \Phi_{ij}^{ab} | \bar{H} | \Phi_0 \rangle = 0, \tag{1.16}$$

where $|\Phi_i^a\rangle$ and $|\Phi_{ij}^{ab}\rangle$ are one- and two-electron excited determinants, respectively ($i, j, k, \ldots$ are occupied spinorbitals and $a, b, c, \ldots$ are virtual). The CCSD ground-state energy E_{CC} (as an approximation to E_0) is then obtained by evaluating

$$E_{\mathrm{CC}} = \langle \Phi_0 | \bar{H} | \Phi_0 \rangle. \tag{1.17}$$

By virtue of satisfying Eqs. (1.15) and (1.16), the effective Hamiltonian $\bar{H}$ has a block structure, where the first column of $\bar{H}$ is zero in the singles and doubles blocks, as illustrated by $\bar{H}^{(\mathrm{EE})}$ in Fig. 1.1.

Since $e^{-\hat{T}} \neq (e^{\hat{T}})^{\dagger}$, the CC effective Hamiltonian is not Hermitian. However, this is a worthy sacrifice because the exponential structure of the CC wave operator is responsible for both the rigorous size-extensivity and comparatively high accuracy of the theory at a low computational cost. The size-extensivity is traced to the connectedness of the effective Hamiltonian,

$$\begin{aligned} \bar{H} &= e^{-\hat{T}} \hat{H} e^{\hat{T}} \\ &= \left(\hat{H} e^{\hat{T}} \right)_{\mathrm{C}}, \end{aligned} \tag{1.18}$$

where "C" indicates the absence of disconnected terms. [71,72] The exponential excitation operator also allows the CC

wave function to include higher excitations than the truncation order of $\hat{T}$ all the way up to simultaneous excitations of all electrons in the system. Electron-correlation effects from such higher-order excitations are folded into each amplitude of the effective Hamiltonian $\bar{H}$, making its constant part $E_{\rm CC}$ much closer to the exact energy than that in the bare Hamiltonian (which is just the HF energy $E_{\rm HF}$, capturing no correlation) or the lowest eigenvalue of $\hat{H}$ in the space of zero-, one-, and two-electron excited determinants, i.e., the ground-state energy of configuration interaction (CI) with singles and doubles (CISD), which lacks size-extensivity.

As implied by the use of distinct symbols $\bar{\mathbf{X}}$ versus $\mathbf{X}$ in Fig. 1.1, higher-order excitation effects are included not only in the constant part (ground-state energy) but also in all the other amplitudes of the effective Hamiltonian operator $\bar{H}$. Therefore, energies of states other than the ground state can also be obtained with higher accuracy by diagonalization of the $\bar{H}$ matrix in the space of excited (EE), ionized (IP), or electron-attached (EA) determinants than by diagonalization of the bare $\hat{H}$ matrix in the respective space (which is CI). This is the idea underlying equation-of-motion coupled-cluster (EOM-CC) theory for excited states, [73–81] IP-EOM-CC for ionized states, [82–85] or EA-EOM-CC for electron-attached states. [86–89] They can also be justified by a linear-response argument applied to ground-state CC. [90–92]

Taking CCSD for excited states as an example, the corresponding method, EOM-CCSD, is stipulated simply as a CISD problem using $\bar{H}$ in lieu of $\hat{H}$ (Fig. 1.1). Therefore, the ℓth excited-state wave function of EOM-CCSD is $\hat{R}(\ell)|\Psi_0\rangle$, where $\hat{R}(\ell)$ is a sum of one- and two-electron linear (CI-like) excitation operators, which satisfies the trans-correlated Schrödinger equation,

$$\bar{H}\hat{R}(\ell)|\Phi_0\rangle = E_\ell \hat{R}(\ell)|\Phi_0\rangle, \tag{1.19}$$

in the matching determinant space, namely,

$$\langle \Phi_i^a|\bar{H}\hat{R}(\ell)|\Phi_0\rangle = E_\ell \langle \Phi_i^a|\hat{R}(\ell)|\Phi_0\rangle, \tag{1.20}$$

$$\langle \Phi_{ij}^{ab}|\bar{H}\hat{R}(\ell)|\Phi_0\rangle = E_\ell \langle \Phi_{ij}^{ab}|\hat{R}(\ell)|\Phi_0\rangle. \tag{1.21}$$

One can act $\hat{R}(\ell)$ on both sides of Eq. (1.11) and subtract its projection onto the same determinants from Eqs. (1.20) and (1.21) to obtain

$$\langle \Phi_i^a|[\bar{H}, \hat{R}(\ell)]|\Phi_0\rangle = \omega_\ell \langle \Phi_i^a|\hat{R}(\ell)|\Phi_0\rangle, \tag{1.22}$$

$$\langle \Phi_{ij}^{ab}|[\bar{H}, \hat{R}(\ell)]|\Phi_0\rangle = \omega_\ell \langle \Phi_{ij}^{ab}|\hat{R}(\ell)|\Phi_0\rangle, \tag{1.23}$$

which is equivalent to the connected form

$$\langle \Phi_i^a | \left(\bar{H} \hat{R}(\ell) \right)_{\rm C} | \Phi_0 \rangle = \omega_\ell \langle \Phi_i^a | \hat{R}(\ell) | \Phi_0 \rangle, \tag{1.24}$$

$$\langle \Phi_{ij}^{ab} | \left(\bar{H} \hat{R}(\ell) \right)_{\rm C} | \Phi_0 \rangle = \omega_\ell \langle \Phi_{ij}^{ab} | \hat{R}(\ell) | \Phi_0 \rangle. \tag{1.25}$$

These equations prove the rigorous size-insensivity of excitation energy $\omega_\ell = E_\ell - E_{\rm CC}$, which then implies its high accuracy. The ground-state determinant (or the zero-electron excitation operator) does not enter the excited-state wave functions because of the block-diagonal structure of the $\bar{H}$ matrix in the first column (see $\bar{H}^{(\rm EE)}$ in Fig. 1.1). In other words, the ground and excited states are decoupled by the similarity transformation. Because of this decoupling, the use of the commutator is equivalent to the original CI problem except for a shift in energy

$$\langle \Phi_i^a | [\bar{H}, \hat{R}(\ell)] | \Phi_0 \rangle = \langle \Phi_i^a | \left(\bar{H} - E_{\rm CC} \right) \hat{R}(\ell) | \Phi_0 \rangle, \tag{1.26}$$

$$\langle \Phi_{ij}^{ab} | [\bar{H}, \hat{R}(\ell)] | \Phi_0 \rangle = \langle \Phi_{ij}^{ab} | \left(\bar{H} - E_{\rm CC} \right) \hat{R}(\ell) | \Phi_0 \rangle. \tag{1.27}$$

Furthermore, unlike the matrix elements of $\hat{H}$ used in CISD, those of $\bar{H}$ are dressed with the size-extensive ground-state correlation effect via the similarity transformation. For example, the matrix elements $\langle \Phi_{ijk}^{abc} | [\bar{H}, \hat{R}_1(\ell)] | \Phi_0 \rangle$ are small as only three-body terms of $\bar{H}$ contribute, so EOM-CCSD implicitly benefits from the inclusion of higher-order excitations relative to CISD. The same logic applies to IP- and EA-EOM-CCSD (see $\bar{H}^{(\rm IP)}$ and $\bar{H}^{(\rm EA)}$ in Fig. 1.1).

Viewing CC and EOM-CC as just the first application of a series of similarity transformations to the Hamiltonian, one can propose a potentially more powerful theory for excited states. The CC effective Hamiltonian $\bar{H}$ can be transformed *a second time* with another exponential excitation operator $\{e^{\hat{S}}\}$ (where the braces bring the operators enclosed by them into a normal-order) to account for higher-order electron-correlation effects in excited states. Such an approach was first considered by Stolarczyk and Monkhorst [93–96] in the development of Fock-space CC (FSCC) theory and subsequently by Nooijen *et al.*, [97–103] who proposed similarity-transformed equation-of-motion coupled-cluster (STEOM-CC) theory.

In the STEOM-CC method with single and double excitations (STEOM-CCSD), [97–103] the second similarity transformation,

$$\bar{\bar{H}} = \{e^{\hat{S}}\}^{-1} \bar{H} \{e^{\hat{S}}\}, \tag{1.28}$$

decouples the 1h determinants from the 2h1p ones in the IP sector and the 1p determinants from the 1h2p ones in the

EA sector, i.e.,

$$\langle \Phi_{ij}^{a} | \bar{\bar{H}} | \Phi_k \rangle = 0, \tag{1.29}$$

$$\langle \Phi_{i}^{ab} | \bar{\bar{H}} | \Phi^c \rangle = 0. \tag{1.30}$$

These can be achieved by the $\hat{S}$ operator containing up to 2h1p and 1h2p operators. [104–109] The matrix representations of the resulting $\bar{\bar{H}}$ operator should have the block tridiagonal structures illustrated by $\bar{\bar{H}}^{(\mathrm{IP})}$ and $\bar{\bar{H}}^{(\mathrm{EA})}$ in Fig. 1.1. The diagonalization of these matrices in the tiny 1h or 1p space (indicated by the dashed boxes in the same figure) is equivalent to IP- or EA-EOM-CCSD, [97–99] which selectively and simultaneously determine all principal IPs or EAs. Furthermore, since IP- and EA-EOM-CCSD have ready-available efficient implementations, they can be used to determine the amplitudes of $\hat{S}$ expediently.

However, the objective of STEOM-CCSD is not to supply an alternative route to IP- or EA-EOM-CCSD but more so to compute excitation energies. Notice that the amplitudes of the $\bar{\bar{H}}$ operator that are made to vanish in Eqs. (1.29) and (1.30) are of the two-electron excitation type. Hence, the $\bar{\bar{H}}$ operator largely, albeit not completely, decouples the one- and two-electron *excited* determinants also, i.e.,

$$\langle \Phi_{ij}^{ab} | \bar{\bar{H}} | \Phi_k^c \rangle \approx 0, \tag{1.31}$$

rendering the $\bar{\bar{H}}^{(\mathrm{EE})}$ matrix an approximate block tridiagonal structure shown in Fig. 1.1. The reason for the incomplete decoupling (the approximate equal sign in the above equation) is that the left-hand side contains three-electron contributions that are insignificant but remain nonzero.

Owing to this matrix structure and the connectedness of $\bar{\bar{H}}$ proven by Nooijen, [110] the diagonalization of this matrix in its tiny singles-singles block (dashed-boxed area of $\bar{\bar{H}}^{(\mathrm{EE})}$ in the figure) yields size-intensive excitation energies of *all predominantly one-electron character simultaneously* that are roughly of the same accuracy and, for certain classes of excitations (such as charge-transfer excitations), distinctly superior to EOM-CCSD. [99, 111] The ground-state energy E_{CC} is unchanged by the second similarity transformation.

In Chapters 3 and 4, we will investigate the utility of the STEOM ansatz for vibrations.

1.5 Vibrational structure theory for one-dimensional periodicity

Here we outline the calculation of phonon dispersion curves for a system with periodicity in one dimension.

The harmonic force constants of a periodic lattice can be obtained in Cartesian coordinates as

$$F_{\mu(0)\nu(m)} = \frac{\partial^2 V}{\partial X_{\mu(0)} \partial X_{\nu(m)}}, \tag{1.32}$$

where V is the electronic energy of the system and $X_{\nu(m)}$ is the νth Cartesian coordinate in the mth unit cell. The dynamical mass-weighted force-constant matrix is then defined by the discrete Fourier transform of the Cartesian force constants

$$F_k^{\mu\nu} = \sum_m m_\mu^{-1/2} m_\nu^{-1/2} F_{\mu(0)\nu(m)} e^{-imka}. \tag{1.33}$$

where m_ν is atomic mass associated with the νth Cartesian coordinates, a is the lattice constant, and k is the linear quasimomentum which can take distinct values defined by

$$k = \frac{2n\pi}{Ka}, \{n \in \mathbb{Z} | 0 \leq n < K\}, \tag{1.34}$$

where K is the number of unit cells.

Diagonalizing the dynamical force constant matrix as a function of the quasimomentum k yields eigenvalues $\omega^2_{pk_p}$ and eigenvectors $C^\mu_{pk_p}$. The pth phonon branch of the phonon dispersion curves is then obtained by plotting the frequency ω_{pk_p} as a function of the linear quasimomentum k_p.

The working equations of the diagrammatically size-consistent vibrational methods described in this work all rely on an expansion of the PES in a Taylor series. The force constants in normal coordinates which define the Taylor-series expansion may be obtained via

$$F_{pk_p} = K^{1/2} \Delta_{k_p} \sum_\kappa m_\kappa^{-1/2} C^{\kappa^*}_{pk_p} F_{\kappa(0)}, \tag{1.35}$$

$$F_{pk_pqk_q} = K^0 \Delta_{k_p+k_q} \sum_{\kappa,\lambda} \sum_{m_1} m_\kappa^{-1/2} m_\lambda^{-1/2} C^{\kappa^*}_{pk_p} C^{\lambda^*}_{qk_q} F_{\kappa(0)\lambda(m_1)} e^{i(m_1 k_q)a}, \tag{1.36}$$

$$F_{pk_pqk_qrk_r} = K^{-1/2} \Delta_{k_p+k_q+k_r} \sum_{\kappa,\lambda,\mu} \sum_{m_1,m_2} m_\kappa^{-1/2} m_\lambda^{-1/2} m_\mu^{-1/2} C^{\kappa^*}_{pk_p} C^{\lambda^*}_{qk_q} C^{\mu^*}_{rk_r} F_{\kappa(0)\lambda(m_1)\mu(m_2)} e^{i(m_1 k_q + m_2 k_r)a}, \tag{1.37}$$

$$\begin{aligned} F_{pk_pqk_qrk_rsk_s} = {} & K^{-1} \Delta_{k_p+k_q+k_r+k_s} \sum_{\kappa,\lambda,\mu,\nu} \sum_{m_1,m_2,m_3} m_\kappa^{-1/2} m_\lambda^{-1/2} m_\mu^{-1/2} m_\nu^{-1/2} \\ & \times C^{\kappa^*}_{pk_p} C^{\lambda^*}_{qk_q} C^{\mu^*}_{rk_r} C^{\nu^*}_{sk_s} F_{\kappa(0)\lambda(m_1)\mu(m_2)\nu(m_3)} e^{i(m_1 k_q + m_2 k_r + m_3 k_s)a}, \end{aligned} \tag{1.38}$$

where Δ_k enforces the momentum conservation condition. That is $\Delta_k = 1$ if $k = 2n\pi/a$ where n is an integer and Δk is

zero otherwise. Since the normal coordinates are centered at the equilibrium lattice structure, we have

$$F_{p_{k_p}} = 0, \tag{1.39}$$

$$F_{p_{k_p} q_{k_q}} = \delta_{pq} \Delta_{k_p + k_q} \omega^2_{p_{k_p}}. \tag{1.40}$$

1.6 Figure

$$
\hat{H}^{(\mathrm{EE})} = \begin{array}{c} \\ \langle\Phi_0| \\ \langle\Phi_i^a| \\ \langle\Phi_{ij}^{ab}| \end{array} \begin{array}{c} \begin{array}{ccc} |\Phi_0\rangle & |\Phi_i^a\rangle & |\Phi_{ij}^{ab}\rangle \end{array} \\ \begin{bmatrix} E_{\mathrm{HF}} & \mathbf{0} & \mathbf{X} \\ \mathbf{0} & \mathbf{X} & \mathbf{X} \\ \mathbf{X} & \mathbf{X} & \mathbf{X} \end{bmatrix} \end{array}
$$

$$
\bar{H}^{(\mathrm{EE})} = \begin{array}{c} \\ \langle\Phi_0| \\ \langle\Phi_i^a| \\ \langle\Phi_{ij}^{ab}| \end{array} \begin{array}{c} \begin{array}{ccc} |\Phi_0\rangle & |\Phi_i^a\rangle & |\Phi_{ij}^{ab}\rangle \end{array} \\ \begin{bmatrix} E_{\mathrm{CC}} & \bar{\mathbf{X}} & \bar{\mathbf{X}} \\ \mathbf{0} & \bar{\mathbf{X}} & \bar{\mathbf{X}} \\ \mathbf{0} & \bar{\mathbf{X}} & \bar{\mathbf{X}} \end{bmatrix} \end{array}
$$

$$
\bar{H}^{(\mathrm{IP})} = \begin{array}{c} \\ \langle\Phi_i| \\ \langle\Phi_{ij}^a| \end{array} \begin{array}{c} \begin{array}{cc} |\Phi_i\rangle & |\Phi_{ij}^a\rangle \end{array} \\ \begin{bmatrix} \bar{\mathbf{X}} & \bar{\mathbf{X}} \\ \bar{\mathbf{X}} & \bar{\mathbf{X}} \end{bmatrix} \end{array}
$$

$$
\bar{H}^{(\mathrm{EA})} = \begin{array}{c} \\ \langle\Phi^a| \\ \langle\Phi_i^{ab}| \end{array} \begin{array}{c} \begin{array}{cc} |\Phi^a\rangle & |\Phi_i^{ab}\rangle \end{array} \\ \begin{bmatrix} \bar{\mathbf{X}} & \bar{\mathbf{X}} \\ \bar{\mathbf{X}} & \bar{\mathbf{X}} \end{bmatrix} \end{array}
$$

$$
\bar{\bar{H}}^{(\mathrm{IP})} = \begin{array}{c} \\ \langle\Phi_i| \\ \langle\Phi_{ij}^a| \end{array} \begin{array}{c} \begin{array}{cc} |\Phi_i\rangle & |\Phi_{ij}^a\rangle \end{array} \\ \begin{bmatrix} \bar{\bar{\mathbf{X}}} & \bar{\bar{\mathbf{X}}} \\ \mathbf{0} & \bar{\bar{\mathbf{X}}} \end{bmatrix} \end{array}
$$

$$
\bar{\bar{H}}^{(\mathrm{EA})} = \begin{array}{c} \\ \langle\Phi^a| \\ \langle\Phi_i^{ab}| \end{array} \begin{array}{c} \begin{array}{cc} |\Phi^a\rangle & |\Phi_i^{ab}\rangle \end{array} \\ \begin{bmatrix} \bar{\bar{\mathbf{X}}} & \bar{\bar{\mathbf{X}}} \\ \mathbf{0} & \bar{\bar{\mathbf{X}}} \end{bmatrix} \end{array}
$$

$$
\bar{\bar{H}}^{(\mathrm{EE})} = \begin{array}{c} \\ \langle\Phi_0| \\ \langle\Phi_i^a| \\ \langle\Phi_{ij}^{ab}| \end{array} \begin{array}{c} \begin{array}{ccc} |\Phi_0\rangle & |\Phi_i^a\rangle & |\Phi_{ij}^{ab}\rangle \end{array} \\ \begin{bmatrix} E_{\mathrm{CC}} & \bar{\bar{\mathbf{X}}} & \bar{\bar{\mathbf{X}}} \\ \mathbf{0} & \bar{\bar{\mathbf{X}}} & \bar{\bar{\mathbf{X}}} \\ \mathbf{0} & \approx \mathbf{0} & \bar{\bar{\mathbf{X}}} \end{bmatrix} \end{array}
$$

Figure 1.1: Structure of the bare ($\hat{H}$), singly ($\bar{H}$), and doubly ($\bar{\bar{H}}$) similarity-transformed Hamiltonian of electronic CCSD in the excited (EE), ionized (IP), and electron-attached (EA) sectors. The blocks whose elements are zero and approximately zero are represented by $\mathbf{0}$ and $\approx \mathbf{0}$, respectively, while the others by $\mathbf{X}$, $\bar{\mathbf{X}}$, and $\bar{\bar{\mathbf{X}}}$. The blue-colored blocks are the ones expressly made to vanish by the similarity transformation. E_{HF} and E_{CC} denote the HF and CCSD energy, respectively, for the ground state. The dashed-boxed areas are the formal diagonalization spaces of EOM-CCSD ($\bar{H}^{(\mathrm{EE})}$), IP-EOM-CCSD ($\bar{H}^{(\mathrm{IP})}$), EA-EOM-CCSD ($\bar{H}^{(\mathrm{EA})}$), and STEOM-CCSD ($\bar{\bar{H}}^{(\mathrm{EE})}$). Diagonalization in the dashed-boxed area of $\bar{\bar{H}}^{(\mathrm{IP})}$ ($\bar{\bar{H}}^{(\mathrm{EA})}$) is equivalent to IP-EOM-CCSD (EA-EOM-CCSD) for principal IPs (EAs).

Chapter 2

Higher-order diagrammatic vibrational coupled-cluster theory

2.1 Introduction

In this chapter,[1] we present rigorously (i.e., diagrammatically) size-consistent VCC theory for the ground and excited states, the latter through the EOM formalism. We call them XVCCm and EOM-XVCCm theories, respectively, where m stands for the highest excitation rank considered. We propose a rational and expedient method of deriving their algebraic definitions using the rules of normal-ordered second quantization and Feynman–Goldstone diagrams. We demonstrate its utility through the derivation of low-order XVCC and EOM-XVCC equations. The formalisms thus derived are valid for any single reference Hartree product of harmonic-oscillator modals along delocalized, rectilinear coordinates, such as XVSCF(n), [9] XVSCF[n], [10] and the closely related self-consistent-phonon (SCP) method [112–116] as well as the harmonic approximation. In its current implementation, XVCC is ill-equipped for a PES with multiple minima along one coordinate. Some diagrammatic contributions are shown to vanish in the XVSCF and SCP reference, making them more favorable, although higher-order XVCC and EOM-XVCC are increasingly insensitive to the reference choice. XVCC and EOM-XVCC with the XVSCF[n] reference are found to be equivalent to the VCC formalism first developed by Prasad and coworkers, [40, 45] shedding light on the relationship between the two VCC theories and XVCC theory: the VCC theory of Prasad and coworkers and XVCC theory are diagrammatically size-consistent and infinite-basis counterparts of the VCC theory of Christiansen and coworkers in a truncated Taylor-series PES, if no other approximations are made.

We furthermore derive and implement high-order XVCCm and EOM-XVCCm equations up to $m = 8$ or octuple excitations, with the aid of computerized derivation, optimization, and code synthesis. We apply these methods to the zero-point energies and frequencies of the fundamentals, overtones, and combinations as well as Fermi-resonant modes of the water and formaldehyde molecules, using quartic force fields (QFF's). [117] A comparative analysis is performed for the results of these methods and of XVSCF(n), XVSCF[n], size-extensive second-order vibrational many-body perturbation theory (XVMP2), [14] and full VCI. It shows that XVCCm and EOM-XVCCm with m equal to the truncation rank of the Taylor-series PES are uniformly accurate and stable for both resonant and nonresonant

[1] The work in this chapter has been published in Ref. 132. Reprint permission is granted by AIP.

modes and are likely the methods with the greatest practical utility of all considered.

2.2 Theory

2.2.1 XVCC formalism

We express the mth-order XVCC (XVCCm) wave function for the zero-point (ground) state (labeled by subscript '0') as

$$|\Psi_0\rangle = e^{\hat{T}}|\Phi_0\rangle, \tag{2.1}$$

where $|\Phi_0\rangle$ is a reference wave function. The latter, in turn, is a Hartree product of harmonic-oscillator modals (which include but are not limited to those from the harmonic approximation to the PES),

$$|\Phi_0\rangle = \prod_p |0_p\rangle, \tag{2.2}$$

where $|n_p\rangle$ denotes the harmonic-oscillator wave function with quantum number n_p and frequency ω_p along the pth normal, first-order Dyson, [11] or other delocalized rectilinear coordinate. Operator $\hat{T}$ is the sum of the single, double, through m-fold cluster excitation operators,

$$\hat{T} = \hat{T}_1 + \hat{T}_2 + \cdots + \hat{T}_m, \tag{2.3}$$

with

$$\hat{T}_n = \frac{1}{n!} \sum_{p_1,p_2,\ldots,p_n} \tau^{p_1 p_2 \cdots p_n} \hat{a}^\dagger_{p_1} \hat{a}^\dagger_{p_2} \cdots \hat{a}^\dagger_{p_n} \tag{2.4}$$

$$= \frac{1}{n!} \sum_{p_1,p_2,\ldots,p_n} \tau^{p_1 p_2 \cdots p_n} \{\hat{a}^\dagger_{p_1} \hat{a}^\dagger_{p_2} \cdots \hat{a}^\dagger_{p_n}\}, \tag{2.5}$$

where $\tau^{p_1 p_2 \cdots p_n}$ is an excitation amplitude, the value of which is to be determined by solving the amplitude equations (see below). Operator $\hat{a}^\dagger_p$ and its adjoint $\hat{a}_p$ are the ladder operators for the harmonic-oscillator modals, i.e.,

$$\hat{a}_p|n_p\rangle = n_p^{1/2}|n_p - 1\rangle, \tag{2.6}$$

$$\hat{a}^\dagger_p|n_p\rangle = (n_p + 1)^{1/2}|n_p + 1\rangle. \tag{2.7}$$

The braces $\{\cdots\}$ in Eq. (2.5) bring the operators enclosed by them into a normal order. [13] Two or more of the mode indices $(p_1, p_2, \ldots, p_n)$ in Eq. (2.4) are permitted to be coincident.

We require that the wave function of Eq. (2.1) satisfy the vibrational Schrödinger equation in the space of Hartree products reachable by $\hat{T}$ from $|\Phi_0\rangle$:

$$\langle\Phi_0|\hat{H}e^{\hat{T}}|\Phi_0\rangle = \langle\Phi_0|E_0^{(m)}e^{\hat{T}}|\Phi_0\rangle, \tag{2.8}$$

and

$$\langle\Phi_{p_1p_2\cdots p_n}|\hat{H}e^{\hat{T}}|\Phi_0\rangle = \langle\Phi_{p_1p_2\cdots p_n}|E_0^{(m)}e^{\hat{T}}|\Phi_0\rangle, \tag{2.9}$$

for all $p_1, p_2, \ldots, p_n$ and each n $(1 \le n \le m)$. Here, $E_0^{(m)}$ is the XVCCm total energy and

$$|\Phi_{p_1p_2\cdots p_n}\rangle = \hat{a}_{p_1}^\dagger\hat{a}_{p_2}^\dagger\cdots\hat{a}_{p_n}^\dagger|\Phi_0\rangle. \tag{2.10}$$

The number of the amplitude equations expressed collectively by Eq. (2.9) is equal to the number of unknown excitation amplitudes $\{\tau\}$ in Eq. (2.4). Furthermore, it can be shown below that $E_0^{(m)}$, which is also unknown, is eliminated from Eq. (2.9). Hence, by solving Eq. (2.9), we obtain $\{\tau\}$. Substituting the latter in the energy equation [Eq. (2.8)], we determine $E_0^{(m)}$.

The reference wave function $|\Phi_0\rangle$ can be furnished by any of the following: XVSCF(n), [9] XVSCF[n], [10] SCP, [112–116] or the harmonic approximation. They differ from one another in the coordinates, their center, and the modal frequencies, [11] but they all share the same form: the Hartree product of harmonic-oscillator modals. The XVCCm formalisms are essentially unchanged by the choice of the references except that some terms may vanish in some references. The foregoing definition of XVCCm and the working equations derived in the following are valid for any of these references.

One may notice at this stage a striking difference between electronic CC and XVCC. Since the one-mode basis functions of XVCC are harmonic-oscillator wave functions, which need not be stored numerically, XVCC can take account of an infinite number of them implicitly. This means that, even when the Hamiltonian is truncated after the n-body term $(n \ge 3)$ for a molecule with N vibrational degrees of freedom, neither XVCCn nor XVCCN is exact mathematically, though XVCCm is shown below to be rapidly convergent with m in practice. In other words, XVCC is an infinite-basis or basis-free method despite the finiteness of its equations. This is where XVCC and Christiansen's VCC (Ref. 48) also differ from each other fundamentally. The excitation space reached by $\hat{T}$ is limited by the number of basis functions included in VCC, whereas it is not in XVCC.

The VCC ansatz of Prasad and coworkers [40, 45] is the same as above, but it is predicated on a reference Hartree product of Gaussian modals along normal coordinates, whose centers and widths are varied to minimize its energy. This reference method is identified as the XVSCF[n] method. [10] Therefore, XVCCm with the XVSCF[n] reference corresponds to the VCC theory of Prasad and coworkers, [40, 45] although XVCCm is defined for more general reference Hartree products, including XVSCF(n), SCP, and the harmonic approximation.

2.2.2 Algebraic derivation of XVCC

Here, we illustrate an algebraic derivation of working equations of XVCCm using the normal-ordered second quantization and Wick's theorem. [13] We use, as an example, XVCC1 or XVCC with single excitations (XVCCS) for a vibrational Hamiltonian with a QFF.

This Hamiltonian can be written in the normal-ordered second-quantized form [13] as

$$\begin{aligned}\hat{H} &= E_0^{(0)} + \sum_p h^p\{\hat{a}_p^\dagger\} + \sum_p h_p\{\hat{a}_p\} + \frac{1}{2!}\sum_{p,q} h^{pq}\{\hat{a}_p^\dagger\hat{a}_q^\dagger\} + \sum_{p,q} h_q^p\{\hat{a}_p^\dagger\hat{a}_q\} + \frac{1}{2!}\sum_{p,q} h_{pq}\{\hat{a}_p\hat{a}_q\} \\ &+ \frac{1}{3!}\sum_{p,q,r} h^{pqr}\{\hat{a}_p^\dagger\hat{a}_q^\dagger\hat{a}_r^\dagger\} + \frac{1}{2!}\sum_{p,q,r} h_r^{pq}\{\hat{a}_p^\dagger\hat{a}_q^\dagger\hat{a}_r\} + \frac{1}{2!}\sum_{p,q,r} h_{qr}^p\{\hat{a}_p^\dagger\hat{a}_q\hat{a}_r\} + \frac{1}{3!}\sum_{p,q,r} h_{pqr}\{\hat{a}_p\hat{a}_q\hat{a}_r\} \\ &+ \frac{1}{4!}\sum_{p,q,r,s} h^{pqrs}\{\hat{a}_p^\dagger\hat{a}_q^\dagger\hat{a}_r^\dagger\hat{a}_s^\dagger\} + \frac{1}{3!}\sum_{p,q,r,s} h_s^{pqr}\{\hat{a}_p^\dagger\hat{a}_q^\dagger\hat{a}_r^\dagger\hat{a}_s\} + \frac{1}{2!2!}\sum_{p,q,r,s} h_{rs}^{pq}\{\hat{a}_p^\dagger\hat{a}_q^\dagger\hat{a}_r\hat{a}_s\} \\ &+ \frac{1}{3!}\sum_{p,q,r,s} h_{qrs}^p\{\hat{a}_p^\dagger\hat{a}_q\hat{a}_r\hat{a}_s\} + \frac{1}{4!}\sum_{p,q,r,s} h_{pqrs}\{\hat{a}_p\hat{a}_q\hat{a}_r\hat{a}_s\}. \end{aligned} \tag{2.11}$$

The constant term in Eq. (2.11), $E_0^{(0)}$, is the total ground-state energy expression of XVSCF, [9, 10, 13] regardless of the actual reference method adopted in the calculation, and given by

$$\begin{aligned}E_0^{(0)} &= V_0 + \frac{1}{4}\sum_p \omega_p + \frac{1}{2}\sum_p \frac{F_{pp}}{(2\omega_p)} \\ &+ \frac{1}{2!2^2}\sum_{p,q} \frac{F_{ppqq}}{(2\omega_p)(2\omega_q)} + \ldots, \end{aligned} \tag{2.12}$$

where V_0 is the value of the PES at the minimum, ω_p is again the frequency of the pth modal, and F's are the force

constants. The Hamiltonian amplitudes, $\{h\}$ in a QFF, are given by

$$h_p = \frac{F_p}{(2\omega_p)^{1/2}} + \frac{1}{2}\sum_q \frac{F_{pqq}}{(2\omega_p)^{1/2}(2\omega_q)}, \tag{2.13}$$

$$h_q^p = \frac{1}{2}\delta_{pq}\omega_p + \frac{F_{pq}}{(2\omega_p)^{1/2}(2\omega_q)^{1/2}} + \frac{1}{2}\sum_r \frac{F_{pqrr}}{(2\omega_p)^{1/2}(2\omega_q)^{1/2}(2\omega_r)}, \tag{2.14}$$

$$h_{pq} = -\frac{1}{2}\delta_{pq}\omega_p + \frac{F_{pq}}{(2\omega_p)^{1/2}(2\omega_q)^{1/2}} + \frac{1}{2}\sum_r \frac{F_{pqrr}}{(2\omega_p)^{1/2}(2\omega_q)^{1/2}(2\omega_r)}, \tag{2.15}$$

$$h_{pqr} = \frac{F_{pqr}}{(2\omega_p)^{1/2}(2\omega_q)^{1/2}(2\omega_r)^{1/2}}, \tag{2.16}$$

$$h_{pqrs} = \frac{F_{pqrs}}{(2\omega_p)^{1/2}(2\omega_q)^{1/2}(2\omega_r)^{1/2}(2\omega_s)^{1/2}}, \tag{2.17}$$

with

$$h_p = h^p, \tag{2.18}$$

$$h_{pq} = h^{pq}, \tag{2.19}$$

$$h_{pqr} = h_r^{pq} = h_{qr}^p = h^{pqr}, \tag{2.20}$$

$$h_{pqrs} = h_s^{pqr} = h_{rs}^{pq} = h_{qrs}^p = h^{pqrs}. \tag{2.21}$$

These amplitudes are invariant to any permutation of indices. With the XVSCF(4) reference, $h_p^p = \omega_p$ holds. In the XVSCF[4] reference, additionally, $h^p = 0$ is true. Furthermore, $h_q^p = 0$ for $p \neq q$ with the SCP reference. The fact that these key quantities of the XVSCF methods naturally emerge in the expression of the normal-ordered Hamiltonian underscores their fundamental significance in many-body vibrational theory. [13]

From Eq. (2.8), we find the XVCCS energy equation to be

$$E_0^{(1)} = \langle\Phi_0|\hat{H}\left(1 + \hat{T}_1 + \frac{1}{2!}\hat{T}_1^2 + \frac{1}{3!}\hat{T}_1^3 + \frac{1}{4!}\hat{T}_1^4\right)|\Phi_0\rangle, \tag{2.22}$$

where $E_0^{(1)}$ is the XVCCS total energy and the Taylor-series of the exponential operator is truncated after the $\hat{T}_1^4$ term because the higher-order terms cannot contribute in a QFF (see below). The XVCCS amplitude equation, Eq. (2.9),

similarly reduces to

$$E_0^{(1)}\tau^p = \langle\Phi_0|\{\hat{a}_p\}\hat{H} \times \left(1 + \hat{T}_1 + \frac{1}{2!}\hat{T}_1^2 + \frac{1}{3!}\hat{T}_1^3 + \frac{1}{4!}\hat{T}_1^4 + \frac{1}{5!}\hat{T}_1^5\right)|\Phi_0\rangle, \tag{2.23}$$

in a QFF. Here, the Taylor-series can be terminated after the $\hat{T}_1^5$ term (see below).

Wick's theorem states that the vacuum expectation value of a product of two or more normal-ordered series of operators is the sum of all full contractions with no internal contractions. [13, 118] It also states that the vacuum expectation value of just one normal-ordered series is zero. [13, 118]

Using this theorem, one can evaluate the first term of Eq. (2.22) as

$$\langle\Phi_0|\hat{H}|\Phi_0\rangle = E_0^{(0)}. \tag{2.24}$$

The second term has only one nonzero full contraction:

$$\begin{aligned}\langle\Phi_0|\hat{H}\hat{T}_1|\Phi_0\rangle &= \sum_{p,q} h_p\tau^q\langle\Phi_0|\{\hat{a}_p\}\{\hat{a}_q^\dagger\}|\Phi_0\rangle, \\ &= \sum_p h_p\tau^p.\end{aligned} \tag{2.25}$$

The third term has two nonzero full contractions:

$$\begin{aligned}&\langle\Phi_0|\frac{1}{2!}\hat{H}\hat{T}_1^2|\Phi_0\rangle \\ &= \frac{1}{2!2!}\sum_{p,q,r,s} h_{pq}\tau^r\tau^s\langle\Phi_0|\{\hat{a}_p\hat{a}_q\}\{\hat{a}_r^\dagger\}\{\hat{a}_s^\dagger\}|\Phi_0\rangle, \\ &+ \frac{1}{2!2!}\sum_{p,q,r,s} h_{pq}\tau^r\tau^s\langle\Phi_0|\{\hat{a}_p\hat{a}_q\}\{\hat{a}_r^\dagger\}\{\hat{a}_s^\dagger\}|\Phi_0\rangle, \\ &= \frac{1}{2}\sum_{p,q} h_{pq}\tau^p\tau^q.\end{aligned} \tag{2.26}$$

The fourth and fifth terms are evaluated similarly, yielding

$$\frac{1}{3!}\langle\Phi_0|\hat{H}\hat{T}_1^3|\Phi_0\rangle = \frac{1}{3!}\sum_{p,q,r} h_{pqr}\tau^p\tau^q\tau^r, \tag{2.27}$$

and

$$\frac{1}{4!}\langle\Phi_0|\hat{H}\hat{T}_1^4|\Phi_0\rangle = \frac{1}{4!}\sum_{p,q,r,s} h_{pqrs}\tau^p\tau^q\tau^r\tau^s. \tag{2.28}$$

Since the Hamiltonian with a QFF has only up to four-body operators, the $\hat{T}_1^5$ term and higher in the exponential operator cannot produce a full contraction.

Together, the XVCCS energy is given by

$$\begin{aligned} E_0^{(1)} &= E_0^{(0)} + \sum_p h_p\tau^p + \frac{1}{2!}\sum_{p,q} h_{pq}\tau^p\tau^q \\ &\quad + \frac{1}{3!}\sum_{p,q,r} h_{pqr}\tau^p\tau^q\tau^r + \frac{1}{4!}\sum_{p,q,r,s} h_{pqrs}\tau^p\tau^q\tau^r\tau^s. \end{aligned} \tag{2.29}$$

It may be noticed that each of the second and subsequent terms is connected in the sense that every factor has at least one common summation index with another factor. This ensures the extensivity of $E_0^{(1)}$. [23, 24]

The connectedness of the energy equation is a universal feature of XVCCm for all m. For future convenience, therefore, we introduce an XVCCm energy equation alternative to Eq. (2.8), which reads

$$\Delta E_0^{(m)} = \langle\Phi_0|\left(\hat{H}_\mathrm{N}e^{\hat{T}}\right)_\mathrm{C}|\Phi_0\rangle, \tag{2.30}$$

where $\hat{H}_\mathrm{N} = \hat{H} - E_0^{(0)}$, $\Delta E_0^{(m)} = E_0^{(m)} - E_0^{(0)}$, and $(\cdots)_\mathrm{C}$ deletes terms that are disconnected. We call this the energy equation of XVCCm.

The XVCCS amplitude equation can likewise be derived by Wick's theorem. The first term of Eq. (2.23) has one nonzero full contraction:

$$\langle\Phi_0|\{\hat{a}_p\}\hat{H}|\Phi_0\rangle = \langle\Phi_0|\{\hat{a}_p\}\{\hat{a}_q^\dagger\}|\Phi_0\rangle = h^p. \tag{2.31}$$

The second term has two nonzero full contractions:

$$\begin{aligned} \langle\Phi_0|\{\hat{a}_p\}H\hat{T}_1|\Phi_0\rangle &= E_0^{(0)}\sum_q \tau^q\langle\Phi_0|\{\hat{a}_p\}\{\hat{a}_q^\dagger\}|\Phi_0\rangle \\ &\quad + \sum_{q,r,s} h_r^q\tau^s\langle\Phi_0|\{\hat{a}_p\}\{\hat{a}_q^\dagger\}\hat{a}_r\{\hat{a}_s^\dagger\}|\Phi_0\rangle \\ &= E_0^{(0)}\tau^p + \sum_q h_q^p\tau^q. \end{aligned} \tag{2.32}$$

The third term has four such contractions:

$$
\begin{aligned}
&\langle\Phi_0|\{\hat{a}_p\}\frac{1}{2}\hat{H}\hat{T}_1^2|\Phi_0\rangle \\
&= \frac{1}{2!}\sum_{q,r,s} h_q \tau^r \tau^s \langle\Phi_0|\{\hat{a}_p\}\{\hat{a}_q\}\{\hat{a}_r^\dagger\}\{\hat{a}_s^\dagger\}|\Phi_0\rangle \\
&+ \frac{1}{2!}\sum_{q,r,s} h_q \tau^r \tau^s \langle\Phi_0|\{\hat{a}_p\}\{\hat{a}_q\}\{\hat{a}_r^\dagger\}\{\hat{a}_s^\dagger\}|\Phi_0\rangle \\
&+ \frac{1}{2!}\frac{1}{2!}\sum_{q,r,s,t,u} h^q_{rs} \tau^t \tau^u \langle\Phi_0|\{\hat{a}_p\}\{\hat{a}_q^\dagger \hat{a}_r \hat{a}_s\}\{\hat{a}_t^\dagger\}\{\hat{a}_u^\dagger\}|\Phi_0\rangle \\
&+ \frac{1}{2!}\frac{1}{2!}\sum_{q,r,s,t,u} h^q_{rs} \tau^t \tau^u \langle\Phi_0|\{\hat{a}_p\}\{\hat{a}_q^\dagger \hat{a}_r \hat{a}_s\}\{\hat{a}_t^\dagger\}\{\hat{a}_u^\dagger\}|\Phi_0\rangle \\
&= \sum_q h_q \tau^q \tau^p + \frac{1}{2}\sum_{q,r} h^p_{qr} \tau^q \tau^r .
\end{aligned}
\tag{2.33}
$$

The remainder are evaluated similarly, yielding

$$
\begin{aligned}
\frac{1}{3!}\langle\Phi_0|\{\hat{a}_p\}\hat{H}\hat{T}_1^3|\Phi_0\rangle &= \frac{1}{2!}\sum_{q,r} h_{qr}\tau^q\tau^r\tau^p \\
&\quad + \frac{1}{3!}\sum_{q,r,s} h^p_{qrs}\tau^q\tau^r\tau^s, \qquad (2.34)\\
\frac{1}{4!}\langle\Phi_0|\{\hat{a}_p\}\hat{H}\hat{T}_1^4|\Phi_0\rangle &= \frac{1}{3!}\sum_{q,r,s} h_{qrs}\tau^q\tau^r\tau^s\tau^p, \qquad (2.35)\\
\frac{1}{5!}\langle\Phi_0|\{\hat{a}_p\}\hat{H}\hat{T}_1^5|\Phi_0\rangle &= \frac{1}{4!}\sum_{q,r,s,t} h_{qrst}\tau^q\tau^r\tau^s\tau^t\tau^p. \qquad (2.36)
\end{aligned}
$$

The higher-order terms in the exponential operator cannot produce a full contraction and are zero.

Combining these, we find the XVCCS amplitude equation to read

$$
\begin{aligned}
E_0^{(1)}\tau^p &= E_0^{(0)}\tau^p + \sum_q h_q\tau^q\tau^p + \frac{1}{2!}\sum_{q,r} h_{qr}\tau^q\tau^r\tau^p \\
&\quad + \frac{1}{3!}\sum_{q,r,s} h_{qrs}\tau^q\tau^r\tau^s\tau^p + \frac{1}{4!}\sum_{q,r,s,t} h_{qrst}\tau^q\tau^r\tau^s\tau^t\tau^p \\
&\quad + h^p + \sum_q h^p_q\tau^q + \frac{1}{2!}\sum_{q,r} h^p_{qr}\tau^q\tau^r \\
&\quad + \frac{1}{3!}\sum_{q,r,s} h^p_{qrs}\tau^q\tau^r\tau^s .
\end{aligned}
\tag{2.37}
$$

Note that the first five terms in the right-hand side are disconnected in the sense that there is a factor (τ^p) that has no common summation index with any other factor; each of them is, therefore, a simple product of two factors.

Factoring these disconnected terms, we can rewrite the above equation as

$$\begin{aligned} E_0^{(1)}\tau^p &= \left(E_0^{(0)} + \sum_q h_q\tau^q + \frac{1}{2!}\sum_{q,r} h_{qr}\tau^q\tau^r \right. \\ &\quad \left. + \frac{1}{3!}\sum_{q,r,s} h_{qrs}\tau^q\tau^r\tau^s + \frac{1}{4!}\sum_{q,r,s,t} h_{qrst}\tau^q\tau^r\tau^s\tau^t\right)\tau^p \\ &\quad + h_p + \sum_q h_q^p\tau^q + \frac{1}{2!}\sum_{q,r} h_{qr}^p\tau^q\tau^r \\ &\quad + \frac{1}{3!}\sum_{q,r,s} h_{qrs}^p\tau^q\tau^r\tau^s \qquad (2.38) \\ &= E_0^{(1)}\tau^p + h_p + \sum_q h_q^p\tau^q + \frac{1}{2!}\sum_{q,r} h_{qr}^p\tau^q\tau^r \\ &\quad + \frac{1}{3!}\sum_{q,r,s} h_{qrs}^p\tau^q\tau^r\tau^s, \qquad (2.39) \end{aligned}$$

where we use the fact that the sum in the parenthesis is equal to $E_0^{(1)}$ as per Eq. (2.29). We can, therefore, further simplify the amplitude equation into

$$\begin{aligned} T_1^{(1)} &\equiv h^p + \sum_q h_q^p\tau^q + \frac{1}{2!}\sum_{q,r} h_{qr}^p\tau^q\tau^r \\ &\quad + \frac{1}{3!}\sum_{q,r,s} h_{qrs}^p\tau^q\tau^r\tau^s = 0. \qquad (2.40) \end{aligned}$$

Notice that this amplitude equation consists of connected terms only.

In fact, we can recast the amplitude equations of XVCCm in general into a form that is equivalent to, but more convenient than Eq. (2.9):

$$\langle\Phi_{p_1p_2\cdots p_n}|\left(\hat{H}_{\mathrm{N}}e^{\hat{T}}\right)_{\mathrm{C}}|\Phi_0\rangle = 0, \qquad (2.41)$$

for all $p_1, p_2, \ldots, p_n$ and all n ($1 \le n \le m$). We call this the T_n amplitude equation of XVCCm. The diagrammatic derivations of XVCC and the EOM-XVCC formulations to be discussed below are based on Eqs. (2.30) and (2.41).

We now outline a general, systematic derivation of the connected form of the XVCCm equations. The vibrational Schrödinger equation for a general XVCC wave function can be written as

$$\hat{H}_{\mathrm{N}}e^{\hat{T}}|\Phi_0\rangle = \Delta E_0^{(m)}e^{\hat{T}}|\Phi_0\rangle. \qquad (2.42)$$

Multiplying Eq. (2.42) by $e^{\hat{T}}$ from the left yields

$$e^{-\hat{T}}\hat{H}_{\mathrm{N}}e^{\hat{T}}|\Phi_0\rangle = \Delta E_0^{(m)}|\Phi_0\rangle. \tag{2.43}$$

The similarity transformed Hamiltonian can be rewritten using the Baker-Campbell-Hausdorff expansion as

$$e^{-\hat{T}}\hat{H}_{\mathrm{N}}e^{\hat{T}} = \hat{H}_{\mathrm{N}} + [\hat{H}_{\mathrm{N}}, \hat{T}] + \frac{1}{2}\left[\left[\hat{H}_{\mathrm{N}}, \hat{T}\right], \hat{T}\right] + \cdots . \tag{2.44}$$

Unlike in electronic CC, this expansion is formally infinite for vibrations and is only truncated after truncating the Hamiltonian. Evaluation of the commutators in Eq. (2.44) eliminates all disconnected terms. Furthermore, the only nonzero connected terms are those in which $\hat{H}_{\mathrm{N}}$ is the leading operator, thus we obtain the final connected form of the Hamiltonian

$$e^{-\hat{T}}\hat{H}_{\mathrm{N}}e^{\hat{T}} = \left(\hat{H}_{\mathrm{N}}e^{\hat{T}}\right)_{\mathrm{C}}. \tag{2.45}$$

Substituing the connected form of the Hamiltonian into Eq. (2.43) and projecting onto the space spanned by $\hat{T}$ yields the connected forms of the energy and amplitude equations given in Eqs. (2.30) and (2.41) respectively.

2.2.3 Diagrammatic derivation of XVCC

The equations of XVCC can be derived even more expediently with Feynman–Goldstone diagrams, which is equivalent to the normal-ordered second-quantized derivation; a diagram corresponds to all topologically related Wick's contractions. Here, we introduce the rules of drawing closed diagrams for XVCC energy equations and open diagrams for XVCC amplitude equations as well as the rules of translating them into algebraic expressions. These rules differ from those for XVMP energies and self-energies. [119] We illustrate their application to XVCCm with $m = 1$ (XVCCS) and $m = 2$ (XVCCSD) in this subsection.

We recast each term in the normal-ordered Hamiltonian, $\hat{H}$, into diagrammatic forms, as shown in Fig. 2.1. There is a term-by-term correspondence with the Hamiltonian defined by Eq. (2.11). The cluster excitation operators, $\{\hat{T}_n\}$, are expressed diagrammatically in Fig. 2.2.

Table 2.1 lists the rules to generate diagrams of the XVCCm energy and amplitude equations in an nth-order Taylor-series PES. Applying these rules, we find the energy diagrams of XVCCS in a QFF ($n = 4$) to be those in Fig.

2.3. The energy diagrams of XVCCSD in a QFF are the union of Figs. 2.3 and 2.4. Hence,

$$\Delta E_0^{(1)} = \sum_{i=1}^{4} E_i, \tag{2.46}$$

$$\Delta E_0^{(2)} = \sum_{i=1}^{8} E_i, \tag{2.47}$$

where the summands are the algebraic interpretation of the diagrams. Since each $\hat{T}_k$ vertex in an energy diagram has only upgoing lines (signifying the fact that they describe an excitation process), all of its lines have no choice but to connect with the $\hat{H}_\mathrm{N}$ vertex, making the whole diagram always connected when closed, guaranteeing its thermodynamic extensivity as per the extensive diagram theorem. [23, 24, 120]

Table 2.2 provides a set of rules to translate these diagrams into algebraic expressions. For example, diagram E_4 of Fig. 2.3 can be labeled as shown in Fig. 2.5 using rules 1 through 5 of the table. Following the remaining rules, we find the algebraic expression of the whole diagram to be

$$E_4 \equiv \frac{1}{4!} \sum_{p,q,r,s} h_{pqrs} \tau^p \tau^q \tau^r \tau^s, \tag{2.48}$$

where the $1/4!$ factor comes from rule 8 because there are four equivalent $\hat{T}_1$ vertices. It is straightforward to confirm that the algebraic interpretations of E_1, E_2, and E_3 obtained with Table 2.2 agree exactly with the second, third, and fourth term of the XVCCS energy expression [Eq. (2.29)], respectively.

Likewise, the application of the rules in Table 2.2 to the diagrams in Fig. 2.4 leads to the XVCCSD energy equation:

$$\Delta E_0^{(2)} = \Delta E_0^{(1)} + E_5 + E_6 + E_7 + E_8 \tag{2.49}$$

$$\begin{aligned} = \Delta E_0^{(1)} &+ \frac{1}{2!} \sum_{p,q} h_{pq} \tau^{pq} + \frac{1}{2!} \sum_{p,q,r} h_{pqr} \tau^p \tau^{qr} \\ &+ \frac{1}{2!}\frac{1}{2!}\frac{1}{2!} \sum_{p,q,r,s} h_{pqrs} \tau^{pq} \tau^{rs} \\ &+ \frac{1}{2!}\frac{1}{2!} \sum_{p,q,r,s} h_{pqrs} \tau^p \tau^q \tau^{rs}. \end{aligned} \tag{2.50}$$

The factor of $(1/2!)^3$ in the penultimate term (diagram E_7) arises from the fact that there are one pair of equivalent $\hat{T}_2$ vertices and two pairs of equivalent lines.

Table 2.1 also outlines rules to enumerate all diagrams in the XVCC*m* amplitude equations. Unlike energy diagrams, a diagram in the T_l amplitude equation is open with l external lines. Such diagrams can be disconnected, in which case they must be deleted as per rule 3.

Figure 2.6 lists all four connected diagrams of the XVCCS T_1 amplitude equation in a QFF, which can thus be written as

$$0 = \sum_{i=1}^{4} S_i \equiv T_1^{(1)}, \tag{2.51}$$

where S_i is the algebraic interpretation of the corresponding diagram. The T_1 amplitude equation of XVCCSD in a QFF is diagrammatically expressed by Figs. 2.6 and 2.7. The T_2 amplitude equation of the same method is defined with the diagrams in Fig. 2.8. The T_1 and T_2 amplitude equations of XVCCSD are thus formally written as

$$0 = \sum_{i=1}^{12} S_i \equiv T_1^{(2)}, \tag{2.52}$$

$$0 = \sum_{i=1}^{12} D_i \equiv T_2^{(2)}. \tag{2.53}$$

The interpretation rules in Table 2.2 apply to open diagrams in these amplitude equations also. For example, lines and vertices in diagram S_4 can be labeled as shown in Fig. 2.9. Its algebraic expression then reads

$$S_4 = \frac{1}{3!} \sum_{q,r,s} h^p_{qrs} \tau^q \tau^r \tau^s. \tag{2.54}$$

Applying the same rules to diagrams S_1, S_2, and S_3 and substituting the results in Eq. (2.51) reproduces the T_1 amplitude equation [Eq. (2.40)] derived algebraically.

The T_1 amplitude equation of XVCCSD in a QFF is likewise obtained directly from Figs. 2.6 and 2.7:

$$0 = T_1^{(2)} \tag{2.55}$$

$$\begin{aligned} = {} & T_1^{(1)} + \sum_q h_q \tau^{qp} + \frac{1}{2!} \sum_{q,r} h^p_{qr} \tau^{qr} + \sum_{q,r} h_{qr} \tau^q \tau^{rp} \\ & + \frac{1}{2!} \sum_{q,r,s} h^p_{qrs} \tau^q \tau^{rs} + \frac{1}{2!} \sum_{q,r,s} h_{qrs} \tau^{qr} \tau^{sp} \\ & + \frac{1}{2!} \sum_{q,r,s} h_{qrs} \tau^q \tau^r \tau^{sp} + \frac{1}{2!} \sum_{q,r,s,t} h_{qrst} \tau^q \tau^{rs} \tau^{tp} \\ & + \frac{1}{3!} \sum_{q,r,s,t} h_{qrst} \tau^q \tau^r \tau^s \tau^{tp}, \end{aligned} \tag{2.56}$$

where $T_1^{(1)}$ is given algebraically in Eq. (2.40).

Similarly, the T_2 amplitude equation of the same method can directly result from Fig. 2.8 and reads

$$
\begin{aligned}
0 &= T_2^{(2)} \qquad (2.57)\\
&= \frac{1}{2!}\hat{P}(pq)h^{pq} + \frac{1}{2!}\hat{P}(pq)\sum_r h_r^{pq}\tau^r + \hat{P}(pq)\sum_r h_r^p\tau^{rq}\\
&\quad + \frac{1}{2!}\frac{1}{2!}\hat{P}(pq)\sum_{r,s} h_{rs}^{pq}\tau^{rs} + \frac{1}{2!}\frac{1}{2!}\hat{P}(pq)\sum_{r,s} h_{rs}^{pq}\tau^r\tau^s\\
&\quad + \hat{P}(pq)\sum_{r,s} h_{rs}^p\tau^r\tau^{sq} + \frac{1}{2!}\hat{P}(pq)\sum_{r,s} h_{rs}\tau^{rp}\tau^{sq}\\
&\quad + \frac{1}{2!}\hat{P}(pq)\sum_{r,s,t} h_{rst}^p\tau^{rs}\tau^{tq} + \frac{1}{2!}\hat{P}(pq)\sum_{r,s,t} h_{rst}^p\tau^r\tau^s\tau^{tq}\\
&\quad + \frac{1}{2!}\hat{P}(pq)\sum_{r,s,t} h_{rst}\tau^r\tau^{sp}\tau^{tq}\\
&\quad + \frac{1}{2!}\frac{1}{2!}\hat{P}(pq)\sum_{r,s,t,u} h_{rstu}\tau^{rs}\tau^{tp}\tau^{uq}\\
&\quad + \frac{1}{2!}\frac{1}{2!}\hat{P}(pq)\sum_{r,s,t,u} h_{rstu}\tau^r\tau^s\tau^{tp}\tau^{uq}, \qquad (2.58)
\end{aligned}
$$

where $\hat{P}(p_1\cdots p_n)$ yields the sum of $n!$ permutations of indices $\{p_1,\ldots,p_n\}$ in the term it acts on (cf., rule 7 of Table 2.2). For instance,

$$\hat{P}(pq)\sum_r h_r^p\tau^{rq} = \sum_r h_r^p\tau^{rq} + \sum_r h_r^q\tau^{rp}. \qquad (2.59)$$

In the same way, the diagrammatic energy and amplitude equations of XVCCm for $m \leq 8$ in a QFF are derived and documented in Appendix A. They were generated with the aid of computer algebra based on the rules provided in Tables 2.1. The algebraic equations can be easily generated by application of the rules provided in Table 2.2.

2.2.4 EOM-XVCC formalism

In a vibrational analysis, it is usually the frequencies (excitation energies) that are of greater interest than the zero-point energies (total energies in the ground state). Here, we stipulate and implement an excited-state XVCC theory using the EOM formalism, [73–77, 81] which is equivalent to CC linear response [78–80, 90–92] for excitation energies.

The EOM-XVCCm theory can be viewed as a CI for excited states using the XVCC effective Hamiltonian $\bar{H}_\mathrm{N}$ defined as

$$\bar{H}_\mathrm{N} = \left(\hat{H}_\mathrm{N}e^{\hat{T}}\right)_\mathrm{C}, \qquad (2.60)$$

where $\hat{T}$ is truncated after the m-fold cluster excitation operator [Eq. (2.3)] and all of its amplitudes should have been

determined by a preceding XVCCm calculation.

Let $\hat{R}$ be a linear excitation operator truncated after the same rank,

$$\hat{R} = r_0 + \hat{R}_1 + \hat{R}_2 + \cdots + \hat{R}_m, \tag{2.61}$$

with

$$\hat{R}_n = \frac{1}{n!} \sum_{p_1,p_2,\cdots p_n} r^{p_1 p_2 \cdots p_n} \hat{a}^\dagger_{p_1} \hat{a}^\dagger_{p_2} \cdots \hat{a}^\dagger_{p_n} \tag{2.62}$$

$$= \frac{1}{n!} \sum_{p_1,p_2,\cdots p_n} r^{p_1 p_2 \cdots p_n} \{\hat{a}^\dagger_{p_1} \hat{a}^\dagger_{p_2} \cdots \hat{a}^\dagger_{p_n}\}, \tag{2.63}$$

where $r^{p_1 p_2 \cdots p_n}$ is an excitation amplitude. We require that the excited-state wave function $\hat{R}|\Phi_0\rangle$ satisfy the Schrödinger equation with the modified Hamiltonian $\bar{H}_\mathrm{N}$ in the space of Hartree products reachable by $\hat{R}$ from $|\Phi_0\rangle$. That is,

$$\langle\Phi_0|\bar{H}_\mathrm{N}\hat{R}|\Phi_0\rangle = \langle\Phi_0|\Delta E^{(m)}_\ell \hat{R}|\Phi_0\rangle, \tag{2.64}$$

$$\langle\Phi_{p_1 p_2 \cdots p_n}|\bar{H}_\mathrm{N}\hat{R}|\Phi_0\rangle = \langle\Phi_{p_1 p_2 \cdots p_n}|\Delta E^{(m)}_\ell \hat{R}|\Phi_0\rangle, \tag{2.65}$$

for all $p_1, \ldots, p_n$ and all n ($1 \le n \le m$), where $\Delta E^{(m)}_\ell = E^{(m)}_\ell - E^{(0)}_0$ and $E^{(m)}_\ell$ is the total EOM-XVCCm energy of the ℓth excited state. The constant term r_0 is formally necessary in Eq. (2.61) for excited states of the same symmetry as the ground state. Although $\hat{R}$ and its amplitudes vary with ℓ and should thus carry a ℓ identifier, it is suppressed for brevity.

Equations (2.64) and (2.65) define EOM-XVCCm as an eigenvalue problem with a non-Hermitian matrix of $\bar{H}_\mathrm{N}$, which thus has both left and right eigenvectors with $\hat{R}$ corresponding to the latter. They can, however, be further simplified by using the fact that T amplitudes in $\bar{H}_\mathrm{N}$ satisfy the XVCCm equations. Equation (2.30) and (2.41) indicate that $|\Phi_0\rangle$ satisfies the Schrödinger equation with $\bar{H}_\mathrm{N}$ in the same Hartree-product space. This implies

$$\langle\Phi_0|\hat{R}\bar{H}_\mathrm{N}|\Phi_0\rangle = \langle\Phi_0|\hat{R}\Delta E^{(m)}_0|\Phi_0\rangle, \tag{2.66}$$

$$\langle\Phi_{p_1 p_2 \cdots p_n}|\hat{R}\bar{H}_\mathrm{N}|\Phi_0\rangle = \langle\Phi_{p_1 p_2 \cdots p_n}|\hat{R}\Delta E^{(m)}_0|\Phi_0\rangle, \tag{2.67}$$

because $\hat{R}^\dagger|\Phi_0\rangle \cup \{\hat{R}^\dagger|\Phi_{p_1 p_2 \cdots p_n}\rangle\}$ spans the same space as $|\Phi_0\rangle \cup \{|\Phi_{p_1 p_2 \cdots p_n}\rangle\}$. Subtracting these from Eqs. (2.64) and (2.65), we obtain

$$\langle\Phi_0|[\bar{H}_\mathrm{N}, \hat{R}]|\Phi_0\rangle = \bar{\omega}^{(m)}_\ell r_0, \tag{2.68}$$

$$\langle\Phi_{p_1 p_2 \cdots p_n}|[\bar{H}_\mathrm{N}, \hat{R}]|\Phi_0\rangle = \bar{\omega}^{(m)}_\ell r^{p_1 p_2 \cdots p_n}, \tag{2.69}$$

where $\bar{\omega}_\ell^{(m)} = \Delta E_\ell^{(m)} - \Delta E_0^{(m)}$ and is the EOM-XVCCm transition energy (frequency) to the ℓth excited state.

Equation (2.69) is the ansatz for EOM-XVCCm for frequencies, which can also be written as

$$\langle \Phi_{p_1 p_2 \cdots p_n} | \left(\left(\hat{H}_\mathrm{N} e^{\hat{T}} \right)_\mathrm{C} \hat{R} \right)_\mathrm{C} | \Phi_0 \rangle \quad = \quad \bar{\omega}_\ell^{(m)} r^{p_1 p_2 \cdots p_n}, \tag{2.70}$$

for all $p_1, \ldots, p_n$ and all n ($1 \leq n \leq m$). We call this the R_n amplitude equation of EOM-XVCCm. The nested connectedness requirement is always met when the term is simply connected because both $\hat{T}$ and $\hat{R}$ are excitation operators and can only directly connect with $\hat{H}_\mathrm{N}$, but not with each other.

Equation (2.70), therefore, refers to a set of equations whose number is equal to the number of unknowns (excluding r_0) minus one (because $\bar{\omega}_\ell^{(m)}$ is also unknown) and, with an appropriate normalization condition, can determine $\bar{\omega}_\ell^{(m)}$ and all the amplitudes in $\hat{R}$ except r_0. The value of r_0, in turn, can be determined by Eq. (2.68), though it is not necessary if only frequencies are sought. Equation (2.70) satisfies the intensive diagram theorem, [23, 24] ensuring the size consistency of EOM-XVCCm for total excited-state energies and frequencies, despite its CI-like structure.

Just like the electronic counterpart, EOM-XVCCm can also be derived by applying the first-order time-dependent perturbation (linear-response) theory to XVCCm. This derivation (not repeated here because it is identical to the electronic case [92]) elegantly explains why the truncation ranks of $\hat{T}$ and $\hat{R}$ should be the same. EOM-XVCCm with the XVSCF[n] reference is the same as excited-state VCC of Prasad and coworkers. [40, 45]

2.2.5 Algebraic derivation of EOM-XVCC

Here, we illustrate the normal-ordered second-quantized derivation of the amplitude equations of EOM-XVCCm using $m = 1$ (EOM-XVCCS) in a QFF as an example.

The left-hand side of Eq. (2.70) in the case of $m = 1$ reads

$$\begin{aligned}
&\langle \Phi_0 | \{\hat{a}_p\} \left(\left(\hat{H}_\mathrm{N} e^{\hat{T}_1} \right)_\mathrm{C} \hat{R}_1 \right)_C | \Phi_0 \rangle \\
&= \langle \Phi_0 | \{\hat{a}_p\} \left(\hat{H}_\mathrm{N} \hat{R}_1 \right)_\mathrm{C} | \Phi_0 \rangle + \langle \Phi_0 | \{\hat{a}_p\} \left(\hat{H}_\mathrm{N} \hat{T}_1 \hat{R}_1 \right)_\mathrm{C} | \Phi_0 \rangle \\
&\quad + \frac{1}{2!} \langle \Phi_0 | \{\hat{a}_p\} \left(\hat{H}_\mathrm{N} \hat{T}_1^2 \hat{R}_1 \right)_\mathrm{C} | \Phi_0 \rangle,
\end{aligned} \tag{2.71}$$

where we use the facts that the nested connectedness means simple connectedness in this case and that the terms containing higher powers of $\hat{T}_1$ cannot yield any connected contributions.

The first term of Eq. (2.71) has only one full contraction:

$$\begin{aligned}\langle\Phi_0|\{\hat{a}_p\}\left(\hat{H}_\mathrm{N}\hat{R}_1\right)_\mathrm{C}|\Phi_0\rangle &= \sum_{q,r,s} h^q_r r^s \langle\Phi_0|\{\hat{a}_p\}\{\hat{a}^\dagger_q\hat{a}_r\}\{\hat{a}^\dagger_s\}|\Phi_0\rangle \\ &= \sum_q h^p_q r^q, \end{aligned} \tag{2.72}$$

which is connected. The next term has two:

$$\begin{aligned}&\langle\Phi_0|\{\hat{a}_p\}\left(\hat{H}_\mathrm{N}\hat{T}_1\hat{R}_1\right)_\mathrm{C}|\Phi_0\rangle \\ &= \frac{1}{2!}\sum_{q,r,s,t,u} h^q_{rs}\tau^t r^u \langle\Phi_0|\{\hat{a}_p\}\{\hat{a}^\dagger_q\hat{a}_r\hat{a}_s\}\{\hat{a}^\dagger_t\}\{\hat{a}^\dagger_u\}|\Phi_0\rangle \\ &+ \frac{1}{2!}\sum_{q,r,s,t,u} h^q_{rs}\tau^t r^u \langle\Phi_0|\{\hat{a}_p\}\{\hat{a}^\dagger_q\hat{a}_r\hat{a}_s\}\{\hat{a}^\dagger_t\}\{\hat{a}^\dagger_u\}|\Phi_0\rangle \\ &= \sum_{q,r} h^p_{qr}\tau^q r^r, \end{aligned} \tag{2.73}$$

which are also connected. The last term also yields connected full contractions only, leading to

$$\frac{1}{2!}\langle\Phi_0|\{\hat{a}_p\}\left(\hat{H}_\mathrm{N}\hat{T}_1^2\hat{R}_1\right)_\mathrm{C}|\Phi_0\rangle = \frac{1}{2!}\sum_{q,r,s} h^p_{qrs}\tau^q\tau^r r^s. \tag{2.74}$$

Together, we obtain the R_1 amplitude equation of EOM-XVCCS in a QFF as

$$\begin{aligned} R^{(1)}_1 &\equiv \sum_q h^p_q r^q + \sum_{q,r} h^p_{qr}\tau^q r^r + \sum_{q,r,s}\frac{1}{2!}h^p_{qrs}\tau^q\tau^r r^s \\ &= \bar{\omega}^{(1)}_\ell r^p. \end{aligned} \tag{2.75}$$

2.2.6 Diagrammatic derivation of EOM-XVCC

The diagrammatic forms of the $\hat{R}_n$ operators are given in Fig. 2.10. They are isomorphic to the diagrams of the $\hat{T}_n$ operators with the only difference being the colors of the vertices. The rules to generate all diagrams entering the amplitude equations of EOM-XVCCm are given in Table 2.3. The rules for interpreting these diagrams algebraically are provided in Table 2.2.

As an illustration, we derive the R_1 amplitude equation of EOM-XVCCS in a QFF diagrammatically. Diagrams in this equation are drawn in Fig. 2.11. The R_1 amplitude equation can thus be formally written as

$$R^{(1)}_1 \equiv S'_1 + S'_2 + S'_3 = \bar{\omega}^{(1)}_\ell r^p. \tag{2.76}$$

Diagram S'_3 may be labeled as shown in Fig. 2.12 according to the rules in Table 2.2. The corresponding algebraic translation is,

$$S'_3 \equiv \frac{1}{2!} \sum_{q,r,s} h^p_{qrs} \tau^q \tau^r r^s, \tag{2.77}$$

where the $1/2!$ factor is due to a pair of equivalent $\hat{T}_1$ vertices. The other two diagrams can be interpreted similarly, yielding the same R_1 amplitude equation as Eq. (2.75).

The diagrammatic equations of EOM-XVCCm for $m \leq 8$ were generated with the aid of computer algebra based on the rules provided in Tables 2.3 and are documented in Appendix B. For brevity, the EOM-XVCCm equations were drawn using the vertices of the transformed Hamiltonian $\bar{H}$ which are defined in Appendix C. The algebraic expressions are generated by application of the rules in Table 2.2.

2.3 Automated computer implementation

The XVCCm and EOM-XVCCm methods with $m = 1$ through 8 in a QFF were implemented. The Hamiltonian employed was the pure vibrational one, neglecting any coupling between vibrations and rotations. The XVSCF(4), XVSCF[4], or the harmonic reference wave function was used ('4' standing for the QFF). The choice of the reference wave function is indicated by a suffix as in XVCCm(4), XVCCm[4], or XVCCm{4}, respectively; "{n}" suffix indicates the use of a harmonic reference with the nth-order PES.

The T_n amplitude equations of XVCCm were solved with a standard Newton–Krylov algorithm, [121] implemented in IGMRES, available from SCIPY. The initial values of τ were zero. The R_n amplitude equations of EOM-XVCCm with $m \geq 2$ were solved with the iterative Arnoldi method, a non-Hermitian generalization of the Lanczos method, [122–124] available in ARPACK. [125] The eigenvalue convergence criterion was set to machine precision. The Arnoldi method does not require the matrix elements of $\bar{H}_\mathrm{N}$ stored in memory; instead, it evaluates the left-hand sides of the R_n amplitude equations [Eq. (2.70)] directly for several trial r vectors. This allows a small subset of low-lying excited-state roots to be determined in a memory-efficient manner. On the other hand, the EOM-XVCCS problem was solved by diagonalization of the $\bar{H}_\mathrm{N}$ matrix, solving Eqs. (2.64) and (2.65) for all excited-state energies instead.

The XVCCm and EOM-XVCCm diagrammatic equations were derived by a symbolic algebra program using the rules presented in Tables 2.1 and 2.3. These diagrammatic equations were then translated also by the same symbolic algebra program into the algebraic form according to the interpretation rules given in Table 2.2. Terms that originate from a single diagram and are thus related by a permutation operator were identified and consolidated. When the resulting expressions are evaluated literally, the operation costs of XVCCm and EOM-XVCCm in an nth-order Taylor-series PES can scale as steeply as $O(N^{n+m})$, where N is the number of modes. To reduce the cost, three types algorithm

optimizations were performed computationally before the automatic synthesis of c++ codes was carried out. [126,127] The optimizations considered in this work were the strength reduction of the matrix chain products, intermediate reuse, and factorization. [126] The details of each optimization procedure are given below.

2.3.1 Strength reduction

The algebraic equations of XVCC and EOM-XVCC are sums of products of matrices (i.e., force constants h, τ amplitudes, and r amplitudes). The operation cost of evaluating a product of more than two matrices is greatly reduced by carrying out a series of binary matrix multiplications. Suppose a matrix chain product $E = ABCD$, where A through E are matrices of some dimension (including possibly scalars). This product can be evaluated stepwise as

$$I_1 = CD, I_2 = BI_1, E = AI_2, \tag{2.78}$$

where I_1 and I_2 are the so-called *intermediate* matrices. Alternatively, the same product may be evaluated as

$$I_3 = AB, I_4 = CI_3, E = DI_4. \tag{2.79}$$

Both orders of multiplication give the same final result (E) but at generally different operation and memory costs. Strength reduction determines the *sequential* multiplication order with the minimal operation cost for each product by blanket search; it neglects *parallel* multiplication such as $(AB)(CD)$.

The result of this procedure is depicted in Fig. 2.13 for one diagram of the T_3 amplitude equation of XVCCm [see Eq. (A.4)]. It is algebraically defined as

$$\left(T_{17}\right)_{pqr} = \frac{1}{2!}\frac{1}{2!}\hat{P}(pqr)\sum_{s,t,u,v} W_{stuv}\tau^{v}\tau^{tup}\tau^{sqr}. \tag{2.80}$$

A literal evaluation of this equation involves an $O(N^7)$ arithmetic operations, as it must perform N^4 multiplications and additions to evaluate each of N^3 elements of T_{17}, where N is the number of modes. However, the same result can be obtained at an $O(N^4)$ cost by breaking the quaternary matrix multiplication into three separate binary matrix multiplications carried out in the following order. First, the force constant matrix is multiplied with τ^v, which has no external index.

$$\left(T_{17\mathrm{a}}\right)_{stu} = \sum_{v} h_{stuv}\tau^{v}. \tag{2.81}$$

This step involves N^4 multiplications and additions and defines an intermediate, $T_{17\mathrm{a}}$, of dimension N^3. This interme-

diate is then multiplied by τ^{tup} at an $O(N^4)$ cost to define another intermediate, T_{17b}, of dimension N^2.

$$\left(T_{17b}\right)_{ps} = \sum_{tu} \tau^{tup} \left(T_{17a}\right)_{stu}. \tag{2.82}$$

Finally, T_{17} is obtained by multiplication of intermediate T_{17b} by τ^{sqr} at an $O(N^4)$ cost:

$$\left(T_{17}\right)_{pqr} = \frac{1}{2!}\frac{1}{2!}\hat{P}(pqr) \sum_{s} \tau^{sqr} \left(T_{17b}\right)_{ps}. \tag{2.83}$$

Therefore, the cost of evaluating diagram T_{17} was reduced from $O(N^7)$ to $O(N^4)$.

2.3.2 Intermediate reuse

This optimization simply stores an intermediate appearing two or more times in the whole equation and reuses it without recalculating. Consider the following sum-of-product expression of matrices: $E = A(BC) + D(BC)$. If the strength reduction procedure suggests the optimal multiplication orders specified by the parentheses, intermediate $I_1 = BC$ is calculated only once and stored for reuse. Hence, the whole sum is evaluated as

$$I_1 = BC, E = AI_1 + DI_1. \tag{2.84}$$

The number of multiplications and additions as a function of N required to evaluate all the amplitude equations of XVCCm and EOM-XVCCm with no optimization and with strength reduction and intermediate reuse are compared in Table 2.4. For all methods with $m \geq 2$, strength reduction leads to a great reduction in the operation cost from $O(N^{m+4})$ to $O(N^{m+2})$. Generally, for an nth order PES, the optimal scaling of XVCCm and EOM-XVCCm is $O(N^{m+\lfloor n/2 \rfloor})$ when $m \geq n$ and is no greater than $O(N^{n+\lfloor (m-1)/2 \rfloor})$ when $m < n$. A proof of this statement is given in Appendix D.

2.3.3 Factorization

The operation cost of XVCC and EOM-XVCC can be further reduced by factorization. Let us consider the sum-of-product matrix equation, $E = A(BC) + A(BD)$, where the parentheses indicate the optimal order of multiplication for each product. This sum can be evaluated as

$$I_1 = C + D, I_2 = BI_1, E = AI_2. \tag{2.85}$$

Two multiplications by the common matrix factor B in $I_2 = BC + BD$ are consolidated into one by factorization, $I_2 = B(C + D)$, reducing the multiplication cost by half. Also, two multiplications by A are also merged into one,

further halving the multiplication cost. This procedure should not be confused with intermediate reuse.

Factorability of equations depends on the multiplication order of each product, making strength reduction and factorization a coupled optimization problem. Since a complete solution of this coupled problem is exponentially complex, we approach it as two separate, sequential optimizations. Strength reduction is performed first for each product, whereupon factorization is carried out by blanket search without altering the order of multiplication. Hence, a sum of intermediates multiplied by the same final matrix and the same permutation operator is factored; in this work, the permutation operator itself is not decomposed into a product of smaller permutation operators, which increases factorability. [126] The resulting new intermediates are sums of matrices and they are recursively factored. An example of the procedure is given below and drawn in Fig. 2.14:

$$D_6 = \hat{P}(pq) \sum_{rs} \tau^{rp} \left(\tau^s h^q_{rs} \right), \tag{2.86}$$

$$D_8 = \frac{1}{2!} \hat{P}(pq) \sum_{rst} \tau^{rp} \left(\tau^{st} h^q_{rst} \right), \tag{2.87}$$

$$D_9 = \frac{1}{2!} \hat{P}(pq) \sum_{rst} \tau^{rp} \left(\tau^s \left(\tau^t h^q_{rst} \right) \right), \tag{2.88}$$

$$D_{17} = \frac{1}{2!} \hat{P}(pq) \sum_{rst} \tau^{rp} \left(\tau^{stq} h_{rst} \right), \tag{2.89}$$

$$D_{23} = \frac{1}{2!} \hat{P}(pq) \sum_{rstu} \tau^{rp} \left(\tau^{stq} \left(\tau^u h_{rstu} \right) \right), \tag{2.90}$$

where the parentheses specify the optimal order of multiplication for each product determined by the preceding strength reduction step. Factorization does not alter these orders. When evaluating the sum of these five terms, the common factor τ^{rp} is pulled out:

$$\left(D_{\text{sum}} \right)_{pq} = \hat{P}(pq) \sum_{r} \tau^{rp} \left(D_{6+8+9+17+23} \right)_{qr}, \tag{2.91}$$

where the intermediate $D_{6+8+9+17+23}$ is the sum of three intermediates:

$$\left(D_{6+8+9+17+23} \right)_{qr} = \left(D_{6+8} \right)_{qr} + \left(D_9 \right)_{qr} + \left(D_{17+23} \right)_{qr}. \tag{2.92}$$

with the subscripts indicating the diagrammatic origin of the intermediates. The first intermediate does not lend itself to any further factorization and is given by

$$\left(D_{6+8} \right)_{qr} = \sum_{s} h^q_{rs} \tau^s + \frac{1}{2!} \sum_{st} h^q_{rst} \tau^{st}. \tag{2.93}$$

Nor does the second intermediate, which is defined as

$$\left(D_9\right)_{qr} = \sum_s \tau^s \left(D_9\right)_{qrs}, \tag{2.94}$$

$$\left(D_9\right)_{qrs} = \frac{1}{2!} \sum_t h^q_{rst} \tau^t. \tag{2.95}$$

The third intermediate is further factored by the common matrix τ^{stq} and is given by

$$\left(D_{17+23}\right)_{qr} = \sum_{st} \tau^{stq} \left(D_{17+23}\right)_{rst}, \tag{2.96}$$

$$\left(D_{17+23}\right)_{rst} = \frac{1}{2!} h_{rst} + \frac{1}{2!} \sum_u h_{rstu} \tau^u. \tag{2.97}$$

The operation costs of XVCCm and EOM-XVCCm after factorization (in addition to strength reduction and intermediate reuse) are listed in Table 2.4. It should be understood that intermediate reuse (combined with factorization) applies to common intermediates appearing two or more times that are either a product or a sum-of-product of matrices. Since factorization is more likely for the final multiplication step in our implementation, it is especially effective when the final step is the most costly. Factorization always reduces a multiplication cost, but replaces an addition cost of product matrices by that of matrix factors. Therefore, it cannot alter the overall *scaling* of the cost function, but generally reduces the prefactor multiplying the leading-order term, while it may increase or decrease prefactors of sub-leading-order terms.

Factorization is more important for EOM-XVCC and for higher values of m. In particular, for $m > 4$, factorization lowers the prefactors on the leading-order term of the cost functions. For $m = 3$ or 4, only the prefactors of the second and third leading-order terms of the cost functions are reduced. For $m = 1$ and 2, the cost is dominated by the multiplication of the force-constant matrix with a matrix of τ amplitudes, which occurs first in each product (see Appendix D); therefore, factorization is found least effective there.

The cost scaling of the final optimized algorithm including strength reduction, intermediate reuse, and factorization was computationally verified on model QFFs. The CPU time spent in one cycle of the iterative solution of XVCCm and EOM-XVCCm ($3 \leq m \leq 5$) as a function of the number of modes N is illustrated in Fig. 2.15. The timing results for each method were fit to a polynomial of the form AN^{m+2} and showed good agreement with the expected scaling.

2.4 Numerical tests

The XVCCm and EOM-XVCCm methods were applied to the vibrational zero-point energies and frequencies of the water and formaldehyde molecules. Their equilibrium structure, normal modes, and QFF's were calculated at the

MP2/aug-cc-pVDZ level using NWCHEM [128] and SINDO. [129] The results were compared with those obtained from full VCI calculations with MAVI [130] using the 20 lowest-lying harmonic-oscillator wave functions of each mode as the basis set. The VCI results were converged to within 0.1 cm^{-1} of the exact solutions for the QFF. Our results were also compared with the XVMP2(4) and XVMP2[4] results, [14] obtained either in the frequency-independent approximation to the self-energy or by solving the Dyson equation with the frequency-dependent self-energy.

2.4.1 Water

Table 2.5 compiles the errors in the XVCCm zero-point energy (E_0) and EOM-XVCCm frequencies (ν) from the VCI results for the water molecule. These errors decrease nearly monotonically with the excitation rank m, reaching the accuracy of a few cm^{-1} at $m = 3$ (CCSDT) for both E_0 and ν. At $m = 4$ (CCSDTQ), the results are generally within tenths of cm^{-1} of the VCI results with a few exceptions. The results for $m \geq 5$ are given in Table 2.6 and are converged with accuracy higher than necessary, e.g., within 0.001 cm^{-1} at $m = 8$.

Note that the VCI results in this table were obtained with 20 basis functions per mode. The number of Hartree products involved in such a calculation grows exponentially with size or as $O(b^N)$, where b is the number of basis functions and N is the number of modes. The numbers of the τ and r amplitudes in XVCCm and EOM-XVCCm, on the other hand, increase only polynomially or as $O(N^m)$. The values of b^N for VCI and N^m for XVCCSDTQ ($N = 3$, $b = 20$, and $m = 4$) are 8,000 and 81, respectively, implying a much severer limitation in VCI's applicability to larger molecules. The number of unknowns in Christiansen's VCC (Ref. 48) grows as $O(b^m)$. Therefore, it too suffers from the consequence of having a finite number of basis functions, unlike XVCCm, which is inherently an infinite-basis method.

The accuracy of E_0 from XVCCm is relatively insensitive to the choice of the reference wave function, despite much larger differences in the results of the reference methods themselves: harmonic approximation, XVSCF(4), and XVSCF[4]. This is in line with the similar observation [81] made in the electronic CC results for correlation energies, which is understood to be due to the single-excitation operator which corrects any deficiency in the reference wave function. Likewise, the XVCCS(4) and XVCCS[4] results of E_0 are close to each other, while the XVSCF(4) results differ considerably from those of XVSCF[4]. This difference is due to the anharmonic shift in the geometry, neglected in XVSCF(4) but included in XVSCF[4]. Diagrammatically, this contribution is largely represented by E_1 of Fig. 2.6 with the $\hat{T}_1$ vertex replaced by its isomorphic vertex of $\hat{H}_N$ (i.e., the open circle filled). The fact that this diagram is found among the XVCCS energy equation means that the effect of anharmonic geometry shift is included in XVCCS regardless of the reference wave function.

XVSCF[4] determines and adopts the first-order Dyson geometry [11] as the center of coordinates, where $h^p = 0$ for all p. The T_1 amplitude equation of XVCCS[4], Eq. (2.40), then has a trivial solution of $\tau^p = 0$ for all p. This

renders the XVCCS correction, $E_0^{(1)} - E_0^{(0)}$ in Eq. (2.29), zero, making the XVCCS[4] and XVSCF[4] values of E_0 identical to each other. This expected behavior is observed in Table 2.5. Furthermore, substituting $\tau^p = 0$ into the R_1 amplitude equation of EOM-XVCCS [Eq. (2.75)], we find the EOM-XVCCS[4] frequencies to be the eigenvalues of the h_q^p matrix, whose eigenvectors are known to define the first-order Dyson coordinates. [11, 13] These eigenvalues are usually, but not always, close to the XVSCF[4] frequencies, [11] the latter being the diagonal elements (h_q^p) of the same matrix. This is also observed in Table 2.5. Therefore, XVCCS can take into account the leading-order effects in E_0 and ν from anharmonic corrections both in geometry and coordinates.

It may be noted that XVMP2 performs considerably better than XVCCSD for E_0. This is in striking contrast with the electronic counterparts; CCSD has been observed to consistently outperform MP2. [15] This difference can be traced to the difference in the rank of the Hamiltonians in the two cases: the electronic Hamiltonian is a two-body operator, whereas the vibrational one is an n-body operator, where n is the rank of the Taylor-series PES ($n = 4$ in this calculation). The most important anharmonic correction to E_0 is the ninth diagram of Eq. (A.1), which involves cubic force constants and first appears at XVCCSDT. This contribution is to a great extent accounted for by the isomorphic diagram in XVMP2 labeled **2C′** in Ref. 14. This explains why only at $m \geq 3$ does XVCCm outperform XVMP2. It is generally recommended to set the value of m equal to n, if not higher, because the overall cost of the calculation is dominated by the $O(N^n)$ step of the force-constant evaluation.

The rather small change in E_0 from XVCCS to XVCCSD can also be understood as follows. The chief contribution of XVCCSD to E_0 is E_5 of Fig. 2.4 This is nearly zero in the XVSCF reference where $h_{pp} = 0$ holds. When the normal coordinates are close to the first-order Dyson coordinates, which is usually the case, $h_{pq} = h_q^p \approx 0$ is also true for $p \neq q$, making the remaining (i.e., off-diagonal) contributions to E_5 insignificant. Furthermore, the smallness of h_{pq} implies the smallness of the T_2 amplitudes. Although XVCCSD has terms which include cubic force constants, they are always multiplied by the small T_2 amplitudes and can hardly alter E_0 of XVCCS. The frequencies from EOM-XVCCSD, on the other hand, are considerably better than EOM-XVCCS and are similar to those of XVMP2. This may be ascribed to the second diagram of Eq. (B.1), included in EOM-XVCCSD, which can describe the same essential cubic corrections accounted for by self-energy diagrams **2e′** and **2f′** (Ref. 14) of XVMP2.

For the zero-point energies and frequencies that are not affected by any resonance, we observe the following general order of accuracy: Harmonic ≈ XVSCF(n) < XVCCS{n} ≈ XVCCS(n) < XVSCF[n] ≈ XVCCS[n] < XVCCSD < XVMP2 < XVCCSDT < XVCCSDTQ ≤ XVCC5 ≤ XVCC6 ≤ XVCC7 ≤ XVCC8, which differs from the order established in electronic-structure theory. [15] In a QFF ($n = 4$), XVCCSDTQ or $m = 4$ already achieves accuracy high enough for practical purposes and XVCCm with $m > n$ seem to have diminishing returns. Here, XVCC stands for both XVCC and EOM-XVCC and the effects of the reference wave functions and the frequency-independent approximation in XVMP2 are insignificant because there are no resonances.

2.4.2 Formaldehyde

The XVCCm and EOM-XVCCm results for the formaldehyde molecule are summarized in Tables 2.7 and 2.8. The calculated zero-point energy and frequencies of the fundamentals (except for ν_1 and ν_5) confirm the general observations made above for the water molecule.

The ν_5 fundamental is known to undergo Fermi resonances with combinations $\nu_3\nu_6$ and $\nu_2\nu_6$. For this mode, XVMP2[4] in the frequency-independent approximation shows a sign of divergent perturbation series, with a large error of -414 cm^{-1} (the VMP2 result is even worse). [14] XVMP2(4) in the same approximation, on the other hand, is reasonable (with an error of 33 cm^{-1}), but breaks down unexpectedly for nonresonant ν_1 with an error of -191 cm^{-1}. [14] Therefore, the behavior of XVMP2 in the frequency-independent approximation is rather unpredictable. This method also lacks roots for Fermi-resonant counterparts.

Solving the Dyson equation with the frequency-dependent XVMP2 self-energy rectifies the aforementioned problems of the frequency-independent approximation. [14] With this approach, the frequency of ν_5 is reproduced within 3 cm^{-1} of VCI and the roots corresponding to Fermi-resonant counterparts, $\nu_3\nu_6$ and $\nu_2\nu_6$, can be located within 30 cm^{-1}. The calculated results of ν_1 also regain stability with an error of less than 10 cm^{-1}. The price one pays is that a numerically cumbersome pole search needs to be performed along each mode.

Without any pole search, EOM-XVCC yields results that display stable convergence and have generally high accuracy for these strongly correlated modes. EOM-XVCCSDT seems to systematically outperform XVMP2 with the frequency-dependent self-energy for all listed modes including the Fermi resonances. EOM-XVCCSDTQ yields near-exact results with the largest error being merely 2.4 cm^{-1}. Remarkably, EOM-XVCCSD, though lacking an $\hat{R}_3$ operator to fully describe cubic anharmonicity, locates all three Fermi-resonant transitions (ν_5, $\nu_3\nu_6$, and $\nu_2\nu_6$) with uniform, medium accuracy. XVSCF and EOM-XVCCS, as expected, do not have roots corresponding to $\nu_3\nu_6$ and $\nu_2\nu_6$ and give rather poor results for ν_1 and ν_5.

The combinations and overtones accessible by XVMP2 with the frequency-dependent self-energy are limited to those that are in resonance with a fundamental, which may be an advantage in some cases, but a disadvantage in others. EOM-XVCCm does not have such limitation and has roots for all low-lying states involving up to m modes and is accurate for those involving up to $(m-1)$ modes. This is analogous to the electronic case: EOM-CCSD has roots for up to two-electron excited states and is accurate for one-electron excitation energies; for accurate results for two-electron excitation energies, one needs to use EOM-CCSDT. [131] Table 2.9 attests to this general trend for two- and three-mode combinations or overtones. The errors in EOM-XVCCSD for two-mode excitations and those in EOM-XVCCSDT for three-mode excitations have on the same order of magnitude as those in EOM-XVCCS for nonresonant fundamentals (ν_2, ν_3, ν_4, and ν_6). EOM-XVCCSDTQ for three-mode excitations, EOM-XVCCSDT for two-mode excitations, and EOM-XVCCSD for nonresonant fundamentals have comparable, high accuracy.

For transition frequencies to strongly correlated states involving at least two modes (Fermi resonances, combinations, and overtones), the following is the order of accuracy: XVCCSD < XVMP2 with pole search < XVCCSDT < XVCCSDTQ < XVCC5 < XVCC6 < XVCC7 ≤ XVCC8. The methods not mentioned in the list either do not have the corresponding roots or tend to display signs of nonconvergence.

2.5 Conclusion

We have presented an accurate, stable, efficient, and widely applicable vibrational CC (XVCC) theory for both zero-point energies and transition frequencies, the latter through the EOM formalism, of a molecule with an anharmonic PES. It relies on a Hartree product of harmonic-oscillator modals as a reference wave function and a truncated Taylor-series as a PES. These assumptions lead to streamlined sets of equations defining XVCC and EOM-XVCC, which mirror exactly those of electronic CC and EOM-CC theories. XVCC and EOM-XVCC are diagrammatically size consistent, free of modal basis sets, and thus an inherently infinite-basis theory.

We have established the rules for enumerating Feynman–Goldstone diagrams for XVCC and EOM-XVCC theories and the ones for translating them into algebraic equations. This method of derivation is not only expedient but also insightful because the diagrammatic topology can more immediately determine size consistency of a theory or its lack thereof as well as the relationships among various diagrammatic theories. The rules are justified by the underlying normal-ordered second-quantized method of derivation, which gives the same equations as the diagrammatic derivation in each case.

XVCC and EOM-XVCC theories are general in the sense that their formalisms are unchanged for any single-reference Hartree product of harmonic-oscillator modals, including the wave functions of XVSCF(n), XVSCF[n], SCP, or the harmonic approximation. Reflecting the centrality of XVSCF (which includes SCP) as the size-consistent single-Hartree-product method in many-body vibrational theory, some diagrammatic contributions in XVCC and EOM-XVCC vanish in this reference, simplifying their equations further. Low-order XVCC and EOM-XVCC results are also the same or very close to the XVSCF results for the same reason.

The VCC theory of Prasad and coworkers [40,45] can be identified as XVCC and EOM-XVCC with the XVSCF[n] reference. XVSCF is a diagrammatic size-consistent simplification of VSCF. Christiansen's VCC theory, [48] which relies on VSCF and modals that are numerically defined, differs completely from XVCC; unlike XVCC, VCC likely inherits many terms that are not size-consistent in the sense that they vanish identically in the thermodynamic limit. In VCC, the rank of disconnected excitations are also limited by the number of basis functions, which is not the case with basis-set-free XVCC.

The XVCCm and EOM-XVCCm methods up to $m = 8$ have been formulated and implemented by computer algebra of the aforementioned diagram logic as well as of algorithmic optimizations such as strength reduction, inter-

mediate reuse, and factorization. The numerical tests of these methods show that the results are smoothly and rapidly convergent towards the exact values. This is in contrast to XVMP2 in the frequency-independent approximation to the self-energy, which displays signs of divergent perturbation series not only for resonant modes, but also for nonresonant modes. While this problem is rectified by solving the Dyson equation with the frequency-dependent self-energy in XVMP2, EOM-XVCC may be said to achieve the same with a more well-studied diagonalization algorithm instead of a pole search. XVCC*m* and EOM-XVCC*m* with $m = n$, where n is the truncation rank of the Taylor-series PES, seem to be ones with the best cost-accuracy balance and hence the greatest practical utility.

2.6 Figures

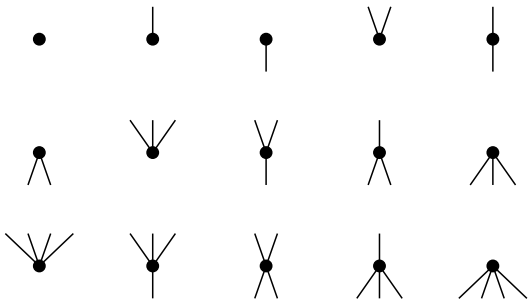

Figure 2.1: Diagrammatic representation of the normal-ordered Hamiltonian $\hat{H}$ with a QFF.

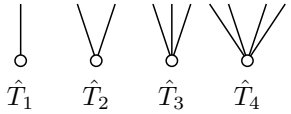

Figure 2.2: Diagrammatic representation of the cluster excitation operators.

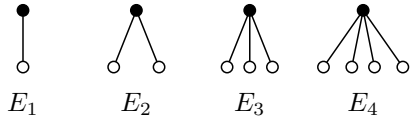

Figure 2.3: Diagrams in the energy equation of XVCCS in a QFF.

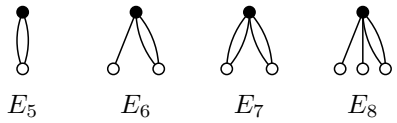

Figure 2.4: Additional diagrams in the energy equation of XVCCSD in a QFF.

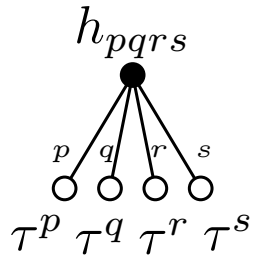

Figure 2.5: Diagram E_4 with labels.

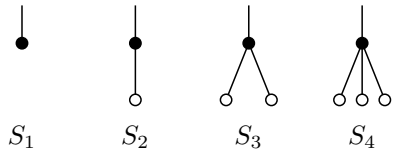

Figure 2.6: Diagrams in the T_1 amplitude equation of XVCCS in a QFF.

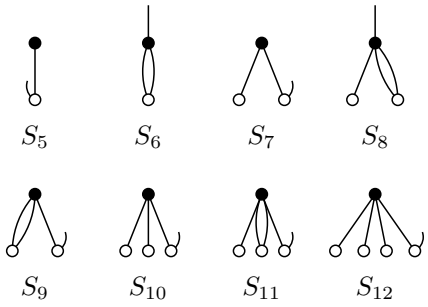

Figure 2.7: Additional diagrams in the T_1 amplitude equation of XVCCSD in a QFF.

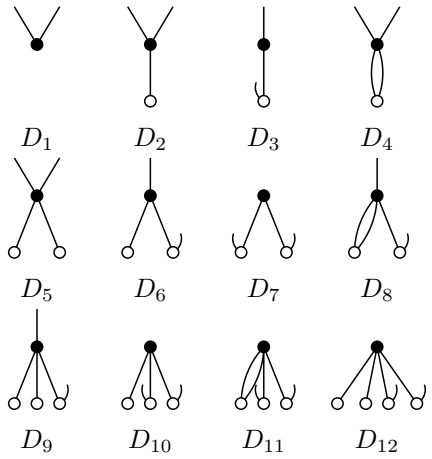

Figure 2.8: Diagrams in the T_2 amplitude equation of XVCCSD in a QFF.

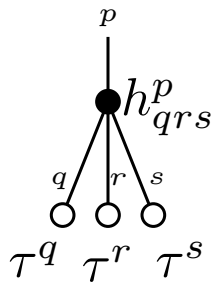

Figure 2.9: Diagram S_4 with labels.

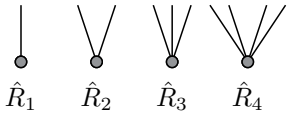

Figure 2.10: Diagrammatic representation of the linear excitation operators.

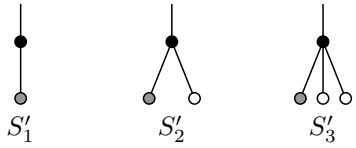

Figure 2.11: Diagrams in the R_1 amplitude equation of EOM-XVCCS in a QFF.

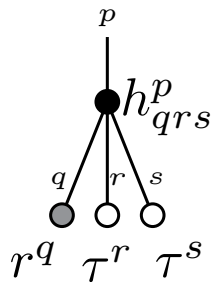

Figure 2.12: Diagram S'_3 with labels.

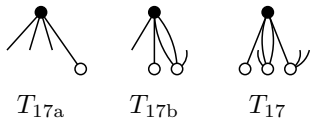

Figure 2.13: Strength reduction of diagram T_{17} in the T_3 amplitude equation of XVCCSDT (see Appendix A).

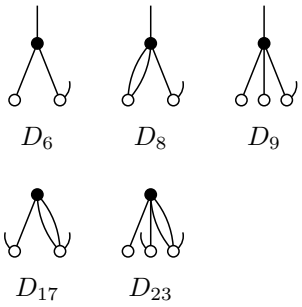

Figure 2.14: Factorable diagrams in the T_2 amplitude equation of XVCCSDT (see Appendix A).

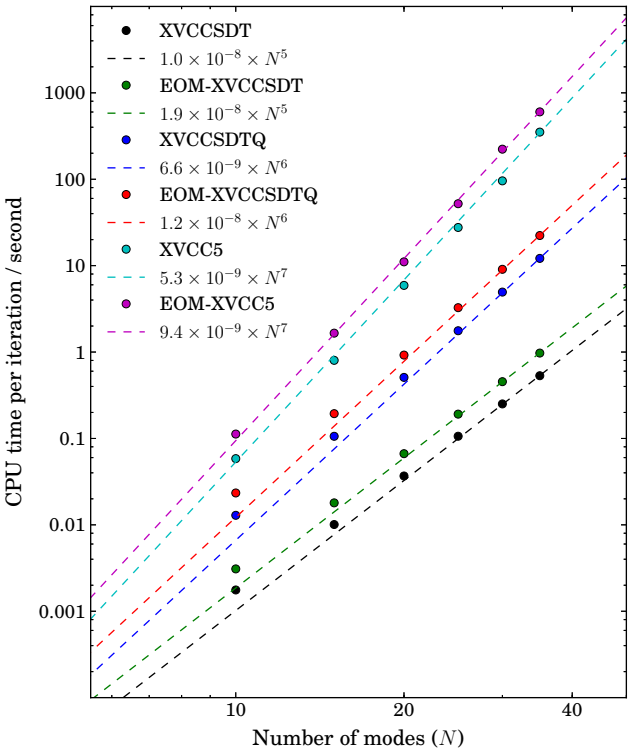

Figure 2.15: CPU time (in seconds) spent in one cycle of the iterative solution of XVCC*m* or EOM-XVCC*m* for a molecule with *N* modes in a QFF.

2.7 Tables

Table 2.1: Rules to draw all closed diagrams in the energy equation and all open diagrams in the T_l amplitude equation of XVCCm in an nth-order Taylor-series PES.

(1) Draw an $\hat{H}_{\mathrm{N}}$ vertex having up to n lines.
(2) Draw 0 to n $\hat{T}_k$ vertices ($1 \leq k \leq m$) beneath the $\hat{H}_{\mathrm{N}}$ vertex.
(3) Connect the lines of the $\hat{T}_k$ vertices with the lines of the $\hat{H}_{\mathrm{N}}$ vertex without altering (upgoing or downgoing) line directions, leaving l external (i.e., dangling) lines to form a connected diagram, which is either closed ($l = 0$) or open ($l > 0$).
(4) Repeat steps (1)–(3) to enumerate all topologically distinct diagrams. If permutation of $\hat{T}$ vertices allows two diagrams to overlap, they are deemed topologically equivalent.

Table 2.2: Rules to translate the closed and open diagrams of XVCC and EOM-XVCC into algebraic expressions.

(1) Label each internal line with a mode index.
An internal line is a line terminated by vertexes at both ends.
(2) Label each external line with a mode index.
An external line is a line terminated by a vertex at only one end.
(3) Associate each $\hat{H}_{\mathrm{N}}$ vertex with a Hamiltonian amplitude h.
The indices of h are given by the labels of the lines connected to that vertex.
(4) Associate each $\hat{T}_k$ vertex with an excitation amplitude τ.
The indices of τ are given by the labels of the lines connected to that vertex.
(5) Associate each $\hat{R}_k$ vertex with an excitation amplitude r.
The indices of r are given by the labels of the lines connected to that vertex.
(6) Sum over all internal line indices.
(7) Sum over all permutations of external line indices.
(8) For each set of n equivalent vertices, multiply by a factor of $(1/n!)$. If permutation of two vertices leaves the diagram unchanged topologically, the two vertices are equivalent.
(9) For each set of m equivalent lines, multiply by a factor of $(1/m!)$. If permutation of two lines leaves the diagram unchanged topologically, the two lines are equivalent.

Table 2.3: Rules to draw all open diagrams in the R_l amplitude equation of EOM-XVCCm in an nth-order Taylor-series PES.

(1) Draw an $\hat{H}_{\mathrm{N}}$ vertex having up to n lines.
(2) Draw an $\hat{R}_h$ vertex ($1 \leq h \leq m$) and zero to $(n-1)$ $\hat{T}_k$ vertices ($1 \leq k \leq m$) beneath the $\hat{H}_{\mathrm{N}}$ vertex.
(3) Connect the lines of the $\hat{R}_h$ and $\hat{T}_k$ vertices with the lines of the $\hat{H}_{\mathrm{N}}$ vertex without altering (upgoing or downgoing) line directions, leaving l external (i.e., dangling) lines to form a connected diagram.
(4) Repeat steps (1)–(3) to enumerate all topologically distinct diagrams. If permutation of $\hat{T}$ vertices allows two diagrams to overlap, they are deemed topologically equivalent.

Table 2.4: The number of multiplications and additions as a function of the number of modes (N) required in evaluating all the amplitude equations of XVCC and EOM-XVCC implemented with no optimization, with strength reduction and intermediate reuse, or with strength reduction, intermediate reuse, and factorization. The three leading terms only are shown.

Method	No optimization	Strength reduction	Factorization
XVCCS	$5N^4 + 4N^3 + 2N^2$	$2N^4 + 4N^3 + 8N^2$	$2N^4 + 4N^3 + 8N^2$
XVCCSD	$11N^6 + 31N^5 + 34N^4$	$13N^4 + 54N^3 + 36N^2$	$13N^4 + 57N^3 + 30N^2$
XVCCSDT	$60N^7 + 119N^6 + 110N^5$	$11N^5 + 165N^4 + 96N^3$	$11N^5 + 127N^4 + 59N^3$
XVCCSDTQ	$241N^8 + 360N^7 + 282N^6$	$24N^6 + 425N^5 + 225N^4$	$24N^6 + 189N^5 + 155N^4$
XVCC5	$799N^9 + 1053N^8 + 720N^7$	$104N^7 + 1061N^6 + 488N^5$	$81N^7 + 347N^6 + 206N^5$
XVCC6	$2577N^{10} + 3086N^9 + 1888N^8$	$175N^8 + 3079N^7 + 1134N^6$	$141N^8 + 1133N^7 + 368N^6$
XVCC7	$8398N^{11} + 9246N^{10} + 5070N^9$	$285N^9 + 8902N^8 + 3156N^7$	$239N^9 + 4141N^8 + 1162N^7$
XVCC8	$28099N^{12} + 28380N^{11} + 13989N^{10}$	$468N^{10} + 26641N^9 + 8991N^8$	$407N^{10} + 16403N^9 + 4170N^8$
EOM-XVCCS	$5N^4 + 3N^3 + 2N^2$	$2N^4 + 4N^3 + 7N^2$	$2N^4 + 4N^3 + 7N^2$
EOM-XVCCSD	$30N^6 + 70N^5 + 54N^4$	$21N^4 + 97N^3 + 63N^2$	$21N^4 + 92N^3 + 55N^2$
EOM-XVCCSDT	$183N^7 + 286N^6 + 220N^5$	$15N^5 + 343N^4 + 189N^3$	$15N^5 + 222N^4 + 93N^3$
EOM-XVCCSDTQ	$729N^8 + 916N^7 + 598N^6$	$34N^6 + 965N^5 + 474N^4$	$34N^6 + 341N^5 + 298N^4$
EOM-XVCC5	$2490N^9 + 2794N^8 + 1614N^7$	$207N^7 + 2649N^6 + 1096N^5$	$141N^7 + 707N^6 + 368N^5$
EOM-XVCC6	$8295N^{10} + 8533N^9 + 4432N^8$	$348N^8 + 8164N^7 + 2782N^6$	$251N^8 + 2527N^7 + 748N^6$
EOM-XVCC7	$27975N^{11} + 26506N^{10} + 12457N^9$	$569N^9 + 24962N^8 + 8309N^7$	$435N^9 + 10275N^8 + 2570N^7$
EOM-XVCC8	$96603N^{12} + 83992N^{11} + 35934N^{10}$	$934N^{10} + 78522N^9 + 25129N^8$	$757N^{10} + 45703N^9 + 10324N^8$

Table 2.5: The calculated zero-point energy (E_0) and frequencies (ν_i) of the fundamental transitions (in cm^{-1}) of the water molecule. Except for VCI, the errors from VCI are shown.

Method[1]	E_0	ν_1	ν_2	ν_3
VCI	4642.4	3682.4	1556.6	3791.5
Harmonic	108.4	139.7	71.7	156.4
XVSCF(4)	104.5	280.2	−17.9	289.4
XVSCF[4]	21.5	105.3	11.7	116.1
XVCCS{4}	21.9	196.5	−1.2	206.7
XVCCS(4)	26.6	197.2	−2.4	207.0
XVCCS[4]	21.5	105.3	11.7	116.1
XVCCSD{4}	22.1	33.6	7.9	34.3
XVCCSD(4)	23.8	38.3	8.5	38.3
XVCCSD[4]	21.5	26.0	6.8	26.6
XVCCSDT{4}	0.2	−1.7	2.2	−2.0
XVCCSDT(4)	0.1	−2.4	2.2	−2.7
XVCCSDT[4]	0.4	−1.7	2.4	−1.9
XVCCSDTQ{4}	0.0	−0.7	0.2	−0.7
XVCCSDTQ(4)	−0.0	−1.0	0.1	−1.0
XVCCSDTQ[4]	0.0	−0.1	0.1	−0.1
XVMP2(4)[2]	4.5	−24.6	3.8	−28.3
XVMP2[4][2]	−1.3	−18.9	2.4	−20.3
XVMP2(4)[3]	4.5	−14.3	3.8	−20.8
XVMP2[4][3]	−1.3	−14.8	2.5	−17.0

[1] XVCC for zero-point energy and EOM-XVCC for frequencies. Suffix '{4}' means the use of a harmonic reference, '(4)' means the use of a XVSCF(4) reference, and '[4]' the use of a XVSCF[4] reference.
[2] In the frequency-independent approximation. [14]
[3] Solutions of the Dyson equation with the frequency-dependent self-energy. [14]

Table 2.6: The calculated zero-point energy (E_0) and frequencies (ν_i) of the fundamental transitions (in cm^{-1}) of the water molecule. The errors from XVCC8 with the corresponding reference wave function are shown.

Method[1]	E_0	ν_1	ν_2	ν_3
XVCC5{4}	−0.02	−0.05	0.02	−0.06
XVCC5(4)	−0.03	−0.12	0.01	−0.12
XVCC5[4]	−0.03	0.00	0.02	0.00
XVCC6{4}	−0.001	0.004	0.004	0.005
XVCC6(4)	−0.001	0.005	0.002	0.006
XVCC6[4]	−0.001	0.006	0.003	0.007
XVCC7{4}	−0.0004	0.003	0.001	0.003
XVCC7(4)	−0.0002	0.004	0.001	0.005
XVCC7[4]	−0.0005	−0.001	0.002	−0.001
XVCC8{4}	0	0	0	0
XVCC8(4)	0	0	0	0
XVCC8[4]	0	0	0	0

[1] XVCC for zero-point energy and EOM-XVCC for frequencies. Suffix '{4}' means the use of a harmonic reference, '(4)' means the use of a XVSCF(4) reference, and '[4]' the use of a XVSCF[4] reference.

Table 2.7: The calculated zero-point energy (E_0) and frequencies (ν_i) of the fundamental transitions (in cm^{-1}) of the formaldehyde molecule. Except for VCI, the errors from VCI are shown.

Method[1]	E_0	ν_1	ν_2	ν_3	ν_4	ν_5	$\nu_3\nu_6$	$\nu_2\nu_6$	ν_6
VCI	5813.6	2837.2	1719.8	1501.5	1160.7	2873.3	2702.8	2989.2	1237.5
Harmonic	74.3	136.2	33.2	38.6	36.2	174.2	...	...	29.4
XVSCF(4)	73.0	185.0	41.0	10.8	−13.7	216.4	...	...	−3.3
XVSCF[4]	22.9	79.0	20.4	9.8	10.6	106.7	...	...	11.2
XVCCS{4}	24.0	134.8	31.9	9.4	−1.3	164.7	...	...	4.0
XVCCS(4)	25.5	134.1	31.9	9.7	−0.8	163.6	...	...	4.4
XVCCS[4]	22.9	79.1	20.9	9.3	10.6	106.7	...	...	11.1
XVCCSD{4}	23.5	30.1	6.7	5.1	6.7	38.1	31.6	34.6	6.4
XVCCSD(4)	24.1	31.6	6.6	5.4	7.5	38.9	32.2	35.4	6.8
XVCCSD[4]	22.9	24.2	6.0	4.2	6.0	31.0	35.5	33.0	5.6
XVCCSDT{4}	0.6	0.3	0.5	1.2	1.7	1.9	7.3	2.2	1.4
XVCCSDT(4)	0.6	−0.0	0.5	1.2	1.7	1.8	7.9	2.4	1.4
XVCCSDT[4]	0.8	0.1	0.5	1.2	1.9	1.3	6.1	1.4	1.4
XVCCSDTQ{4}	0.0	−0.2	0.0	0.1	0.1	0.5	2.4	0.9	0.1
XVCCSDTQ(4)	0.0	−0.3	0.0	0.1	0.1	0.4	2.4	0.9	0.1
XVCCSDTQ[4]	0.1	0.2	0.0	0.1	0.0	0.7	2.3	1.0	0.0
XVMP2(4)[2]	1.3	−190.9	0.7	0.9	2.7	33.0	...	...	3.0
XVMP2[4][2]	−1.0	−15.9	0.1	1.3	1.6	−414.3	...	...	1.8
XVMP2(4)[3]	1.3	−6.6	1.4	1.0	2.6	−0.2	6.6	29.3	3.0
XVMP2[4][3]	−1.0	−8.9	0.3	1.4	1.5	2.2	18.0	24.8	1.8

[1] XVCC for zero-point energy and EOM-XVCC for frequencies. Suffix '{4}' means the use of a harmonic reference, '(4)' means the use of a XVSCF(4) reference, and '[4]' the use of a XVSCF[4] reference.
[2] In the frequency-independent approximation. [14]
[3] Solutions of the Dyson equation with the frequency-dependent self-energy. [14]

Table 2.8: The calculated zero-point energy (E_0) and frequencies (ν_i) of the fundamental transitions (in cm^{-1}) of the formaldehyde molecule. The errors from XVCC8 with the corresponding reference wave function are shown.

Method[1]	E_0	ν_1	ν_2	ν_3	ν_4	ν_5	$\nu_3\nu_6$	$\nu_2\nu_6$	ν_6
XVCC5{4}	−0.02	−0.03	0.00	0.01	0.00	0.03	0.33	0.06	0.01
XVCC5(4)	−0.02	−0.06	0.00	0.01	0.00	0.01	0.32	0.05	0.01
XVCC5[4]	−0.02	0.02	0.00	0.01	0.00	0.04	0.26	0.06	0.01
XVCC6{4}	−0.001	0.000	0.001	0.001	−0.001	0.005	0.067	0.011	0.001
XVCC6(4)	−0.001	−0.002	0.000	0.001	−0.001	0.003	0.062	0.010	0.001
XVCC6[4]	0.000	0.002	0.000	0.000	−0.002	0.006	0.052	0.008	0.000
XVCC7{4}	−0.0003	0.0012	0.0002	0.0004	0.0003	0.0010	0.0131	0.0021	0.0005
XVCC7(4)	−0.0002	0.0014	0.0002	0.0004	0.0003	0.0010	0.0124	0.0022	0.0005
XVCC7[4]	−0.0004	−0.0011	0.0002	0.0006	0.0007	−0.0005	0.0100	0.0004	0.0007
XVCC8{4}	0	0	0	0	0	0	0	0	0
XVCC8(4)	0	0	0	0	0	0	0	0	0
XVCC8[4]	0	0	0	0	0	0	0	0	0

[a] XVCC for zero-point energy and EOM-XVCC for frequencies. Suffix '{4}' means the use of a harmonic reference, '(4)' means the use of a XVSCF(4) reference, and '[4]' the use of a XVSCF[4] reference.

Table 2.9: The calculated frequencies of selected overtones and combinations (in cm^{-1}) of the formaldehyde molecule. Except for VCI, the errors from VCI are shown.

Method	(000200)	(000101)	(000002)	(001100)	(010100)	(002000)	(000300)	(000201)
VCI	2318.1	2399.6	2472.5	2660.6	2871.2	3000.8	3464.2	3555.2
EOM-XVCCSD[4]	35.7	28.3	31.0	77.7	38.3	23.2	...	...
EOM-XVCCSDT[4]	7.6	6.0	5.3	5.7	4.5	4.7	62.5	49.6
EOM-XVCCSDTQ[4]	2.1	2.0	2.1	2.0	1.8	2.0	14.2	10.9
EOM-XVCC5[4]	0.1	0.1	0.2	0.1	0.1	0.2	3.3	3.0
EOM-XVCC6[4]	0.0	0.0	0.0	0.0	0.0	0.0	0.5	0.3
EOM-XVCC7[4]	0.0	0.0	0.0	0.0	0.0	0.0	0.1	0.1
EOM-XVCC8[4]	0.0	0.0	0.0	0.0	0.0	0.0	0.0	0.0

Chapter 3

Similarity-transformed equation-of-motion vibrational coupled cluster theory

3.1 Introduction

In the previous chapter, we introduced basis-set free, diagrammatic anharmonic vibrational CC theories for ground-state (zero-point) energies and transition frequencies, referred to as XVCCm and EOM-XVCCm, respectively, where m is the number of modes that are simultaneously excited by the cluster excitation operator $\hat{T}$. [132] The XVCCm and EOM-XVCCm energies are the eigenvalues of the similarity-transformed Hamiltonian $\bar{H}$ as defined by Eq. (1.18), which decouples the ground (zero-point) state and all higher-order excited products up to the mth order, as illustrated in Fig. 3.1 in the case of $m = 4$. For a meaningful anharmonic calculation, m has to be greater than two, rendering the $\bar{H}$ matrix too large for storage or full diagonalization. Hence, a subspace diagonalization algorithm [123, 124, 133] needs to be used to determine its several lowest eigenvalues only.

In a vibrational analysis, however, one is typically less interested in the lowest transition frequencies, but more in the frequencies of all fundamental modes. This is because fundamentals are the only bright modes in infrared absorption (IR) and Raman scattering spectra within the harmonic approximation. Even in the spectra of a realistic molecule with an anharmonic potential energy surface (PES), they tend to be responsible for a vast majority of intense IR and Raman bands since anharmonicity is usually a small perturbation. These are in contrast with electronic transitions, which have a varied degree of two-electron character and whose significance tends to correlate more with their energies than with their one-electron character. Since the fundamentals have transition frequencies spanning one to two orders of magnitude (i.e., from tens to thousands of reciprocal centimeters) and thus tend to be buried in a dense manifold of overtones and combinations, a method that can selectively and simultaneously determine all fundamental frequencies is highly desirable.

The STEOM-CC ansatz can achieve exactly this and is, therefore, uniquely appealing for vibrational analyses. Here, we report its application to anharmonic molecular vibrations in a Taylor-series PES, abbreviated as STEOM-XVCCm, where m has the same meaning as before. It computes all fundamental frequencies accurately, selectively, and simultaneously by diagonalization of the doubly similarity-transformed vibrational Hamiltonian $\bar{\bar{H}}$ matrix in the space of only singly (one-mode) excited Hartree products. The effective Hamiltonian $\bar{\bar{H}}$ is obtained as a second

similarity transformation of the XVCCm similarity-transformed Hamiltonian $\bar{H}$ by Eq. (1.28) such that its singles and higher-order excited Hartree products up to the mth order are decoupled, as shown in Fig. 3.1. This decoupling allows the eigenvalues of $\bar{\bar{H}}$ in the space of single through mth-order excitations to be obtained exactly by its diagonalization in the singles space only.

In this chapter, we stipulate the STEOM-XVCCm ansatz, establish a diagrammatic method of derivations, and implement them up to $m = 4$ in a quartic force field (QFF) with the aid of our previously reported symbolic algebra program. [132] We analyze the results of their applications to the fundamentals of the water, formaldehyde, and ethene molecules, in comparison with the results from the second-order many-body perturbation (XVMP2) [14, 119] approximation to vibrational many-body Green's function (MBGF) theory as well as from the EOM-XVCC4 theory.

We prove the size-intensivity and exact equality of the STEOM-XVCCm frequencies for fundamentals with the EOM-XVCCm frequencies, unlike the electronic case where STEOM-CCSD excitation energies differ from those of EOM-CCSD. The proof is based on the connectedness of $\bar{\bar{H}}$ shown by Nooijen, [110] which is valid for vibrations also, and on the fact that the $\bar{\bar{H}}$ operator in the singles space contains only up to one $\hat{S}$ operator of STEOM-XVCCm, which can then be one-to-one mapped onto the $\hat{R}$ operator of EOM-XVCCm for the same eigenvalue. The relationship between STEOM-XVCCm and EOM-XVCCm for fundamentals is analogous to the equivalence of the principal IPs and EAs obtained from the diagonalization of $\bar{\bar{H}}$ with IP- and EA-EOM-CC.

In this sense, STEOM-XVCCm may be viewed as a particularly convenient root-homing algorithm of EOM-XVCCm, the one that can determine all fundamental frequencies simultaneously instead of one mode at a time. However, it also has a greater theoretical significance as it defines a systematic series of approximations converging at an *exact one-mode theory*, which, therefore, is closely related to MBGF theory based on the Dyson equation, which is also a formally exact one-particle theory. [134]

In this chapter, therefore, we also elucidate the algebraic and diagrammatic correspondence between the STEOM-XVCC one-mode equation and the vibrational Dyson equation with the self-energy expanded in a Feynman–Dyson perturbation series. [14, 119] We show that STEOM-XVCC diagrams for anharmonic corrections and XVMP2 self-energy diagrams share the same topology, and a second-order perturbation approximation to the former reduces to the latter in the frequency-independent approximation. The parallels between STEOM-XVCC and vibrational MBGF have inspired the following three approximations to the former: the diagonal, perturbation, and frequency-independent approximations, all of which have been widely used for the self-energy. The impact of these approximations to the STEOM-XVCC frequencies is measured numerically and will be discussed.

3.2 XVCC

Equations (2.30) and (2.41) suggest that XVCC*m* can also be viewed as a mean-field (single-Hartree-product) method for the trans-correlated Schrödinger equation with the similarity-transformed Hamiltonian,

$$\begin{aligned} \bar{H} &\equiv e^{-\hat{T}}\hat{H}e^{\hat{T}} = \left(\hat{H}e^{\hat{T}}\right)_{\mathrm{C}} && (3.1) \\ &= \bar{h}_0 + \sum_p \bar{h}_p\{\hat{a}_p\} + \sum_p \bar{h}^p\{\hat{a}_p^\dagger\} + \frac{1}{2!}\sum_{p,q}\bar{h}_{pq}\{\hat{a}_p\hat{a}_q\} \\ &\quad + \sum_{p,q}\bar{h}_q^p\{\hat{a}_p^\dagger\hat{a}_q\} + \ldots, && (3.2) \end{aligned}$$

where the normal-ordered vibrational Hamiltonian $\hat{H}$ is defined in Chapter 2. [13] The amplitudes $\bar{h}$'s (whose superscript and subscript indices separately have permutation symmetry) are the tensor contractions of the τ and bare normal-ordered Hamiltonian amplitudes [13, 132] and are thus dressed with higher-order anharmonic effects in a size-consistent manner. In this alternative, but equivalent view, the energy equation [Eq. (2.30)] of XVCC*m* is vastly simplified to

$$\bar{h}_0 = \bar{E}_0^{(m)}, \tag{3.3}$$

whereas the amplitude equation [Eq. (2.41)] is nothing but

$$\bar{h}^{p_1 p_2 \cdots p_n} = 0, \tag{3.4}$$

for all $p_1, p_2 \ldots, p_n$ and each n ($1 \leq n \leq m$).

The algebraic expressions of the amplitudes of $\bar{H}$ can be obtained by straightforward, but tedious applications of the Born–Huang rules, [9, 135] or the method of second quantization. [114, 136, 137] Alternatively, they are derivable by the use of normal-ordered second quantization and Wick's theorem. [13] In the case of XVCC*m* in a QFF, the

constant term is given by

$$\begin{aligned}
\bar{h}_0 &= h_0 + \sum_p h_p \tau^p + \frac{1}{2!}\sum_{p,q} h_{pq}\tau^{pq} + \frac{1}{3!}\sum_{p,q,r} h_{pqr}\tau^{pqr} \\
&+ \frac{1}{4!}\sum_{p,q,r,s} h_{pqrs}\tau^{pqrs} + \frac{1}{2!}\sum_{p,q} h_{pq}\tau^p\tau^q + \frac{1}{2!}\sum_{p,q,r} h_{pqr}\tau^p\tau^{qr} \\
&+ \frac{1}{3!}\sum_{p,q,r,s} h_{pqrs}\tau^p\tau^{qrs} + \frac{1}{2!2!2!}\sum_{p,q,r,s} h_{pqrs}\tau^{pq}\tau^{rs} \\
&+ \frac{1}{3!}\sum_{p,q,r} h_{pqr}\tau^p\tau^q\tau^r + \frac{1}{2!2!}\sum_{p,q,r,s} h_{pqrs}\tau^p\tau^q\tau^{rs} \\
&+ \frac{1}{4!}\sum_{p,q,r,s} h_{pqrs}\tau^p\tau^q\tau^r\tau^s,
\end{aligned} \tag{3.5}$$

where h's are the amplitudes of the bare normal-ordered vibrational Hamiltonian $\hat{H}$. [13] The one-mode excitation amplitude reads

$$\begin{aligned}
\bar{h}^p &= h^p + \sum_q h^p_q \tau^q + \sum_q h_q \tau^{qp} + \frac{1}{2!}\sum_{q,r} h^p_{qr}\tau^{qr} + \frac{1}{2!}\sum_{q,r} h_{qr}\tau^{qrp} \\
&+ \frac{1}{3!}\sum_{q,r,s} h^p_{qrs}\tau^{qrs} + \frac{1}{3!}\sum_{q,r,s} h_{qrs}\tau^{qrsp} + \frac{1}{2!}\sum_{q,r} h^p_{qr}\tau^q\tau^r \\
&+ \sum_{q,r} h_{qr}\tau^q\tau^{rp} + \frac{1}{2!}\sum_{q,r,s} h^p_{qrs}\tau^q\tau^{rs} \\
&+ \frac{1}{2!}\sum_{q,r,s} h_{qrs}\tau^q\tau^{rsp} + \frac{1}{3!}\sum_{q,r,s,t} h_{qrst}\tau^q\tau^{rstp} \\
&+ \frac{1}{2!}\sum_{q,r,s} h_{qrs}\tau^{qr}\tau^{sp} + \frac{1}{2!2!}\sum_{q,r,s,t} h_{qrst}\tau^{qr}\tau^{stp} \\
&+ \frac{1}{3!}\sum_{q,r,s,t} h_{qrst}\tau^{qp}\tau^{rst} + \frac{1}{3!}\sum_{q,r,s} h^p_{qrs}\tau^q\tau^r\tau^s \\
&+ \frac{1}{2!}\sum_{q,r,s} h_{qrs}\tau^q\tau^r\tau^{sp} + \frac{1}{2!2!}\sum_{q,r,s,t} h_{qrst}\tau^q\tau^r\tau^{stp} \\
&+ \frac{1}{2!}\sum_{q,r,s,t} h_{qrst}\tau^q\tau^{rs}\tau^{tp} + \frac{1}{3!}\sum_{q,r,s,t} h_{qrst}\tau^q\tau^r\tau^s\tau^{tp}.
\end{aligned} \tag{3.6}$$

However, by far the most expedient and insightful approach is the Feynman–Goldstone diagrammatics. [132, 138] The similarity-transformed Hamiltonian $\bar{H}$ is formally drawn as

$\bar{H}$ =

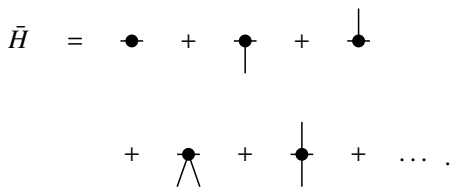

(3.7)

There is a term-by-term correspondence with Eq. (3.2), and a $\bar{h}$ amplitude is expressed by a filled-circle vertex with a single strike-through.

The constant part of this Hamiltonian (the first term in the right-hand side) is a sum of closed, connected diagrams made up of the $\hat{H}$ and $\hat{T}$ vertices:

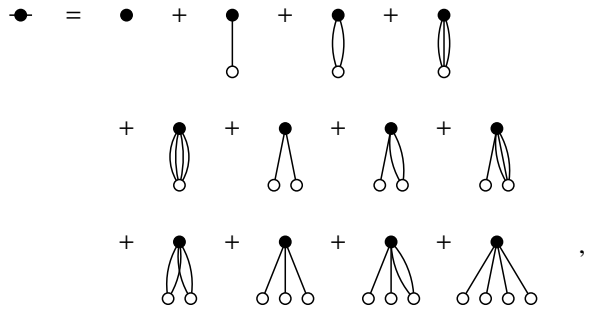

(3.8)

which has a term-by-term correspondence with Eq. (3.5). See Table 2.2 for the rules of translating these diagrams into algebraic expressions. The one-mode excitation operator [the third term of Eq. (3.7)] is

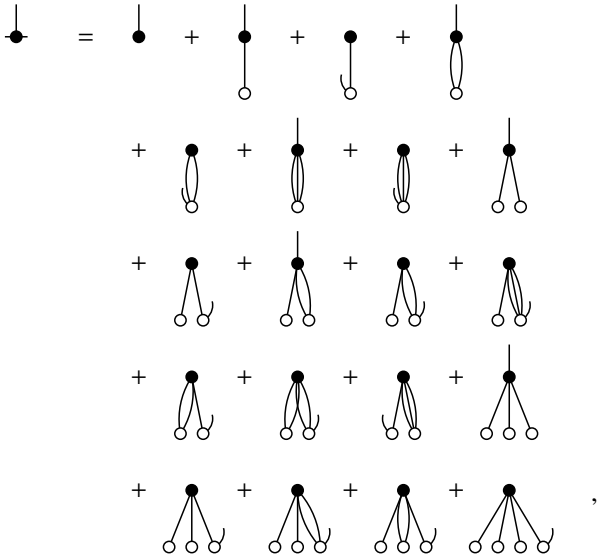

(3.9)

which has a term-by-term correspondence with Eq. (3.6). The diagrammatic definitions of the remaining terms in $\bar{H}$ that are relevant for subsequent discussions are documented in Appendix C. Unlike $\hat{H}$, which is at most an n-mode operator (for an nth-order Taylor-series PES), $\bar{H}$ of XVCCm contains up to an $n(m-1)$-mode excitation operator.

Diagrammatically, the energy and amplitude equations of XVCC4 (XVCCSDTQ) are

(3.10)

and

$$= \quad 0 \quad , \tag{3.11}$$

$$= \quad 0 \quad , \tag{3.12}$$

$$= \quad 0 \quad , \tag{3.13}$$

$$= \quad 0 \quad . \tag{3.14}$$

The algebraic interpretations are given as Eqs. (3.3) and (3.4), respectively. A diagrammatic expansion of each of the left-hand sides in terms of the $\hat{T}$ and $\hat{H}$ amplitudes is given in Appendix C.

3.3 STEOM-XVCC

3.3.1 Ansatz

Here, we introduce the *m*th-order similarity-transformed EOM-XVCC method, abbreviated as STEOM-XVCC*m*, as an *m*th-order CI problem with the *doubly* similarity-transformed Hamiltonian $\bar{\bar{H}}$,

$$\begin{aligned} \bar{\bar{H}} &= \{e^{\hat{S}}\}^{-1} \bar{H} \{e^{\hat{S}}\} \\ &= \{e^{\hat{S}}\}^{-1} e^{-\hat{T}} \hat{H} e^{\hat{T}} \{e^{\hat{S}}\}, \end{aligned} \tag{3.15}$$

where the braces bring the exponential operator in a normal order. [13, 110] The amplitudes of operator $\hat{S}$ are determined so as to decouple singly excited Hartree products from all higher-order excited products up to the *m*th order. Therefore, $\hat{S}$ consists of exactly one lowering operator and n ($2 \leq n \leq m$) raising operators, and can be written as

$$\hat{S} = \hat{S}_{2,1} + \hat{S}_{3,1} + \cdots + \hat{S}_{m,1}, \tag{3.16}$$

with

$$\hat{S}_{n,1} = \frac{1}{n!} \sum_{p_1, p_2, \cdots, p_n} \sum_{q} s_q^{p_1 p_2 \cdots p_n} \{\hat{a}_{p_1}^\dagger \hat{a}_{p_2}^\dagger \cdots \hat{a}_{p_n}^\dagger \hat{a}_q\}, \tag{3.17}$$

where $s_q^{p_1 p_2 \cdots p_n}$ is an excitation-deexcitation amplitude, which is invariant to any permutation of superscript indices but not of the subscript index. Their values are determined by requiring

$$\langle \Phi_{p_1 p_2 \cdots p_n} | \bar{\bar{H}} | \Phi_q \rangle = 0, \tag{3.18}$$

for all q and all $p_1, p_2, \ldots, p_n$ for each n ($2 \leq n \leq m$). We call the equation for a given n the $\hat{S}_{n,1}$-amplitude equation and the whole set the $\hat{S}$-amplitude equations collectively.

As shown in Sec. 3.3.2, this second similarity transformation does not spoil the decoupling of the ground-state Hartree product and all excited products achieved by the first similarity transformation,

$$\langle \Phi_{p_1 p_2 \cdots p_n} | \bar{\bar{H}} | \Phi_0 \rangle = 0, \tag{3.19}$$

making the $\bar{\bar{H}}$ matrix partially block diagonal as depicted in Fig. 3.1 in the case of $m = 4$. This implies that the constant term of the $\bar{\bar{H}}$ operator remains to be the XVCCm energy for the ground state,

$$\langle \Phi_0 | \bar{\bar{H}} | \Phi_0 \rangle = \bar{E}_0^{(m)}. \tag{3.20}$$

Furthermore, the excitation energies of STEOM-XVCCm of predominantly one-mode character can be obtained by the diagonalization of $\bar{\bar{H}}$ in the singles block only (i.e., the area enclosed by dashed lines of $\bar{\bar{H}}$ in Fig. 3.1).

We can, therefore, stipulate STEOM-XVCCm as a CI-singles (CIS) problem (as opposed to the mth-order CI) with the doubly similarity-transformed Hamiltonian $\bar{\bar{H}}$, when one is interested in predominantly one-mode excitations (fundamentals) only. Defining a one-mode excitation operator that brings the ground state to the ℓth singly excited state by

$$\hat{C}_1(\ell) = \sum_p c^p(\ell) \{\hat{a}_p^\dagger\}, \tag{3.21}$$

we require that

$$\langle \Phi_p | \bar{\bar{H}} \hat{C}_1(\ell) | \Phi_0 \rangle = \bar{\bar{E}}_\ell^{(m)} c^p(\ell) \tag{3.22}$$

be satisfied, where $\bar{\bar{E}}_\ell^{(m)}$ is the STEOM-XVCCm total energy of the ℓth excited state, which we will later show is equal to the EOM-XVCCm total energy $\bar{E}_\ell^{(m)}$. Furthermore, Eqs. (3.19) and (3.20) imply

$$\langle \Phi_p | \hat{C}_1(\ell) \bar{\bar{H}} | \Phi_0 \rangle = \bar{E}_0^{(m)} c^p(\ell), \tag{3.23}$$

which, together with Eq. (3.22), leads to

$$\langle \Phi_p | \left(\bar{\bar{H}} \hat{C}_1(\ell) \right)_{\rm C} | \Phi_0 \rangle = \bar{\bar{\omega}}_\ell^{(m)} c^p(\ell), \tag{3.24}$$

where $\bar{\bar{\omega}}_\ell^{(m)} = \bar{\bar{E}}_\ell^{(m)} - \bar{E}_0^{(m)}$, which we will prove is identical to EOM-XVCCm frequency $\bar{\omega}_\ell^{(m)}$ for the ℓth fundamental. We call the above the STEOM-XVCC eigenvalue equation, which is to be solved for frequencies $\bar{\bar{\omega}}$ for all fundamentals at once.

Next, let us consider the diagrammatic expression of the STEOM-XVCCm $\hat{S}$-amplitude equation (3.18) and eigenvalue equation (3.24). Delaying for now the definition of the amplitudes in terms of those of $\hat{H}$, $\hat{T}$, and $\hat{S}$, we can formally write the doubly similarity-transformed Hamiltonian in a normal-ordered form as

$$\begin{aligned} \bar{\bar{H}} \;=\; & \bar{\bar{h}}_0 + \sum_p \bar{\bar{h}}_p \{\hat{a}_p\} + \sum_p \bar{\bar{h}}^p \{\hat{a}_p^\dagger\} \\ & + \frac{1}{2!} \sum_{p,q} \bar{\bar{h}}_{pq} \{\hat{a}_p \hat{a}_q\} + \sum_{p,q} \bar{\bar{h}}_q^p \{\hat{a}_p^\dagger \hat{a}_q\} + \ldots, \end{aligned} \tag{3.25}$$

which is nonterminating. As shown in Sec. 3.3.2, each of the $\bar{\bar{h}}$ amplitudes is connected, allowing its diagrammatic expression to be

$\bar{\bar{H}}$ =

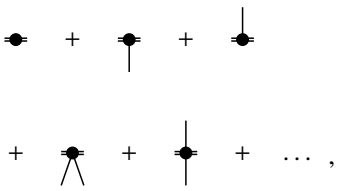

(3.26)

corresponding term-by-term to Eq. (3.25). A filled-circle vertex with a double strike-through denotes an $\bar{\bar{h}}$ amplitude. Since

$$\langle \Phi_{p_1 p_2 \cdots p_n} | \bar{\bar{H}} | \Phi_q \rangle = \sum_{i=1}^{n} \delta_{p_i q} \, \bar{\bar{h}}^{p_1 \cdots p_{i-1} p_{i+1} \cdots p_n} + \bar{\bar{h}}_q^{p_1 p_2 \cdots p_n}, \tag{3.27}$$

and the zeros from the previous transformation are preserved [Eq. (3.19)], the $\hat{S}$-amplitude equation [Eq. (3.18)] can be simplified to

$$\bar{\bar{h}}_q^{p_1 p_2 \cdots p_n} = 0, \tag{3.28}$$

for all q and $p_1, p_2, \ldots, p_n$ for each n ($2 \leq n \leq m$), which is diagrammatically expressed as

(3.29)

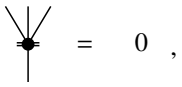

(3.30)

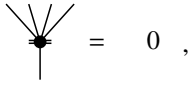

(3.31)

in the case of $m = 4$ (STEOM-XVCC4).

Designating the operator $\hat{C}_1(\ell)$ diagrammatically as

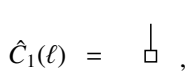

(3.32)

where ℓ dependence is again suppressed, the STEOM-XVCCm eigenvalue equation [Eq. (3.24)] becomes

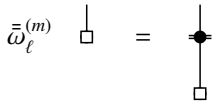

(3.33)

3.3.2 Doubly similarity-transformed Hamiltonian

To arrive at the working equations of STEOM-XVCC, a precise definition and method of calculation of the doubly similarity-transformed Hamiltonian $\bar{\bar{H}}$ need to be established. In this subsection, we show that (1) Nooijen's method of evaluating the inverse of $\{e^{\hat{S}}\}$ is valid for vibrations, (2) the constant part of the $\bar{\bar{H}}$ operator is the same as that of $\bar{H}$, and (3) the zeros of the $\bar{H}$ are preserved by the second similarity transformation. In the next subsection, on these bases, we derive the STEOM-XVCC $\hat{S}$-amplitude and eigenvalue equations, which are shown to be "linearized."

First, we establish a general formula of evaluating $\bar{\bar{H}}$. Because of the presence of a lowering operator in each $\hat{S}_{n,1}$, different components of $\hat{S}_{n,1}$ do not commute, [110] necessitating the normal-ordered exponential in the definition of $\bar{\bar{H}}$. This, in turn, causes the inverse of $\{e^{\hat{S}}\}$ to be not as simply written in a connected form as in the case of the first transformation:

$$\bar{\bar{H}} \equiv \{e^{\hat{S}}\}^{-1} \bar{H} \{e^{\hat{S}}\} \neq \left(\bar{H}\{e^{\hat{S}}\}\right)_{\mathrm{C}}. \tag{3.34}$$

In the electronic case, [110] instead, $\bar{\bar{H}}$ was obtained by solving the equation,

$$\{e^{\hat{S}}\}\bar{\bar{H}} = \bar{H}\{e^{\hat{S}}\}, \tag{3.35}$$

which can be achieved [110] by iteratively improving the left-hand side in the recursive and connected equation,

$$\bar{\bar{H}} = \left(\bar{H}\{e^{\hat{S}}\}\right)_{\mathrm{C}} - \left(\{e^{\hat{S}} - 1\}\bar{\bar{H}}\right)_{\mathrm{C}}, \tag{3.36}$$

or in an equivalent, infinite sum of doubly connected series,

$$\bar{\bar{H}} = \sum_{k=0}^{\infty}(-1)^k \left(\{e^{\hat{S}} - 1\}^k \left(\bar{H}\{e^{\hat{S}}\}\right)_{\mathrm{C}}\right)_{\mathrm{C}}. \tag{3.37}$$

Nothing in the derivations [110] of these expressions is specific to the forms of electronic $\hat{H}$, $\hat{T}$, or $\hat{S}$, and hence these remain correct for the vibrational case. The connectedness of $\bar{\bar{H}}$ and of the eigenvalue equation (3.24) ensures the rigorous size-intensivity of the STEOM-XVCC frequencies.

Second, we prove the invariance of the constant part of the similarity-transformed Hamiltonian operator $\bar{H}$ by the second transformation, i.e., $\bar{\bar{h}}_0 = \bar{h}_0 = \bar{E}_0^{(m)}$ (the XVCCm ground-state energy). To show this, we first note that

$$\{\hat{S}^n\}|\Phi_0\rangle = \langle\Phi_0|\{\hat{S}^n\} = 0 \;\; (n \geq 1), \tag{3.38}$$

because $\hat{S}$ contains at least one lowering and two raising operators. Evaluating the vacuum expectation value of Eq. (3.35), we find

$$\begin{aligned}\langle\Phi_0|\{e^{\hat{S}}\}\bar{\bar{H}}|\Phi_0\rangle &= \langle\Phi_0|\bar{\bar{H}}|\Phi_0\rangle = \bar{\bar{h}}_0 \\ &= \langle\Phi_0|\bar{H}\{e^{\hat{S}}\}|\Phi_0\rangle = \langle\Phi_0|\bar{H}|\Phi_0\rangle = \bar{h}_0 = \bar{E}_0^{(m)},\end{aligned} \tag{3.39}$$

proving the above assertion.

Third, we show that the zeros of $\bar{H}$ are preserved by the second similarity transformation, i.e., $\bar{h}^{p_1 p_2 \cdots p_n} = \bar{\bar{h}}^{p_1 p_2 \cdots p_n} =$

0 for $1 \leq n \leq m$ (see also Fig. 3.1). Starting with Eq. (3.37), we find

$$\begin{aligned}
\bar{\bar{h}}^{p_1 p_2 \cdots p_n} &= \sum_{k=0}^{\infty} (-1)^k \langle \Phi_{p_1 p_2 \cdots p_n} | \left(\{ e^{\hat{S}} - 1 \}^k \left(\bar{H} \{ e^{\hat{S}} \} \right)_{\mathrm{C}} \right)_{\mathrm{C}} | \Phi_0 \rangle = \sum_{k=0}^{\infty} (-1)^k \langle \Phi_{p_1 p_2 \cdots p_n} | \left(\{ e^{\hat{S}} - 1 \}^k \bar{H} \right)_{\mathrm{C}} | \Phi_0 \rangle \\
&= \langle \Phi_{p_1 p_2 \cdots p_n} | \bar{H} | \Phi_0 \rangle - \langle \Phi_{p_1 p_2 \cdots p_n} | \left(\{ \hat{S} \} \bar{H} \right)_{\mathrm{C}} | \Phi_0 \rangle + \frac{1}{2!} \langle \Phi_{p_1 p_2 \cdots p_n} | \left(\{ \hat{S}^2 \} \bar{H} \right)_{\mathrm{C}} | \Phi_0 \rangle + \ldots \\
&= \bar{h}^{p_1 p_2 \cdots p_n} - \sum_{l=1}^{n-1} \sum_{q_1, q_2, \cdots, q_l} \langle \Phi_{p_1 p_2 \cdots p_n} | \{ \hat{S} \} | \Phi_{q_1 q_2 \cdots q_l} \rangle \bar{h}^{q_1 q_2 \cdots q_l} \\
&\quad + \frac{1}{2!} \sum_{l=1}^{n-2} \sum_{q_1, q_2, \cdots, q_l} \langle \Phi_{p_1 p_2 \cdots p_n} | \{ \hat{S}^2 \} | \Phi_{q_1 q_2 \cdots q_l} \rangle \bar{h}^{q_1 q_2 \cdots q_l} + \ldots \\
&= 0,
\end{aligned} \tag{3.40}$$

where we have used Eq. (3.38) in the second equality and also in excluding $l = 0$ from the summations in the penultimate equality (which is further justified by noting that the $l = 0$ contributions are disconnected). The last equality follows from Eq. (3.4). To understand the upper bounds of the summations over l, note that each $\hat{S}$ is at least net one-mode excitation operator. This completes the proof of the preservation of zeros of $\bar{H}$ in $\bar{\bar{H}}$.

3.3.3 Amplitude and eigenvalue equations

The $\hat{S}$-amplitude equation can be expanded by substituting Eq. (3.36) into Eq. (3.18), yielding

$$\begin{aligned}
0 &= \langle \Phi_{p_1 p_2 \cdots p_n} | \left(\bar{H} \{ e^{\hat{S}} \} \right)_{\mathrm{C}} - \left(\{ e^{\hat{S}} - 1 \} \bar{\bar{H}} \right)_{\mathrm{C}} | \Phi_q \rangle \\
&= \langle \Phi_{p_1 p_2 \cdots p_n} | \left(\bar{H} \{ e^{\hat{S}} \} \right)_{\mathrm{C}} | \Phi_q \rangle \\
&\quad - \langle \Phi_{p_1 p_2 \cdots p_n} | \left(\{ e^{\hat{S}} - 1 \} \bar{\bar{H}} \right)_{\mathrm{C}} | \Phi_q \rangle.
\end{aligned} \tag{3.41}$$

The first term in the right-hand side can be simplified to

$$\begin{aligned}
\langle \Phi_{p_1 p_2 \cdots p_n} | \left(\bar{H} \{ e^{\hat{S}} \} \right)_{\mathrm{C}} | \Phi_q \rangle &= \langle \Phi_{p_1 p_2 \cdots p_n} | \bar{H} + \left(\bar{H} \hat{S} \right)_{\mathrm{C}} | \Phi_q \rangle \\
&\quad + \frac{1}{2!} \langle \Phi_{p_1 p_2 \cdots p_n} | \left(\bar{H} \{ \hat{S}^2 \} \right)_{\mathrm{C}} | \Phi_q \rangle + \ldots \\
&= \langle \Phi_{p_1 p_2 \cdots p_n} | \bar{H} + \left(\bar{H} \hat{S} \right)_{\mathrm{C}} | \Phi_q \rangle,
\end{aligned} \tag{3.42}$$

of which the second equality follows from

$$\{ \hat{S}^n \} | \Phi_q \rangle = \langle \Phi_q | \{ \hat{S}^{n-1} \} = 0 \ \ (n \geq 2), \tag{3.43}$$

because $\{ \hat{S}^n \}$ has at least n lowering and $2n$ raising operators and Φ_q is only a one-mode excited Hartree product.

The second term of Eq. (3.41) is expanded by inserting the resolution of the identity, leading to

$$\begin{aligned}
\langle\Phi_{p_1p_2\cdots p_n}|\left(\{e^{\hat{S}}-1\}\bar{\bar{H}}\right)_{\rm C}|\Phi_q\rangle &= \langle\Phi_{p_1p_2\cdots p_n}|\{\hat{S}+\frac{1}{2!}\hat{S}^2+\dots\}|\Phi_0\rangle\langle\Phi_0|\bar{\bar{H}}|\Phi_q\rangle \\
&\quad+\sum_r\langle\Phi_{p_1p_2\cdots p_n}|\{\hat{S}+\frac{1}{2!}\hat{S}^2+\dots\}|\Phi_r\rangle\langle\Phi_r|\bar{\bar{H}}-\bar{E}_0^{(m)}|\Phi_q\rangle \\
&\quad+\sum_{k=2}^{m}\sum_{r_1,r_2,\cdots,r_k}\langle\Phi_{p_1p_2\cdots p_n}|\{\hat{S}+\frac{1}{2!}\hat{S}^2+\dots\}|\Phi_{r_1r_2\cdots r_k}\rangle\langle\Phi_{r_1r_2\cdots r_k}|\bar{\bar{H}}|\Phi_q\rangle \\
&= \sum_r\langle\Phi_{p_1p_2\cdots p_n}|\{\hat{S}+\frac{1}{2!}\hat{S}^2+\dots\}|\Phi_r\rangle\langle\Phi_r|\bar{\bar{H}}-\bar{E}_0^{(m)}|\Phi_q\rangle \\
&= \sum_r\langle\Phi_{p_1p_2\cdots p_n}|\hat{S}|\Phi_r\rangle\langle\Phi_r|\bar{\bar{H}}-\bar{E}_0^{(m)}|\Phi_q\rangle. \qquad (3.44)
\end{aligned}$$

In the second equality, Eq. (3.38) is used to show that the first term in its left-hand side is zero (also the whole term is disconnected). In the same equality, Eq. (3.18) requires the last factor in the third term of the left-hand side to vanish. The last equality comes from Eq. (3.43).

In the very last factor, $\langle\Phi_r|\bar{\bar{H}}-\bar{E}_0^{(m)}|\Phi_q\rangle$, subtracts the constant part from the $\bar{\bar{H}}$ operator so that there is no disconnected contribution. It can be further simplified by using Eq. (3.43) as

$$\begin{aligned}
\langle\Phi_r|\bar{\bar{H}}-\bar{E}_0^{(m)}|\Phi_q\rangle &= \langle\Phi_r|\left(\bar{H}\{e^{\hat{S}}\}\right)_{\rm C}-\bar{E}_0^{(m)}|\Phi_q\rangle \\
&\quad-\langle\Phi_r|\left(\{e^{\hat{S}}-1\}\bar{\bar{H}}\right)_{\rm C}|\Phi_q\rangle \\
&= \langle\Phi_r|\bar{H}+\left(\bar{H}\hat{S}\right)_{\rm C}-\bar{E}_0^{(m)}|\Phi_q\rangle. \qquad (3.45)
\end{aligned}$$

Summarizing, the $\hat{S}$-amplitude equation (3.18) of STEOM-XVCCm can be rewritten in a vastly streamlined form as

$$\langle\Phi_{p_1p_2\cdots p_n}|\bar{\bar{H}}'|\Phi_q\rangle-\sum_r\langle\Phi_{p_1p_2\cdots p_n}|\hat{S}|\Phi_r\rangle\langle\Phi_r|\bar{\bar{H}}'|\Phi_q\rangle=0, \qquad (3.46)$$

for all q and all $p_1, p_2, \dots, p_n$ for each n ($2 \le n \le m$), with

$$\bar{\bar{H}}' \equiv \bar{H}+\left(\bar{H}\hat{S}\right)_{\rm C}-\bar{E}_0^{(m)}. \qquad (3.47)$$

The STEOM-XVCCm eigenvalue equation (3.24) also reduces to

$$\sum_q\langle\Phi_p|\bar{\bar{H}}'|\Phi_q\rangle c^q(\ell)=\bar{\omega}_\ell^{(m)}c^p(\ell). \qquad (3.48)$$

In other words, for the matrix elements of our interest, the $\{e^{\hat{S}}\}$ operator is linearized to $1+\hat{S}$, and the $\bar{\bar{H}}$ operator is

equal to $\bar{\bar{H}}'$ in the diagonalization space of STEOM-XVCC.

3.3.4 Diagrammatic derivation

Here, we illustrate a diagrammatic derivation of the working (matrix-algebraic) equations of the $\hat{S}$-amplitude and eigenvalue equations, taking STEOM-XVCC4 with a QFF as an example. The amplitudes of the $\bar{H}$ operator are assumed to be available from a preceding XVCC4 calculation.

We express the $\hat{S}$ operator truncated at $\hat{S}_{4,1}$ diagrammatically as

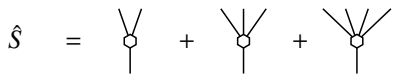

(3.49)

A hexagon vertex designates an amplitude of the $\hat{S}$ operator. The diagrammatic $\hat{S}_{2,1}$-, $\hat{S}_{3,1}$-, and $\hat{S}_{4,1}$-amplitude equations (3.46) are then written as

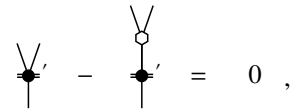

(3.50)

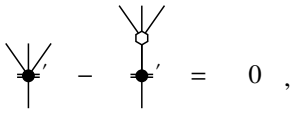

(3.51)

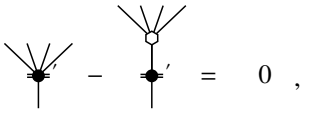

(3.52)

respectively, where a double-strike-through vertex with a " $'$ " denotes an amplitude of $\bar{\bar{H}}'$.

A diagrammatic representation of an amplitude of $\bar{\bar{H}}'$ [Eq. (3.47)] is obtained as a sum of the $\bar{H}$ diagrams and all possible contractions of $\bar{H}$ with one vertex of $\hat{S}$ from below:

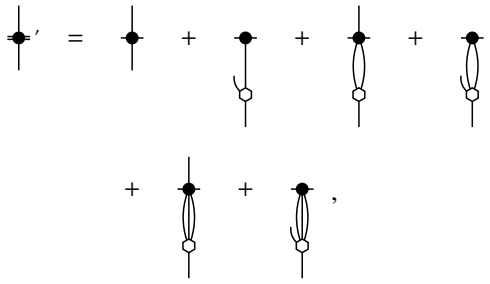

(3.53)

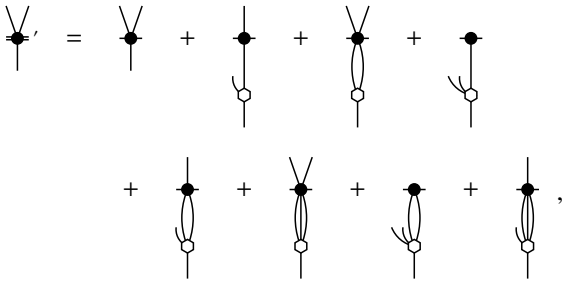

(3.54)

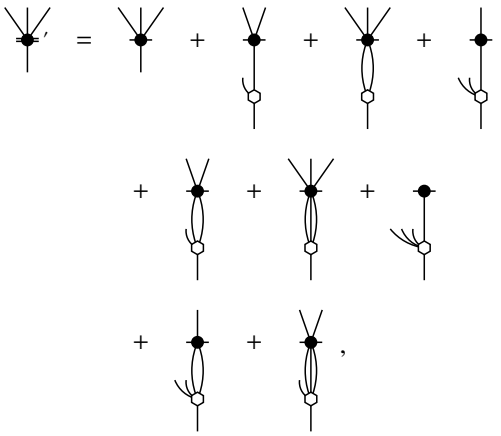

(3.55)

and

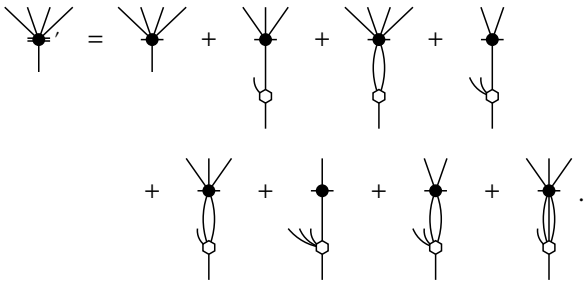

(3.56)

Substituting these into Eqs. (3.50)–(3.52), we can write the $\hat{S}$-amplitude equation in terms of the $\bar{H}$ and $\hat{S}$ vertices.

For instance, the $\hat{S}_{2,1}$-amplitude equation [Eq. (3.50)] is re-expressed as

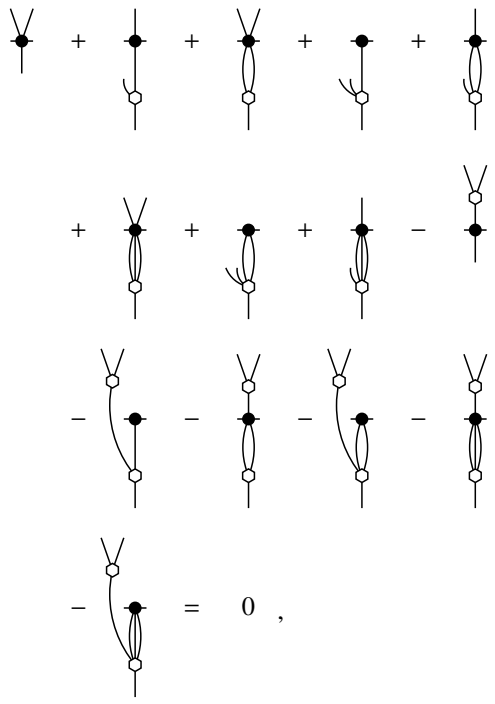

(3.57)

which can be further expanded in terms of the amplitudes of $\hat{H}$, $\hat{S}$, and $\hat{T}$ (not shown). Each of these diagrams is then interpreted algebraically by using the previously established rules for the XVCC and EOM-XVCC diagrams Table 2.2 of with new types of vertices translated appropriately. For instance, an algebraic interpretation of the tenth diagram in the above $\hat{S}_{2,1}$-amplitude equation is

$$\frac{1}{2!}\hat{P}(pq)\sum_{s,t}\bar{h}_s s_r^{st} s_t^{pq}, \tag{3.58}$$

with the vertex and line labeling illustrated in Fig. 3.2, where $\hat{P}(pq)$ is the permutation operator defined by Eq. (2.59). Repeating this for all diagrams in Eq. (3.57), we obtain the matrix-algebraic $\hat{S}_{2,1}$-amplitude equation of STEOM-

XVCC4, which reads

$$
\begin{aligned}
&\frac{1}{2!}\hat{P}(pq)\bar{h}_r^{pq} + \hat{P}(pq)\sum_s \bar{h}_s^p s_r^{sq} + \frac{1}{2!}\frac{1}{2!}\hat{P}(pq)\sum_{s,t}\bar{h}_{st}^{pq}s_r^{st} \\
&+\frac{1}{2!}\hat{P}(pq)\sum_s \bar{h}_s s_r^{spq} + \frac{1}{2!}\hat{P}(pq)\sum_{s,t}\bar{h}_{st}^{p}s_r^{stq} \\
&+\frac{1}{2!}\frac{1}{3!}\hat{P}(pq)\sum_{s,t,u}\bar{h}_{stu}^{pq}s_r^{stu} + \frac{1}{2!}\frac{1}{2!}\hat{P}(pq)\sum_{s,t}\bar{h}_{st}s_r^{stpq} \\
&+\frac{1}{3!}\hat{P}(pq)\sum_{s,t,u}\bar{h}_{stu}^{p}s_r^{stuq} - \frac{1}{2!}\hat{P}(pq)\sum_s \bar{h}_r^s s_s^{pq} \\
&-\frac{1}{2!}\hat{P}(pq)\sum_{s,t}\bar{h}_s s_r^{st}s_t^{pq} - \frac{1}{2!}\frac{1}{2!}\hat{P}(pq)\sum_{s,t,u}\bar{h}_{st}^{u}s_r^{st}s_u^{pq} \\
&-\frac{1}{2!}\frac{1}{2!}\hat{P}(pq)\sum_{s,t,u}\bar{h}_{st}s_r^{stu}s_u^{pq} - \frac{1}{2!}\frac{1}{3!}\hat{P}(pq)\sum_{s,t,u,v}\bar{h}_{stu}^{v}s_r^{stu}s_v^{pq} \\
&-\frac{1}{2!}\frac{1}{3!}\hat{P}(pq)\sum_{s,t,u,v}\bar{h}_{stu}s_r^{stuv}s_v^{pq} = 0,
\end{aligned}
\tag{3.59}
$$

which corresponds term-by-term with Eq. (3.57).

Equation (3.53) is also the kernel of the STEOM-XVCC4 eigenvalue equation (3.24), defining all elements of the matrix to be diagonalized. The matrix-algebraic interpretation of this equation is

$$
\begin{aligned}
\langle\Phi_p|\bar{\bar{H}}'|\Phi_q\rangle \quad = \quad & \bar{h}_q^p + \sum_r \bar{h}_r s_q^{rp} + \frac{1}{2!}\sum_{r,s}\bar{h}_{rs}^p s_q^{rs} \\
&+\frac{1}{2!}\sum_{r,s}\bar{h}_{rs}s_q^{rsp} + \frac{1}{3!}\sum_{r,s,t}\bar{h}_{rst}^p s_q^{rst} \\
&+\frac{1}{3!}\sum_{r,s,t}\bar{h}_{rst}s_q^{rstp},
\end{aligned}
\tag{3.60}
$$

according to the rules in Table 2.2 applied to the diagrammatic counterpart [Eq. (3.53)].

The singly similarity-transformed Hamiltonian $\bar{H}$ amplitudes that become necessary in XVCC4, EOM-XVCC4, and STEOM-XVCC4 are given explicitly in terms of the bare normal-ordered Hamiltonian $\hat{H}$ amplitudes and $\hat{T}$ amplitudes in Appendix C.

3.4 Comparisons of related theories

3.4.1 STEOM-XVCC versus EOM-XVCC

Here, we prove that the STEOM-XVCCm frequencies for the fundamentals are equal to those of the corresponding roots of EOM-XVCCm. Specifically, for a solution, $\hat{R}(\ell)$, of EOM-XVCCm, we show that there exists a STEOM-

XVCCm solution, $\hat{S}$ and $\{c^p(\ell)\}$, which bears the relation,

$$\sum_q \left(1 + \hat{S}\right)|\Phi_q\rangle c^q(\ell) = \hat{R}(\ell)|\Phi_0\rangle, \tag{3.61}$$

or equivalently,

$$\begin{aligned} r^q(\ell) &= c^q(\ell), & (3.62)\\ r^{p_1p_2\cdots p_n}(\ell) &= \sum_q s_q^{p_1p_2\cdots p_n} c^q(\ell) \ \ (n \geq 2), & (3.63) \end{aligned}$$

sharing the same eigenvalue, $\bar{\omega}_\ell^{(m)} = \bar{\bar{\omega}}_\ell^{(m)}$.

Substituting $\hat{R}(\ell)$ of Eq. (3.61) into the EOM-XVCCm amplitude equation (2.70), we find

$$\begin{aligned} \bar{\omega}_\ell^{(m)} r^{p_1p_2\cdots p_n}(\ell) &= \langle\Phi_{p_1p_2\cdots p_n}|\left(\bar{H}\hat{R}(\ell)\right)_{\rm C}|\Phi_0\rangle \\ &= \sum_q \langle\Phi_{p_1p_2\cdots p_n}|\bar{H}|\Phi_q\rangle c^q(\ell) \\ &\quad + \sum_q \langle\Phi_{p_1p_2\cdots p_n}|\left(\bar{H}\hat{S}\right)_{\rm C}|\Phi_q\rangle c^q(\ell) \\ &= \sum_q \langle\Phi_{p_1p_2\cdots p_n}|\bar{\bar{H}}'|\Phi_q\rangle c^q(\ell) \\ &= \sum_{q,r} \langle\Phi_{p_1p_2\cdots p_n}|\hat{S}|\Phi_r\rangle\langle\Phi_r|\bar{\bar{H}}'|\Phi_q\rangle c^q(\ell) \\ &= \sum_q s_q^{p_1p_2\cdots p_n} \bar{\bar{\omega}}_\ell^{(m)} c^q(\ell) \\ &= \bar{\bar{\omega}}_\ell^{(m)} r^{p_1p_2\cdots p_n}(\ell), \end{aligned} \tag{3.64}$$

for $n \geq 2$. For $n = 1$, we have

$$\begin{aligned} \bar{\omega}_\ell^{(m)} r^p(\ell) &= \langle\Phi_p|\left(\bar{H}\hat{R}(\ell)\right)_{\rm C}|\Phi_0\rangle \\ &= \sum_q \langle\Phi_p|\bar{H} - \bar{E}_0^{(m)}|\Phi_q\rangle c^q(\ell) \\ &\quad + \sum_q \langle\Phi_p|\left(\bar{H}\hat{S}\right)_{\rm C}|\Phi_q\rangle c^q(\ell) \\ &= \sum_q \langle\Phi_p|\bar{\bar{H}}'|\Phi_q\rangle c^q(\ell) \\ &= \bar{\bar{\omega}}_\ell^{(m)} c^p(\ell) = \bar{\bar{\omega}}_\ell^{(m)} r^p(\ell). \end{aligned} \tag{3.65}$$

These prove $\bar{\omega}_\ell^{(m)} = \bar{\bar{\omega}}_\ell^{(m)}$ for the ℓth fundamental, which also implies $\bar{E}_\ell^{(m)} = \bar{\bar{E}}_\ell^{(m)}$. Diagrammatic representations of identities (3.62) and (3.63) are depicted in Fig. 3.3.

This characterizes STEOM-XVCC*m* as a convenient root-homing algorithm of EOM-XVCC*m*, yielding identical frequencies of all fundamentals simultaneously from diagonalization of the $\bar{\bar{H}}'$ matrix in the singles space (see Fig. 3.1). The diagonalization of the $\bar{\bar{H}}$ matrix in a broader space gives different frequencies from EOM-XVCC*m*, as its matrix elements include additional size-extensive correlation effects captured by higher-order excitations generated by $\{e^{\hat{S}}\}$ from each excited state.

3.4.2 Vibrational versus electronic STEOM-CC

In *electronic* STEOM-CCSD, [97,99] we require the 1h-2h1p and 1p-1h2p blocks of $\bar{\bar{H}}$ to vanish, satisfying Eqs. (1.29) and (1.30). For practical reasons an active space is used, [99] but this aspect is not essential for the present discussion. As pointed out in Sec. 1.4, diagonalization of the resulting $\bar{\bar{H}}$ matrix in the IP or EA sector is identically equivalent [99] to IP- and EA-EOM-CCSD for principal IPs and EAs or the corresponding FSCC methods of Lindgren, Mukherjee, and coworkers. [105, 106, 108, 139] It is, therefore, possible to map $\hat{S}$ amplitudes onto the IP- or EA-EOM-CCSD eigenvector $\hat{R}^{\mp}(\ell)$ for the ℓth ionized (the minus sign) or electron-attached (the plus sign) state by the equations, [99]

$$\sum_i \left(1 + \hat{S}^-\right)|\Phi_i\rangle c^i(\ell) = \hat{R}^-(\ell)|\Phi_0\rangle, \tag{3.66}$$

$$\sum_a \left(1 + \hat{S}^+\right)|\Phi^a\rangle c^a(\ell) = \hat{R}^+(\ell)|\Phi_0\rangle, \tag{3.67}$$

where $\hat{S} = \hat{S}^- + \hat{S}^+$ with

$$\hat{S}^- = \frac{1}{2}\sum_{i,j,k,a} s_{ij}^{ak}\{\hat{a}^\dagger\hat{i}\hat{j}\hat{k}^\dagger\}, \tag{3.68}$$

$$\hat{S}^+ = \frac{1}{2}\sum_{a,b,c,i} s_{ic}^{ab}\{\hat{a}^\dagger\hat{b}^\dagger\hat{c}\hat{i}\}. \tag{3.69}$$

$\{c^i(\ell)\}$ or $\{c^a(\ell)\}$ is the ℓth eigenvector of the $\hat{H}_{\rm eff}$ matrix in the space of the 1h or 1p determinants, which, in turn, is a linearized form of $\bar{\bar{H}}$: [99]

$$\hat{H}_{\rm eff} = \bar{H} + \left(\bar{H}\hat{S}^{\mp}\right)_{\rm C} - E_{\rm CC}, \tag{3.70}$$

where $E_{\rm CC}$ is the CCSD ground-state energy. The linearization of $\{e^{\hat{S}}\}$ into $1 + \hat{S}$ occurs for the same reason as in the vibrational case: the $\{(\hat{S}^{\mp})^n\}$ operator ($n \geq 2$) contains n hole annihilation (particle creation) operators and its action on a 1h (1p) determinant results in zero. In STEOM-CCSD, this equivalence between the $\hat{S}$-amplitude equations and IP- and EA-EOM-CCSD was exploited to determine the $\hat{S}$ amplitudes with the latter methods, which are then used to construct $\bar{\bar{H}}$ in the singles-singles space for excitation energies.

Equations (3.66) and (3.67), which are a basis of the equivalence of the electronic $\hat{S}$-amplitude equation with IP- and EA-EOM-CCSD, mirror Eq. (3.61), which has been used to prove the equivalence of STEOM-XVCC and EOM-XVCC in Sec. 3.4.1. In both cases, the doubly similarity-transformed Hamiltonian is linearized in the space of diagonalization to compute $\{c^q(\ell)\}$ (for principal IPs and EAs or for fundamentals). In fact, the proof of the latter equivalence in Sec. 3.4.1 borrows heavily from Ref. 99 on the electronic case, and $\hat{H}_{\text{eff}}$ of the electronic STEOM-CC is isomorphic to $\bar{\bar{H}}'$ of the vibrational STEOM-XVCC. Taken together, STEOM-XVCC can be viewed as exactly analogous to the first step (the $\hat{S}$-amplitude equation) of electronic STEOM-CC, or more specifically, EA-EOM-CC. This view may be supported by noting that a vibrational excitation ($\hat{a}_p^\dagger$) is most analogous to an electron attachment ($\hat{a}^\dagger$), as opposed to, e.g., an electronic excitation ($\hat{a}^\dagger\hat{\imath}$), which seems to have no counterpart in vibration.

In the second step of the electronic STEOM-CC, we diagonalize the $\bar{\bar{H}}$ matrix in the space of singly excited determinants. The corresponding step does not exist in the vibrational STEOM-XVCC; recall that the diagonalization of the vibrational $\bar{\bar{H}}'$ matrix in the space of one-mode excited products is more analogous to the diagonalization of the electronic $\hat{H}_{\text{eff}}$ matrix in the 1p determinant space as mentioned above.

The $\bar{\bar{H}}$ operator of the electronic STEOM-CC in the space of singly excited determinants is not linearized. This is because such a determinant Φ_i^a has a two-spinorbital difference from the ground-state determinant Φ_0, and a non-linear operator such as $\{\hat{S}^+\hat{S}^-\}$ or $\{\hat{S}^-\hat{S}^+\}$ can act on it to yield a non-vanishing result. These nonlinear excitations caused by $\{e^{\hat{S}}\}$ fold in higher-order correlation effects in the doubly similarity-transformed Hamiltonian $\bar{\bar{H}}$ amplitudes, making the STEOM-CCSD excitation energies differ from and, in many cases (such as for charge-transfer excitations), distinctly superior to the EOM-CCSD excitation energies. [97, 99] In contrast, the vibrational STEOM-XVCC frequencies are identical to the corresponding EOM-XVCC frequencies, as shown above. This argument may attach greater significance and interest to diagonalization of the vibrational $\bar{\bar{H}}$ outside the space of one-mode excited products where $\{e^{\hat{S}}\}$ no longer truncates at the linear term. For example, one could diagonalize $\bar{\bar{H}}$ over the space of two-mode excitations to obtain frequencies of overtones and combinations that are different from the corresponding EOM-XVCC frequencies. This is analogous to the calculation of double electron affinites in DEA-STEOM-CC. [97] Since $\bar{\bar{H}}$ does not have an exact block triangular structure, this is an approximation, but it is expected that the coupling to higher excitations is already highly suppressed by the sequential similarity transformations. The neglected coupling can always be accounted for by diagonalizing $\bar{\bar{H}}$ in the space of two- through m-mode excitations which may define an *extended*-STEOM-XVCCm method. [101]

FSCC and IP- or EA-EOM-CC can be formulated alternatively by the eigenvalue-independent partitioning technique of Sinha *et al.*, [140] which shares features similar to STEOM-CC. [99] At the level equivalent to EA-EOM-CCSD, in this technique, the $\bar{\bar{H}}$ matrix in the EA sector (denoted by $\bar{\bar{\mathbf{H}}}^{(\text{EA})}$) is partitioned into components in the 1p

(P) and 1h2p (Q) spaces as

$$\bar{\bar{\mathbf{H}}}^{(\mathrm{EA})} = \begin{bmatrix} \bar{\bar{\mathbf{H}}}_{PP} & \bar{\bar{\mathbf{H}}}_{PQ} \\ \bar{\bar{\mathbf{H}}}_{QP} & \bar{\bar{\mathbf{H}}}_{QQ} \end{bmatrix} \tag{3.71}$$

$$= \begin{bmatrix} \mathbf{1}_{PP} & \mathbf{0} \\ -\mathbf{S}^{+}_{QP} & \mathbf{1}_{QQ} \end{bmatrix} \begin{bmatrix} \bar{\mathbf{H}}_{PP} & \bar{\mathbf{H}}_{PQ} \\ \bar{\mathbf{H}}_{QP} & \bar{\mathbf{H}}_{QQ} \end{bmatrix} \begin{bmatrix} \mathbf{1}_{PP} & \mathbf{0} \\ \mathbf{S}^{+}_{QP} & \mathbf{1}_{QQ} \end{bmatrix}, \tag{3.72}$$

where $\mathbf{S}^{+}_{QP}$ is the matrix representation of $\hat{S}^{+}$, whose elements are determined such that $\bar{\bar{\mathbf{H}}}_{QP} = \mathbf{0}$, which is expanded as

$$\mathbf{0} = \bar{\bar{\mathbf{H}}}_{QP} \tag{3.73}$$

$$= \bar{\mathbf{H}}_{QP} + \bar{\mathbf{H}}_{QQ}\mathbf{S}^{+}_{QP} - \mathbf{S}^{+}_{QP}\left(\bar{\mathbf{H}}_{PP} + \bar{\mathbf{H}}_{PQ}\mathbf{S}^{+}_{QP}\right) \tag{3.74}$$

$$= \bar{\bar{\mathbf{H}}}'_{QP} - \mathbf{S}^{+}_{QP}\bar{\bar{\mathbf{H}}}'_{PP}, \tag{3.75}$$

with

$$\bar{\bar{\mathbf{H}}}' = \bar{\mathbf{H}} + \bar{\mathbf{H}}\mathbf{S}^{+}_{QP} - E_{\mathrm{CC}}\mathbf{1}. \tag{3.76}$$

The principal EAs are obtained as eigenvalues of $\bar{\bar{\mathbf{H}}}'_{PP}$. It is evident that Eqs. (3.75) and (3.76) are the matrix representations of the *electronic* STEOM-CCSD working equations, whose vibrational counterparts are Eqs. (3.46) and (3.47), respectively. This technique, therefore, can be viewed as utilizing the linearization of $\{e^{\hat{S}}\}$ in the QP and PP projections of $\bar{\bar{H}}$ from the outset. STEOM-XVCCm can also be reformulated as the eigenvalue-independent partitioning technique with the P space spanning all one-mode excited products and Q all two- to m-mode excited products.

3.4.3 STEOM-XVCC versus MBGF

STEOM-XVCCm is a one-mode theory that is convergent toward the exact solution of the vibrational Schrödinger equation with increasing m. It should, therefore, bear some formal relationship with the vibrational MBGF, which is also an exact one-mode theory. XVMP2 (Ref. 14) is an example of the vibrational MBGF with its self-energy approximated by a second-order perturbation theory. Here, we elucidate the relationship between these two methods.

The exact one-mode Green's function is an N-by-N matrix (N is the number of modes), whose elements are

defined [141] by

$$\{\mathbf{G}(\nu)\}_q^p = \sum_n \frac{\langle\Psi_0|\hat{A}_p|\Psi_n\rangle\langle\Psi_n|\hat{A}_q^\dagger|\Psi_0\rangle}{\nu-(E_n-E_0)} + \sum_n \frac{\langle\Psi_0|\hat{A}_q^\dagger|\Psi_n\rangle\langle\Psi_n|\hat{A}_p|\Psi_0\rangle}{-\nu-(E_n-E_0)}, \tag{3.77}$$

where Ψ_n and E_n are the exact wave function and energy of the nth vibrational state and $\hat{A}_p = \hat{A}_p^\dagger = \hat{a}_p + \hat{a}_p^\dagger$. The first and second terms are the retarded and advanced Green's functions, respectively. We seek poles of the Green's function, i.e., the frequency ν that is equal to one of the exact vibrational transition frequencies, $E_n - E_0$, causing a divergence in $\mathbf{G}(\nu)$.

This Green's function is subject to a Feynman–Dyson perturbation expansion [141] with the vibrational analog of the Møller–Plesset partitioning [13] of the normal-ordered Hamiltonian: $\hat{H} = \hat{H}^{(0)} + \hat{H}^{(1)}$. With the SCP reference in a QFF, the perturbation operator $\hat{H}^{(1)}$ is essentially the sum of the normal-ordered cubic and quartic force-constant operators. The zeroth-order Green's function then reduces to

$$\{\mathbf{G}^{(0)}(\nu)\}_q^p = \frac{\delta_{pq}}{\nu-\omega_p} + \frac{\delta_{pq}}{-\nu-\omega_p} = \delta_{pq}\frac{2\omega_p}{\nu^2-\omega_p^2}. \tag{3.78}$$

Defining the self-energy $\mathbf{\Sigma}(\nu)$ by the Dyson equation,

$$\mathbf{G}(\nu) = \mathbf{G}^{(0)}(\nu) + \mathbf{G}^{(0)}(\nu)\mathbf{\Sigma}(\nu)\mathbf{G}(\nu), \tag{3.79}$$

we find the exact transition frequency ν to be a solution of the one-mode eigenvalue equation (inverse Dyson equation) [14] of the form

$$\sum_q \left(\delta_{pq}\frac{\omega_p}{2} + \{\mathbf{\Sigma}(\nu)\}_q^p\right)c^q = \frac{\nu^2}{2\omega_p}c^p, \tag{3.80}$$

where $2\omega_i\{\mathbf{\Sigma}(\nu)\}_q^p$ serves as an effective anharmonic correction to the pqth element of the quadratic force-constant matrix. The eigenvector $\{c^p\}$ defines an anharmonicity-dressed set of coordinates, which may be called the Dyson coordinates, [11] i.e., a vibrational analogue of the Dyson orbitals. [142, 143]

Expanding the self-energy in a perturbation series with the SCP reference in a QFF, we find the second-order correction to be diagrammatically expressed [14] as

$\{\mathbf{\Sigma}^{(2)}(\nu)\}_q^p =$ 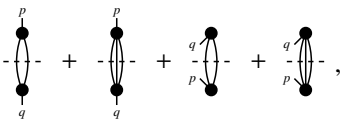 (3.81)

which is algebraically interpreted [14] as

$$\begin{aligned}\{\mathbf{\Sigma}^{(2)}(\nu)\}_q^p &= \frac{1}{2!}\sum_{r,s}\frac{h_{rs}^p h_q^{rs}}{\nu-\omega_r-\omega_s} \\ &+\frac{1}{3!}\sum_{r,s,t}\frac{h_{rst}^p h_q^{rst}}{\nu-\omega_r-\omega_s-\omega_t} \\ &+\frac{1}{2!}\sum_{r,s}\frac{h_{qrs}h^{prs}}{-\nu-\omega_r-\omega_s} \\ &+\frac{1}{3!}\sum_{r,s,t}\frac{h_{qrst}h^{prst}}{-\nu-\omega_r-\omega_s-\omega_t},\end{aligned} \tag{3.82}$$

in the same order of the terms as the diagrammatic equation. A dashed line, called the resolvent line, in each diagram represents a denominator that depends on the root (ν) of the Dyson equation. Note that the first two diagrams (terms) have $+\nu$ in their denominators and originate from the retarded Green's function, whereas the other two with $-\nu$ in their denominators come from the advanced Green's function.

Solving Eq. (3.79) with its $\mathbf{\Sigma}(\nu)$ approximated by $\mathbf{\Sigma}^{(2)}(\nu)$ for ν, we obtain the second-order approximation to the vibrational frequencies in XVMP2. [14] In the original paper, we invoked the diagonal approximation,

$$\{\mathbf{\Sigma}^{(2)}(\nu)\}_q^p \approx \delta_{pq}\{\mathbf{\Sigma}^{(2)}(\nu)\}_p^p, \tag{3.83}$$

without or further with the frequency-independent ("non-self-consistent") approximation,

$$\{\mathbf{\Sigma}^{(2)}(\nu)\}_q^p \approx \delta_{pq}\{\mathbf{\Sigma}^{(2)}(\omega_p)\}_p^p. \tag{3.84}$$

To clarify the relationship of STEOM-XVCC to XVMP2, let us point out that the following alternative, definition [141] (distinguished by a prime) of the exact one-mode Green's function also contains the entire information about the exact vibrational spectrum:

$$\{\mathbf{G}'(\nu)\}_q^p = \sum_n \frac{\langle\Psi_0|\hat{a}_p|\Psi_n\rangle\langle\Psi_n|\hat{a}_q^\dagger|\Psi_0\rangle}{\nu-(E_n-E_0)}, \tag{3.85}$$

with the corresponding zeroth-order Green's function,

$$\{\mathbf{G}'^{(0)}(\nu)\}_q^p = \frac{\delta_{pq}}{\nu-\omega_p}. \tag{3.86}$$

The exact one-mode eigenvalue (inverse Dyson) equation then reads

$$\sum_q \left(\delta_{pq}\omega_p + \{\mathbf{\Sigma}'(\nu)\}_q^p\right) c^q = \nu c^p, \tag{3.87}$$

where $\{\mathbf{\Sigma}'(\nu)\}_q^p$ represents an anharmonic correction to the pqth element of the Hamiltonian matrix (or roughly a SCP frequency) and the eigenvector $\{c^q\}$ relates to (if not immediately defines) the Dyson coordinates. In the diagonal approximation, the above equation reduces to

$$\omega_p + \{\mathbf{\Sigma}'(\nu)\}_p^p = \nu. \tag{3.88}$$

In the diagonal, frequency-independent approximation, it further simplifies to

$$\omega_p + \{\mathbf{\Sigma}'(\omega_p)\}_p^p = \nu. \tag{3.89}$$

We now show how this form of the Dyson equation maps onto the STEOM-XVCC eigenvalue equation (3.48) with the corresponding self-energy containing the same diagrammatic contributions as Eq. (3.81) at the second order, but in frequency-independent approximation. More specifically, the second-order approximation of $\langle\Phi_p|\bar{\bar{H}}'|\Phi_q\rangle$ of Eq. (3.47) or (3.53) corresponds to $\delta_{pq}\omega_p + \{\mathbf{\Sigma}'^{(2)}(\nu)\}_q^p$ in the above equation, where $\{\mathbf{\Sigma}'^{(2)}(\nu)\}_q^p$ is given by Eq. (3.82) or (3.81) with ν replaced by an appropriate reference frequency (ω_p or ω_q), i.e.,

$$\begin{aligned}
\{\mathbf{\Sigma}'^{(2)}\}_q^p \quad = \quad & \frac{1}{2!}\sum_{r,s}\frac{h_{rs}^p h_q^{rs}}{\omega_q - \omega_r - \omega_s} \\
& + \frac{1}{3!}\sum_{r,s,t}\frac{h_{rst}^p h_q^{rst}}{\omega_q - \omega_r - \omega_s - \omega_t} \\
& + \frac{1}{2!}\sum_{r,s}\frac{h_{qrs} h^{prs}}{-\omega_p - \omega_r - \omega_s} \\
& + \frac{1}{3!}\sum_{r,s,t}\frac{h_{qrst} h^{prst}}{-\omega_p - \omega_r - \omega_s - \omega_t},
\end{aligned} \tag{3.90}$$

in a QFF. The derivation of this will be given below.

The zeroth-order approximation to $\bar{\bar{H}}'$ is simply

$$\langle\Phi_p|\bar{\bar{H}}'^{(0)}|\Phi_q\rangle = \langle\Phi_p|\hat{H}|\Phi_q\rangle = \delta_{pq}\omega_p, \tag{3.91}$$

in the SCP reference. The first-order correction $\langle\Phi_p|\bar{\bar{H}}'^{(1)}|\Phi_q\rangle$ is zero. Starting with Eq. (3.47), we find its second-order

correction formally written as

$$\langle \Phi_p | \bar{\bar{H}}'^{(2)} | \Phi_q \rangle = \langle \Phi_p | \bar{H}^{(2)} + \left(\bar{H}^{(1)} \hat{S}^{(1)} \right)_{\mathrm{C}} | \Phi_q \rangle. \tag{3.92}$$

Again, using STEOM-XVCC4 in a QFF as a concrete example, the diagrammatic expression of the above reads

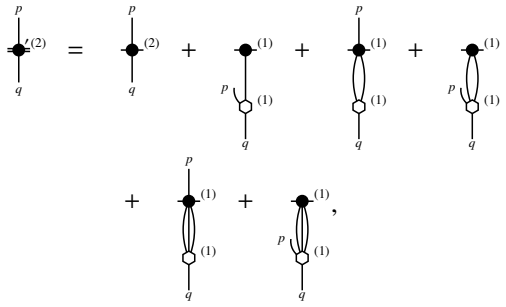

(3.93)

where a parenthesized integer denotes the perturbation order of each vertex. Note that the perturbation order of a $\hat{T}$ and $\hat{S}$ amplitude is at least one. The second and fourth terms in the right-hand side vanish in the SCP reference because

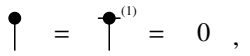

(3.94)

and

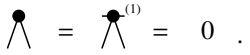

(3.95)

The first term in the right-hand side is expanded as

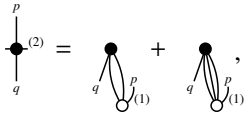

(3.96)

in which an open-circle vertex with '(1)' represents a first-order perturbation correction to the $\hat{T}$ amplitude. It satisfies the first-order approximations to the $\hat{T}$-amplitude equations [Eqs. (A.4) and (A.5)], which are depicted diagrammatically

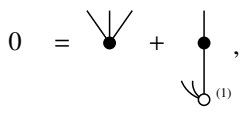

(3.97)

and

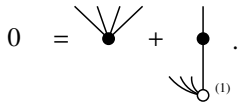

(3.98)

The first-order $\hat{T}_3$-amplitude equation is algebraically interpreted as

$$0 = \frac{1}{3!}\hat{P}(pqr)h^{pqr} + \frac{1}{2!}\hat{P}(pqr)\sum_s h^r_s(\tau^{(1)})^{pqs}, \tag{3.99}$$

which can be immediately solved:

$$(\tau^{(1)})^{pqr} = \frac{h^{pqr}}{-\omega_p - \omega_q - \omega_r}, \tag{3.100}$$

where in the SCP reference $h^r_s = \delta_{rs}\omega_r$. This is expressed diagrammatically as

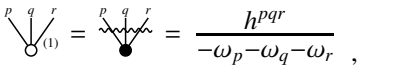

(3.101)

where the wiggly line is a frequency-independent resolvent line. Likewise, the second-order approximation to the $\hat{T}_4$ amplitude is

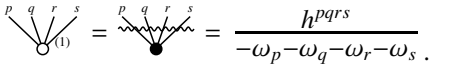

(3.102)

Substitution of these expressions into Eq. (3.96) leads to the last two terms of Eq. (3.90).

The remaining, nonzero terms of Eq. (3.93) involve the first-order corrections to the $\hat{S}$ amplitudes, which satisfy the first-order approximation to the $\hat{S}$-amplitude equation (3.46):

$$\begin{aligned}&\langle\Phi_{p_1\cdots p_n}|\bar{\bar{H}}'^{(1)}|\Phi_q\rangle - \sum_r \langle\Phi_{p_1\cdots p_n}|\hat{S}^{(1)}_{n,1}|\Phi_r\rangle\langle\Phi_r|\bar{\bar{H}}'^{(0)}|\Phi_q\rangle = \\ &\langle\Phi_{p_1\cdots p_n}|\bar{\bar{H}}'^{(1)}|\Phi_q\rangle - (s^{(1)})^{p_1\cdots p_n}_q\omega_q = 0.\end{aligned} \tag{3.103}$$

where we have used Eq. (3.91).

In the case of STEOM-XVCC4 in a QFF, the corresponding diagrammatic equations (3.50)–(3.52) reduce to

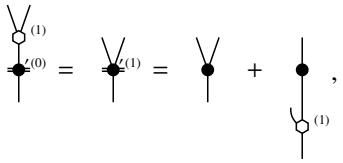

(3.104)

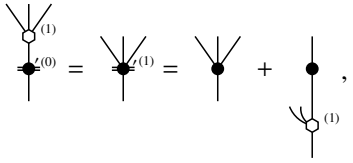

(3.105)

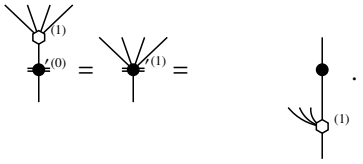

(3.106)

The first of the above three equations can be algebraically interpreted as

$$\begin{aligned} \frac{1}{2!}\hat{P}(pq)(s^{(1)})_r^{pq}\omega_r &= \frac{1}{2!}\hat{P}(pq)h_r^{pq} \\ &\quad +\hat{P}(pq)\sum_s h_s^q(s^{(1)})_r^{ps}, \end{aligned} \tag{3.107}$$

which can be readily solved for the first-order correction to $\hat{S}_{2,1}$:

$$(s^{(1)})_r^{pq} = \frac{h_r^{pq}}{\omega_r - \omega_p - \omega_q}. \tag{3.108}$$

The above equation may be diagrammatically depicted as

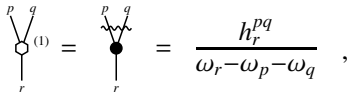

(3.109)

where, again, a wiggly line is a frequency-independent resolvent line, understood to be interpreted algebraically as

indicated above. Likewise, the first-order corrections to the $\hat{S}_{3,1}$ and $\hat{S}_{4,1}$ are

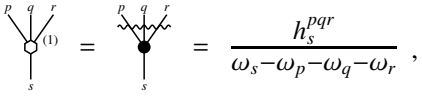

$$= \frac{h_s^{pqr}}{\omega_s - \omega_p - \omega_q - \omega_r} \,, \tag{3.110}$$

and

$$= \quad 0 \quad . \tag{3.111}$$

The latter is a consequence of the QFF approximation to the PES and causes the last term in Eq. (3.93) to vanish. Substituting them in Eq. (3.96), we recover the first two terms of Eq. (3.90).

Together, the diagrammatic expression of the second-order approximation of STEOM-XVCC4 (QFF) effective Hamiltonian $\bar{\tilde{H}}'^{(2)}$ in the space of singles reads

$\{\mathbf{\Sigma}'^{(2)}(\nu)\}_q^p =$

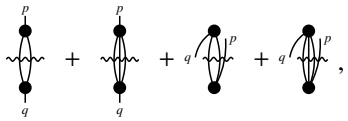

, (3.112)

whose algebraic interpretation is Eq. (3.90). This diagrammatic equation differs from the XVMP2 self-energy [Eq. (3.81)] only in the resolvent lines. The former is a frequency-independent approximation to the latter.

Both the Feynman–Dyson (XVMPn) perturbation series [14] of the self-energy and the perturbation approximation to the STEOM-XVCC discussed here are convergent at the exact solutions of the vibrational Schrödinger equation, but at different rates. The frequency-independent approximation is inherent in the latter, which should somehow recuperate the effect of frequency dependence in the self-energy in a perturbative manner. It may be speculated that this is achieved through the linked-disconnected diagrams in higher-order perturbation corrections of STEOM-XVCC just as in IP- and EA-EOM-CC or ΔMPn for electrons. [134, 144]

3.5 Approximate STEOM-XVCC methods

Inspired by the relationship between STEOM-XVCC and MBGF discussed in Sec. 3.4.3, we introduce three approximations to STEOM-XVCC: the diagonal, perturbation, and frequency-independent approximations.

3.5.1 Diagonal approximation

The diagonal approximation to STEOM-XVCC neglects all off-diagonal elements of $\langle\Phi_p|\bar{\bar{H}}'|\Phi_q\rangle$ both in the $\hat{S}$-amplitude equation (3.46) and eigenvalue equation (3.48). We call this approximation '1' and the method 1-STEOM-XVCCm. The 1-STEOM-XVCC frequencies are the diagonal elements of the singles block of the doubly similarity-transformed Hamiltonian,

$$\bar{\bar{\omega}}_q^{[1]} \quad = \quad \langle\Phi_q|\bar{\bar{H}}'|\Phi_q\rangle, \tag{3.113}$$

where the '[1]' superscript merely indicates approximation 1 and should not be taken as a perturbation order. The amplitude equation also reduces to

$$\begin{aligned}&\langle\Phi_{p_1\cdots p_n}|\bar{\bar{H}}'|\Phi_q\rangle - \langle\Phi_{p_1\cdots p_n}|\hat{S}^{[1]}|\Phi_q\rangle\langle\Phi_q|\bar{\bar{H}}'|\Phi_q\rangle = \\ &\langle\Phi_{p_1\cdots p_n}|\bar{\bar{H}}'|\Phi_q\rangle - (s^{[1]})_q^{p_1\cdots p_n}\bar{\bar{\omega}}_q^{[1]} = 0,\end{aligned} \tag{3.114}$$

where $\bar{\bar{H}}'$ is defined by Eq. (3.47) with $\hat{S}^{[1]}$ that is the solution of the above equation. The frequency $\bar{\bar{\omega}}_q^{[1]}$ is no longer equal to the corresponding EOM-XVCCm frequency $\bar{\omega}_q$ and is, therefore, dressed with a double overbar in addition to the '[1]' superscript. Diagrammatically, the $\hat{S}$-amplitude equations of the 1-STEOM-XVCC4 method in a QFF are expressed as

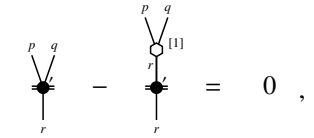

(3.115)

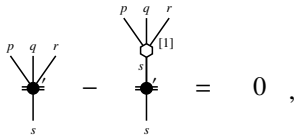

(3.116)

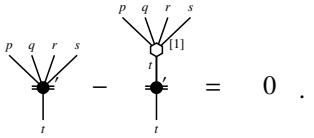

(3.117)

The internal line in the second term is no longer associated with a summation over the mode index, but instead is restricted to the downward external mode index.

While this approximation does not reduce the overall size dependence of arithmetic operation cost (scaling), which is $O(N^7)$ with the number of modes N for STEOM-XVCC4 in a QFF (see below), it decouples the $\hat{S}$-amplitude

equation into individual equations for each fundamental, which are still nonlinear, but allow a subset of roots to be determined. In STEOM-XVCC*m* without the diagonal approximation, on the other hand, all roots must be determined simultaneously.

3.5.2 Perturbation approximation

Here, we apply a first-order perturbation approximation only to the left-hand side of the $\hat{S}$-amplitude equation of 1-STEOM-XVCC*m* [Eq. (3.114)] by partitioning the singly similarity-transformed Hamiltonian, $\bar{H} = \bar{H}^{(0)} + \bar{H}^{(1)}$, where $\bar{H}^{(0)}$ consists of zero- and diagonal two-mode operators of $\bar{H}$ (as opposed to $\hat{H}$ in Sec. 3.4.3) We call this approximation '2' and the method 2-STEOM-XVCC*m*. The frequencies of this method are given by

$$\bar{\bar{\omega}}_q^{[2]} = \langle \Phi_q | \bar{\bar{H}}' | \Phi_q \rangle, \tag{3.118}$$

which is formally the same as in the diagonal approximation, but $\bar{\bar{H}}'$ is defined with the $\hat{S}^{[2]}$ that satisfies

$$\begin{aligned} &\langle \Phi_{p_1 \cdots p_n} | \bar{\bar{H}}'^{[2]} | \Phi_q \rangle - \langle \Phi_{p_1 \cdots p_n} | \hat{S}^{[2]} | \Phi_q \rangle \langle \Phi_q | \bar{\bar{H}}' | \Phi_q \rangle = \\ &\langle \Phi_{p_1 \cdots p_n} | \bar{\bar{H}}'^{[2]} | \Phi_q \rangle - (s^{[2]})_q^{p_1 \cdots p_n} \bar{\bar{\omega}}_q^{[2]} = 0, \end{aligned} \tag{3.119}$$

where $\bar{\bar{H}}'^{[2]}$ is the first-order perturbation correction to $\bar{\bar{H}}'$, i.e.,

$$\begin{aligned} \langle \Phi_{p_1 \cdots p_n} | \bar{\bar{H}}'^{[2]} | \Phi_q \rangle &= \langle \Phi_{p_1 \cdots p_n} | \bar{H}^{(1)} | \Phi_q \rangle \\ &\quad + \langle \Phi_{p_1 \cdots p_n} | \left(\bar{H}^{(0)} \hat{S}^{[2]} \right)_{\mathrm{C}} | \Phi_q \rangle \\ &= \frac{1}{n!} \hat{P}(p_1 \cdots p_n) \bar{h}_q^{p_1 \cdots p_n} \\ &\quad + \hat{P}(p_1 \cdots p_n) \sum_{p_1} \bar{h}_{p_1}^{p_1} (s^{[2]})_q^{p_1 \cdots p_n}, \end{aligned} \tag{3.120}$$

for $n \geq 2$. Again, the superscript '[2]' designates approximation 2 and has nothing to do with a perturbation order. The diagonal approximation is always implied in approximation 2.

For 2-STEOM-XVCC4 in a QFF, these amplitude equations are diagrammatically depicted as

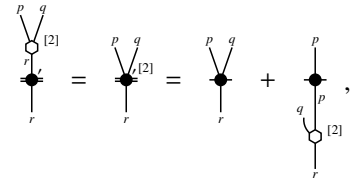

(3.121)

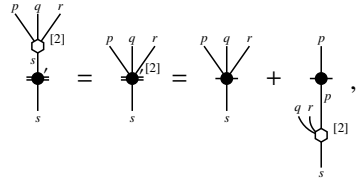

(3.122)

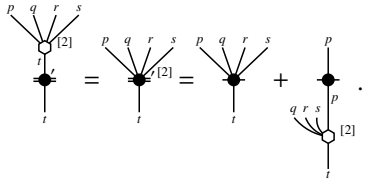

(3.123)

The first of the three equations is algebraically interpreted as

$$\frac{1}{2!}\hat{P}(pq)(s^{[2]})_r^{pq}\bar{\bar{\omega}}_r^{[2]} \quad = \quad \frac{1}{2!}\hat{P}(pq)\bar{h}_r^{pq} + \hat{P}(pq)\bar{h}_q^{q}(s^{[2]})_r^{pq}, \tag{3.124}$$

which can be solved analytically:

$$(s^{[2]})_r^{pq} = \frac{\bar{h}_r^{pq}}{\bar{\bar{\omega}}_r^{[2]} - \bar{h}_p^{p} - \bar{h}_q^{q}}. \tag{3.125}$$

The amplitudes of $\hat{S}^{[2]}_{3,1}$ and $\hat{S}^{[2]}_{4,1}$ are likewise obtained without numerically solving nonlinear equations, but by a one-shot evaluation of the general formula:

$$(s^{[2]})_q^{p_1 p_2 \cdots p_n} = \frac{\bar{h}_q^{p_1 p_2 \cdots p_n}}{\bar{\bar{\omega}}_q^{[2]} - \hat{P}(p_1 p_2 \cdots p_n)\bar{h}_{p_1}^{p_1}}. \tag{3.126}$$

Substituting this into Eq. (3.60), we find the 2-STEOM-XVCC4 (QFF) frequencies to be written in a closed form:

$$\begin{aligned}
\bar{\bar{\omega}}_s^{[2]} &= \bar{h}_s^s + \sum_p \frac{\bar{h}_p \bar{h}_s^{ps}}{\bar{\bar{\omega}}_s^{[2]} - \bar{h}_p^p - \bar{h}_s^s} \\
&+ \frac{1}{2!} \sum_{p,q} \frac{\bar{h}_{pq}^s \bar{h}_s^{pq}}{\bar{\bar{\omega}}_s^{[2]} - \bar{h}_p^p - \bar{h}_q^q} \\
&+ \frac{1}{2!} \sum_{p,q} \frac{\bar{h}_{pq} \bar{h}_s^{pqs}}{\bar{\bar{\omega}}_s^{[2]} - \bar{h}_p^p - \bar{h}_q^q - \bar{h}_s^s} \\
&+ \frac{1}{3!} \sum_{p,q,r} \frac{\bar{h}_{pqr}^s \bar{h}_s^{pqr}}{\bar{\bar{\omega}}_s^{[2]} - \bar{h}_p^p - \bar{h}_q^q - \bar{h}_r^r} \\
&+ \frac{1}{3!} \sum_{p,q,r} \frac{\bar{h}_{pqr} \bar{h}_s^{pqrs}}{\bar{\bar{\omega}}_s^{[2]} - \bar{h}_p^p - \bar{h}_q^q - \bar{h}_r^r - \bar{h}_s^s},
\end{aligned} \tag{3.127}$$

which may be viewed as an inverse Dyson equation (3.88) in the diagonal approximation, but with frequency-dependent denominators. The right-hand side can be evaluated at an $O(N^5)$ arithmetic-operation cost (where N is the number of modes) for one mode or at an $O(N^6)$ cost for all (N) fundamentals.

Similarity of this approximation to XVMP2 is evident. Equations (3.121)–(3.123) mirror Eqs. (3.104)–(3.106), which are used to underscore the relationship between STEOM-XVCC and XVMP2 in Sec. 3.4.3. The major difference, however, is the presence of $\bar{\bar{\omega}}_s^{[2]}$ in the denominators, reviving the frequency dependence in the third and fifth terms in the right-hand side of Eq. (3.127), which now resemble more closely the first two terms of the frequency-dependent second-order self-energy of Eq. (3.82). This, in turn, permits multiple solutions for a single equation (3.127), which is one of the important advantages of the inverse Dyson equation (3.87). The other two terms of Eq. (3.82) are hidden in $\bar{h}_s^s$ (the first term) of Eq. (3.127), which still lacks frequency dependence.

3.5.3 Frequency-independent approximation

If we apply the first-order perturbation approximation with the Hamiltonian partitioning $\bar{H} = \bar{H}^{(0)} + \bar{H}^{(1)}$ consistently to both the left- and right-hand sides of the 1-STEOM-XVCC amplitude equations (3.114), we obtain

$$\begin{aligned}
&\langle \Phi_{p_1 \cdots p_n} | \bar{\bar{H}}'^{[2]} | \Phi_q \rangle - \langle \Phi_{p_1 \cdots p_n} | \hat{S}^{[3]} | \Phi_q \rangle \langle \Phi_q | \bar{H}^{(0)} | \Phi_q \rangle = \\
&\langle \Phi_{p_1 \cdots p_n} | \bar{\bar{H}}'^{[2]} | \Phi_q \rangle - (s^{[3]})_q^{p_1 \cdots p_n} \bar{h}_q^q = 0,
\end{aligned} \tag{3.128}$$

which has a solution for the $\hat{S}^{[3]}$ amplitudes:

$$(s^{[3]})_q^{p_1 p_2 \cdots p_n} = \frac{\bar{h}_q^{p_1 p_2 \cdots p_n}}{\bar{h}_q^q - \hat{P}(p_1 p_2 \cdots p_n) \bar{h}_{p_1}^{p_1}}. \tag{3.129}$$

Substitution of this into Eq. (3.113), leads to the 3-STEOM-XVCC frequencies as

$$\bar{\tilde{\omega}}_q^{[3]} = \langle \Phi_q | \bar{\tilde{H}}' | \Phi_q \rangle, \tag{3.130}$$

where $\bar{\tilde{H}}'$ is constructed with the $\hat{S}^{[3]}$ amplitudes. The 3-STEOM-XVCC method is a frequency-independent approximation to 2-STEOM-XVCC or a more consistent second-order perturbation approximation to 1-STEOM-XVCC.

The 3-STEOM-XVCC4 frequencies in a QFF are, therefore, also given in a closed form:

$$\begin{aligned}
\bar{\tilde{\omega}}_s^{[3]} = {} & \bar{h}_s^s + \sum_p \frac{\bar{h}_p \bar{h}_s^{ps}}{-\bar{h}_p^p} + \frac{1}{2!} \sum_{p,q} \frac{\bar{h}_{pq}^s \bar{h}_s^{pq}}{\bar{h}_s^s - \bar{h}_p^p - \bar{h}_q^q} \\
& + \frac{1}{2!} \sum_{p,q} \frac{\bar{h}_{pq} \bar{h}_s^{pqs}}{-\bar{h}_p^p - \bar{h}_q^q} + \frac{1}{3!} \sum_{p,q,r} \frac{\bar{h}_{pqr}^s \bar{h}_s^{pqr}}{\bar{h}_s^s - \bar{h}_p^p - \bar{h}_q^q - \bar{h}_r^r} \\
& + \frac{1}{3!} \sum_{p,q,r} \frac{\bar{h}_{pqr} \bar{h}_s^{pqrs}}{-\bar{h}_p^p - \bar{h}_q^q - \bar{h}_r^r},
\end{aligned} \tag{3.131}$$

which is another incarnation of the inverse Dyson equation (3.89) in the diagonal and frequency-independent approximations. The cost scaling of this method is $O(N^6)$ for all N fundamentals.

3.6 Computer implementation

STEOM-XVCCm and its approximations defined in Sec. 3.5 were implemented for a XVSCF reference with a QFF up to $m = 4$, using a symbolic computing program [132] automating the formula derivations and code synthesis. The $\hat{S}$-amplitude equations, such as Eq. (3.59), and eigenvalue equation (3.60) are fully expanded in terms of the $\hat{H}$, $\hat{T}$, and $\hat{S}$ amplitudes (rather than of the $\bar{H}$ amplitudes) by this program. They are transformed into an efficient computational sequence (a sum of binary tensor contractions) [126, 132, 145] and translated into c++ computer codes. The asymptotic cost functions with the number of modes (N) of the optimal computational sequences for each method discussed below were determined by the symbolic computing program (although the same can be easily inferred analytically from working equations).

The nonlinear $\hat{S}$-amplitude equations of STEOM-XVCC and 1-STEOM-XVCC were solved iteratively with a Newton–Krylov algorithm, available from SCIPY, which utilized the LGRMES method to approximate the Jacobian. [146,147] This procedure could be sped up dramatically if an approximate inverse of the Jacobian matrix was available, which in this study was supplied by that of 3-STEOM-XVCC. An initial guess of the $\hat{S}$ amplitudes was also furnished by 3-STEOM-XVCC, in which large amplitudes ($|s| \geq 1$), often signaling Fermi resonances, were replaced by zero to avoid slow convergence. The self-consistent roots of the Dyson-like equation (3.127) of 2-STEOM-XVCC were located with MINPACK's HYBRD algorithm available via SCIPY. [148]

Table 3.1 summarizes the characteristics of the STEOM-XVCC4 approximations as well as the EOM-XVCC4 and XVMP2 methods. [14, 132] In STEOM-XVCC, the peak operation cost is incurred during the construction of the necessary parts of the $\bar{\bar{H}}'$ matrix, which is $O(N^7)$ for a QFF. The subsequent diagonalization of the singles block of this $\bar{\bar{H}}'$ matrix only costs $O(N^3)$, and, therefore, no cost reduction occurs by seeking any less than the whole set of N fundamentals in STEOM-XVCC.

Calculating all fundamentals by fully diagonalizing the $\bar{H}$ matrix of EOM-XVCC4 in a QFF will be a prohibitive $O(N^{12})$ task. However, EOM-XVCC is implemented in an efficient iterative subspace diagonalization algorithm, [132] which determines only a requested number of several lowest roots. The cost of a contraction of the $\bar{H}$ matrix and a trial vector, which is the overall cost-determining step, is $O(N^6)$ in EOM-XVCC4 with a QFF. [132] Therefore, a root-homing algorithm that is as efficient as the subspace diagonalization algorithm (not considered in this work) should bring down the scaling of EOM-XVCC4 to $O(N^7)$ for all N fundamentals. In other words, STEOM-XVCC and EOM-XVCC give the identical fundamental frequencies (see Sec. 3.4.1) at an identical asymptotic cost. The usefulness of STEOM-XVCC, therefore, lies in the convenience it offers in providing a whole set of fundamentals simultaneously, which has special significance in vibrational analyses.

The diagonal approximation used in 1-, 2-, and 3-STEOM-XVCC decouples the coupled set of the $\hat{S}$-amplitude equations into individual ones, allowing one fundamental frequency to be determined at a one-rank lower cost function. This approximation alone, however, does not change the overall scaling of cost for all N fundamentals, which is still $O(N^7)$ in 1-STEOM-XVCC. The perturbation approximation to the $\hat{S}$-amplitude equations, adopted in 2- and 3-STEOM-XVCC, reduces the overall cost scaling for all N fundamentals from $O(N^7)$ to $O(N^6)$. An iterative algorithm for the root search in the self-consistent Dyson-like equation of 2-STEOM-XVCC is efficient and does not affect the scaling of cost.

The XVMP2 methods [14] also treat one mode at a time (irrespective of the diagonal or frequency-independent approximation to the self-energy) at an $O(N^4)$ cost for all N fundamentals, when a QFF is used.

Figure 3.4 numerically confirms that the asymptotic limits of the cost functions of STEOM-XVCC4 for all N fundamentals and of 1-STEOM-XVCC4 and 2-STEOM-XVCC4 for one fundamental are reached already at $N = 20$. It also provides the reader with a sense of how expensive/inexpensive these calculations are and how quickly the cost rises with N.

3.7 Numerical tests

The vibrational frequencies of the water, formaldehyde, and ethene molecules were calculated with the various approximations of STEOM-XVCC4, EOM-XVCC4, and XVMP2. Their equilibrium structures, normal coordinates, and QFF's were calculated at the MP2/aug-cc-pVTZ level using NWCHEM [128] and SINDO. [129] The reference wave

function was furnished by the XVSCF[4] method. [10]

3.7.1 Water

Table 3.2 lists the errors in the frequencies of the water molecule calculated by the various methods relative to the EOM-XVCC4 benchmark. As analytically proven in Sec. 3.4.1 and thus expected, STEOM-XVCC4 gives the identical results as EOM-XVCC4 for the fundamentals. The diagonal approximation in 1-STEOM-XVCC causes negligible errors of no more than 1 cm^{-1}.

The frequencies of the 2- and 3-STEOM-XVCC4 methods, which are without and with the frequency-independent approximation, respectively, are similar to each other. This parallels the results of XVMP2 with and without the frequency-independent approximation to the self-energy. Since none of the fundamental modes of the water molecule are appreciably affected by any resonance, the self-energy is roughly constant with frequency. Therefore, a self-consistent solution of the Dyson equation does not differ much from the non-self-consistent one (i.e., in the frequency-independent approximation).

Both 2- and 3-STEOM-XVCC4 noticeably outperform XVMP2 for ν_1 and ν_3, which experience Morse-like PES. This may be understood that the strong one-mode anharmonicity in these PES cannot be adequately described by a second-order perturbation theory of XVMP2. While 2- and 3-STEOM-XVCC4 also invokes a similar perturbation theory argument, its zeroth-order Hamiltonian is a part of $\bar{H}$ (not $\hat{H}$) and, therefore, they take into account much greater degree of anharmonic effects.

3.7.2 Formaldehyde

The results for the formaldehyde molecule in Table 3.3 confirm the general observations made above for the water molecule, except for ν_5.

The ν_5 fundamental is known to undergo a Fermi resonance with combinations $\nu_3\nu_6$ and $\nu_2\nu_6$. For this mode, both XVMP2 in the frequency-independent approximation and 3-STEOM-XVCC4 (also invoking the frequency-independent approximation) suffer from large errors in excess of 400 and 100 cm^{-1}, respectively. In either case, the self-consistent solution of the Dyson equation by XVMP2 (without the frequency-independent approximation) or by 2-STEOM-XVCC4 rectifies this problem and reproduces the ν_5 frequency within 5 cm^{-1} of the EOM-XVCC4 result. Furthermore, roots corresponding to the combinations $\nu_3\nu_6$ and $\nu_2\nu_6$ exist in the same Dyson equation. The accuracy for these roots is somewhat poorer than for the fundamental. Overall, 2- and 3-STEOM-XVCC4 are comparable in accuracy with XVMP2 and frequency-independent XVMP2, respectively, for fundamentals unaffected by resonance and those strongly affected by a resonance.

In a STEOM-XVCC4 or 1-STEOM-XVCC4 calculation, exactly 6 fundamental frequencies are obtained by diag-

onalizing the 6×6 $\bar{\bar{H}}'$ matrix in the singles space with one common set of $\hat{S}$ amplitudes. These eigenvalues are the frequencies listed in the columns labeled ν_1 through ν_6 (but not in the columns of the combinations). The frequencies of the combinations $\nu_3\nu_6$ and $\nu_2\nu_6$ were obtained as follows: We seek a different solution of the nonlinear $\hat{S}$-amplitude equation, starting with an initial guess with a large magnitude assigned to $s_5^{3,6}$ (if $\nu_3\nu_6$ is the target) in its iterative solution algorithm. A more accurate initial guess may be obtained by first performing an inexpensive EOM-XVCC calculation (such as EOM-XVCC2) for the target root and inverting the corresponding $\hat{R}$ amplitudes into guess $\hat{S}$ amplitudes via Eq. (3.62). Once the $\hat{S}$ amplitudes for the target root are determined, we then construct the $\bar{\bar{H}}'$ matrix in the singles space with this different set and diagonalize it. The eigenvalues for all fundamentals other than ν_5 are unchanged, but that for ν_5 now reports the frequency for $\nu_3\nu_6$. The existence of multiple solution sets of the $\hat{S}$-amplitude equations more or less corresponds to the frequency dependence of the $\hat{S}$ amplitudes in 2-STEOM-XVCC, permitting multiple roots of a Dyson equation.

Remarkably, the 1-STEOM-XVCC4 frequencies of $\nu_3\nu_6$ and $\nu_2\nu_6$ are as accurate (relative to EOM-XVCC4) as they are for the other fundamentals unaffected by resonance. In other words, the diagonal approximation and the resulting absence of coordinate mixing hardly influence the ability of STEOM-XVCC to describe the states that undergo significant anharmonic mode-mode coupling. This can be understood by recalling the equivalence of STEOM-XVCC and EOM-XVCC discussed in Sec. 3.4.1, or specifically Fig. 3.3. A large $\hat{R}_3$ amplitude needed to describe a resonance caused by cubic anharmonicity can still be fully accounted for by an equally large $\hat{S}$ amplitude combined with nearly unit $\{c^p(k)\}$ vector.

3.7.3 Ethene

Table 3.4 compiles the results for the ethene molecule. This molecule has a number of modes (ν_1, ν_2, ν_5, ν_8, and ν_{10}) whose anharmonic effects are not fully recuperated by XVMP2. In particular, ν_5 appears to be affected by some resonance, causing XVMP2 in the frequency-independent approximation to suffer from a large error of -237 cm^{-1}. The 3-STEOM-XVCC4 method, which is also frequency independent, has a large, if not larger, error of -43 cm^{-1}.

For ethene also, we observe that 1-STEOM-XVCC4 is an exceedingly accurate approximation to STEOM-XVCC4, suggesting that the off-diagonal elements of the $\bar{\bar{H}}'$ matrix are negligible. The 2- and 3-STEOM-XVCC4 frequencies behave similarly as those of XVMP2 without and with the frequency-independent approximation, respectively, although the former are much more expensive than the latter. This underscores the exceptionally good performance of second-order perturbation theory for MBGF in anharmonic vibrational problems.

3.8 Conclusion

We have introduced STEOM-XVCC*m* (with *m* being the truncation rank of the $\hat{T}$ and $\hat{S}$ operators) for a simultaneous calculation of anharmonic vibrational frequencies of all fundamentals. We have proved that the STEOM-XVCC*m* frequencies are size-intensive and identical to EOM-XVCC*m*, rendering STEOM-XVCC a convenient root-homing algorithm for fundamentals, which have special significance in understanding and simulating IR and Raman spectra. We have also elucidated the relationship between the vibrational and electronic STEOM-CC methods and between STEOM-XVCC and vibrational MBGF, the latter inspiring three approximate STEOM-XVCC methods.

We have presented the diagrammatic and algebraic working equations of STEOM-XVCC4 in a QFF as well as its three approximations, simply named 1-, 2-, and 3-STEOM-XVCC. With the aid of a symbolic computing program, they have been implemented into efficient computer codes, which have been applied to three molecules with varied degree of anharmonicity in their PES's. We numerically confirm the identity of the STEOM-XVCC4 and EOM-XVCC4 frequencies not only for the nominal fundamentals but also Fermi-resonant counterparts coupled with one of the fundamentals. We also show that the diagonal approximation in 1-STEOM-XVCC has negligible (< 1 cm^{-1}) effects on the frequencies and a second-order perturbation approximation to the $\hat{S}$-amplitude equations used in 2-STEOM-XVCC4 makes it behave similar to XVMP2. The frequency-independent approximation to 2-STEOM-XVCC4, called 3-STEOM-XVCC4, also performs similarly with XVMP2 in the frequency-independent approximation, both suffering from large errors for resonant modes. With the much greater operation costs, 2- and 3-STEOM-XVCC may not be the methods of choice in the presence of XVMP2, but STEOM-XVCC and 1-STEOM-XVCC remain a viable alternative to EOM-XVCC for fundamentals.

3.9 Figures

$$
\hat{H} = \begin{array}{c} \\ \langle\Phi_0| \\ \langle\Phi_v| \\ \langle\Phi_{vv}| \\ \langle\Phi_{vvv}| \\ \langle\Phi_{vvvv}| \end{array}
\begin{array}{c}
\begin{array}{ccccc} |\Phi_0\rangle & |\Phi_v\rangle & |\Phi_{vv}\rangle & |\Phi_{vvv}\rangle & |\Phi_{vvvv}\rangle \end{array} \\
\begin{bmatrix}
E_{\mathrm{XVSCF}} & \mathbf{0} & \mathbf{X} & \mathbf{X} & \mathbf{X} \\
\mathbf{0} & \mathbf{X} & \mathbf{X} & \mathbf{X} & \mathbf{X} \\
\mathbf{X} & \mathbf{X} & \mathbf{X} & \mathbf{X} & \mathbf{X} \\
\mathbf{X} & \mathbf{X} & \mathbf{X} & \mathbf{X} & \mathbf{X} \\
\mathbf{X} & \mathbf{X} & \mathbf{X} & \mathbf{X} & \mathbf{X}
\end{bmatrix}
\end{array}
$$

$$
\bar{H} = \begin{array}{c} \\ \langle\Phi_0| \\ \langle\Phi_v| \\ \langle\Phi_{vv}| \\ \langle\Phi_{vvv}| \\ \langle\Phi_{vvvv}| \end{array}
\begin{array}{c}
\begin{array}{ccccc} |\Phi_0\rangle & |\Phi_v\rangle & |\Phi_{vv}\rangle & |\Phi_{vvv}\rangle & |\Phi_{vvvv}\rangle \end{array} \\
\begin{bmatrix}
E_{\mathrm{XVCC}} & \bar{\mathbf{X}} & \bar{\mathbf{X}} & \bar{\mathbf{X}} & \bar{\mathbf{X}} \\
\mathbf{0} & \bar{\mathbf{X}} & \bar{\mathbf{X}} & \bar{\mathbf{X}} & \bar{\mathbf{X}} \\
\mathbf{0} & \bar{\mathbf{X}} & \bar{\mathbf{X}} & \bar{\mathbf{X}} & \bar{\mathbf{X}} \\
\mathbf{0} & \bar{\mathbf{X}} & \bar{\mathbf{X}} & \bar{\mathbf{X}} & \bar{\mathbf{X}} \\
\mathbf{0} & \bar{\mathbf{X}} & \bar{\mathbf{X}} & \bar{\mathbf{X}} & \bar{\mathbf{X}}
\end{bmatrix}
\end{array}
$$

$$
\bar{\bar{H}} = \begin{array}{c} \\ \langle\Phi_0| \\ \langle\Phi_v| \\ \langle\Phi_{vv}| \\ \langle\Phi_{vvv}| \\ \langle\Phi_{vvvv}| \end{array}
\begin{array}{c}
\begin{array}{ccccc} |\Phi_0\rangle & |\Phi_v\rangle & |\Phi_{vv}\rangle & |\Phi_{vvv}\rangle & |\Phi_{vvvv}\rangle \end{array} \\
\begin{bmatrix}
E_{\mathrm{XVCC}} & \bar{\bar{\mathbf{X}}} & \bar{\bar{\mathbf{X}}} & \bar{\bar{\mathbf{X}}} & \bar{\bar{\mathbf{X}}} \\
\mathbf{0} & \bar{\bar{\mathbf{X}}} & \bar{\bar{\mathbf{X}}} & \bar{\bar{\mathbf{X}}} & \bar{\bar{\mathbf{X}}} \\
\mathbf{0} & \mathbf{0} & \bar{\bar{\mathbf{X}}} & \bar{\bar{\mathbf{X}}} & \bar{\bar{\mathbf{X}}} \\
\mathbf{0} & \mathbf{0} & \bar{\bar{\mathbf{X}}} & \bar{\bar{\mathbf{X}}} & \bar{\bar{\mathbf{X}}} \\
\mathbf{0} & \mathbf{0} & \bar{\bar{\mathbf{X}}} & \bar{\bar{\mathbf{X}}} & \bar{\bar{\mathbf{X}}}
\end{bmatrix}
\end{array}
$$

Figure 3.1: Structure of the singly ($\bar{H}$) and doubly ($\bar{\bar{H}}$) similarity-transformed Hamiltonian of XVCC4 as well as of the bare Hamiltonian ($\hat{H}$) in the basis of the Hartree products of XVSCF modals (expressed in a self-explanatory manner). The blocks whose elements are zero are represented by $\mathbf{0}$, while the others by $\mathbf{X}$, $\bar{\mathbf{X}}$, or $\bar{\bar{\mathbf{X}}}$. E_{XVSCF} and E_{XVCC} denote the XVSCF and XVCC4 energy, respectively, for the ground state. The dashed-boxed areas are the formal diagonalization spaces of EOM-XVCC4 ($\bar{H}$) and STEOM-XVCC4 ($\bar{\bar{H}}$).

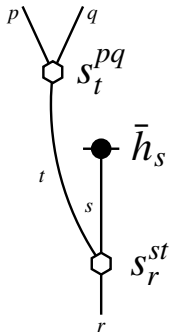

Figure 3.2: The tenth diagram of Eq. (3.57).

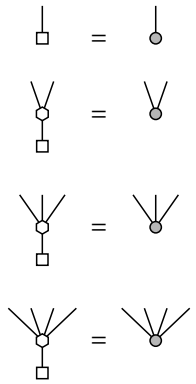

Figure 3.3: Diagrammatic correspondence of the equivalent roots for a fundamental of STEOM-XVCC4 and EOM-XVCC4.

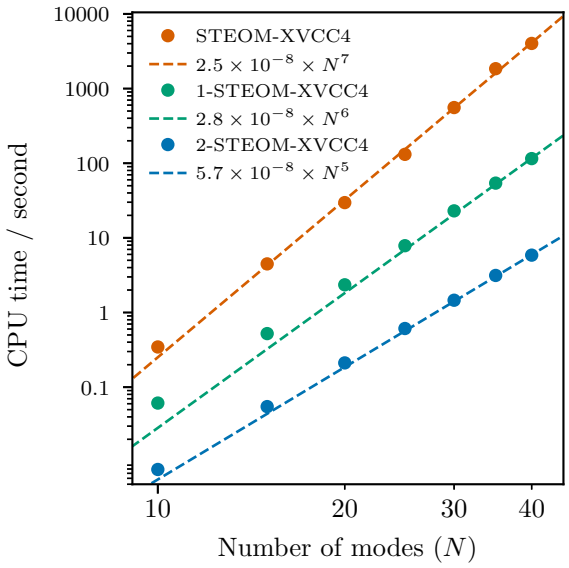

Figure 3.4: CPU time (in seconds) spent in one cycle of the iterative solution of the $\hat{S}$-amplitude equations of STEOM-XVCC4 for all N fundamentals, 1-STEOM-XVCC4 for one fundamental, and 2-STEOM-XVCC4 for one fundamental, as a function of the number of modes N. A QFF is used as a PES.

3.10 Tables

Table 3.1: A summary of the methods considered in this work for a QFF and their asymptotic dependence of cost on the number of modes (N).

Method	Diagonal[1]	Perturbation[1]	ω-independent[1]	1 fundamental	N fundamentals
EOM-XVCC4[2]	No	No	No	$O(N^6)$	$O(N^7)$
STEOM-XVCC4	No	No	No	...	$O(N^7)$
1-STEOM-XVCC4	Yes	No	No	$O(N^6)$	$O(N^7)$
2-STEOM-XVCC4	Yes	Yes	No	$O(N^5)$	$O(N^6)$
3-STEOM-XVCC4	Yes	Yes	Yes	$O(N^5)$	$O(N^6)$
XVMP2[3]	Yes	Yes	No	$O(N^3)$	$O(N^4)$
ω-independent XVMP2[4]	Yes	Yes	Yes	$O(N^3)$	$O(N^4)$

[1] The use of the diagonal, quasi-second-order perturbation, and/or frequency-independent approximations, as defined in Sec. 3.5.
[2] Cost functions assume a root-homing algorithm for fundamentals as efficient as an iterative subspace diagonalization algorithm for several lowest roots. [132]
[3] Vibrational MBGF with the self-energy in the second-order perturbation and diagonal approximations. [14] Cost functions assume a constant number of frequencies at which the self-energy needs to be computed to locate a pole by an interpolation.
[4] Vibrational MBGF with the self-energy in the second-order perturbation, diagonal, and frequency-independent approximations. [14]

Table 3.2: The calculated frequencies (ν_i) of the fundamental transitions (in cm^{-1}) of the water molecule obtained by the methods listed in Table 3.1 using the XVSCF[4] reference in a QFF. Except for EOM-XVCC4, the errors from EOM-XVCC4 are shown.

Method	ν_1	ν_2	ν_3
EOM-XVCC4	3682	1557	3791
STEOM-XVCC4	0	0	0
1-STEOM-XVCC4	−0	0	0
2-STEOM-XVCC4	−4	1	−5
3-STEOM-XVCC4	−7	1	−7
XVMP2	−15	2	−17
ω-independent XVMP2	−19	2	−20

Table 3.3: The same as Table 3.2, but for the formaldehyde molecule.

Method	ν_1	ν_2	ν_3	ν_4	ν_5	$\nu_3\nu_6$	$\nu_2\nu_6$	ν_6
EOM-XVCC4	2837	1720	1502	1161	2874	2705	2990	1238
STEOM-XVCC4	0	0	0	0	0	0^1	0^1	0
1-STEOM-XVCC4	−0	−0	1	0	−0	-1^1	-0^1	0
2-STEOM-XVCC4	−1	−0	1	0	5	13	19	1
3-STEOM-XVCC4	−6	−0	1	0	−111	⋯	⋯	1
XVMP2	−9	0	1	2	1	16	24	2
ω-independent XVMP2	−16	0	1	2	−415	⋯	⋯	2

[1] Obtained with a different set of the $\hat{S}$ amplitudes than the rest.

Table 3.4: The same as Table 3.2, but for the ethene molecule.

Method	ν_1	ν_2	ν_3	ν_4	ν_5	ν_6	ν_7	ν_8	ν_9	ν_{10}	ν_{11}	ν_{12}
EOM-XVCC4	3043	1621	1349	1116	3000	1436	983	3133	815	3112	1223	950
STEOM-XVCC4	0	0	0	0	0	0	0	0	0	0	0	0
1-STEOM-XVCC4	−0	−0	0	0	−0	0	−0	0	0	−0	0	−0
2-STEOM-XVCC4	14	7	1	−1	11	2	−1	9	0	11	1	1
3-STEOM-XVCC4	9	5	1	−1	−43	2	−1	5	0	7	1	0
XVMP2	15	9	2	−2	13	4	−1	8	2	10	2	2
ω-independent XVMP2	5	8	2	−2	−237	3	−1	1	2	1	2	2

Chapter 4

Extended similarity-transformed equation-of-motion vibrational coupled cluster theory

4.1 Introduction

In the previous Chapter, we introduced the STEOM-XVCCm method for the selective and simultaneous calculation of all fundamental modes of a molecule where m stands for the highest excitation rank considered. The method requires two sequential similarity transformations of the vibrational Hamiltonian with exponential excitation operators. The resulting structure of the doubly similarity-transformed Hamiltonian $\bar{\bar{H}}$ is illustrated in Fig. 4.1 using STEOM-XVCC4 as an example. The STEOM-XVCC frequencies are then obtained by diagonalization of the doubly similarity-transformed Hamiltonian $\bar{\bar{H}}$ over the space of one-mode excited Hartree products. As implied by the block structure of $\bar{\bar{H}}$, the one-mode excited products are decoupled from higher-order excited products up to mth order. This decoupling ensures that the STEOM-XVCC frequencies (obtained by blockwise diagonalization) are identical to the eigenvalues of $\bar{\bar{H}}$ in the space of single through mth-order excitations.

Here, we define the extended STEOM-XVCC (Ext-STEOM-XVCC) method for the calculation of overtones and combinations of a molecule. The Ext-STEOM-XVCC frequencies are obtained by diagonalization of $\bar{\bar{H}}$ in the space of two-mode to m-mode excited products as illustrated by the blue dashed-box in Fig. 4.1. Unlike the STEOM-XVCC method, the frequencies of Ext-STEOM-XVCC are not equivalent to those obtained by EOM-XVCC because the matrix elements of $\bar{\bar{H}}$ are dressed with higher-order excitation effects due to the second similarity transformation.

Although not exactly decoupled, it is expected that the coupling between more highly excited Hartree products is also greatly reduced by the two similarity transformations. The doubly transformed Hamiltonian $\bar{\bar{H}}$ then has an approximate upper block triangular form as illustrated in Fig. 4.1. This implies that the eigenvalues of $\bar{\bar{H}}$ may be obtained to good approximation by blockwise diagonalization. Therefore, we also define approximate Ext-STEOM-XVCC methods which are defined by including only up to n-mode excited products in the diagonalization space where $n < m$ as illustrated by the red and green dashed-boxes in Fig. 4.1.

We establish a diagrammatic method for the derivation of the Ext-STEOM-XVCCm equations and the doubly similarity-transformed vibrational Hamiltonian. We derive and implement the Ext-STEOM-XVCCm equations and its approximations for $2 \leq m \leq 4$ with the aid of our previously described symbolic algebra program. We apply these

methods to the frequencies of the overtones and combinations of the water and formaldehyde molecules using quartic force fields (QFF's). A comparative analysis is performed for the results of these methods and of EOM-XVCC*m*.

4.2 Formalism

Here, we introduce the *m*th-order extended similarity-transformed equation-of-motion vibrational coupled-cluster method, abbreviated as Ext-STEOM-XVCC*m*, as an *m*th-order CI problem with the doubly similarity-transformed Hamiltonian $\bar{\bar{H}}$,

$$\bar{\bar{H}} \quad = \quad \{e^{\hat{S}}\}^{-1} e^{-\hat{T}} \hat{H} e^{\hat{T}} \{e^{\hat{S}}\}, \tag{4.1}$$

where the braces bring the exponential operator in a normal order. [13, 110] The operator $\hat{T}$ is the sum of single, double, through *m*-fold cluster excitation operators

$$\hat{T} = \hat{T}_1 + \hat{T}_2 + \cdots + \hat{T}_m, \tag{4.2}$$

with

$$\hat{T}_n = \frac{1}{n!} \sum_{p_1, p_2, \cdots, p_n} \tau^{p_1 p_2 \cdots p_n} \{\hat{a}^\dagger_{p_1} \hat{a}^\dagger_{p_2} \cdots \hat{a}^\dagger_{p_n}\}, \tag{4.3}$$

while the operator $\hat{S}$ is the sum of single, double, through $(m-1)$-fold net excitation operators which contain exactly one lowering operator

$$\hat{S} = \hat{S}_{2,1} + \hat{S}_{3,1} + \cdots + \hat{S}_{m,1}, \tag{4.4}$$

with

$$\hat{S}_{n,1} = \frac{1}{n!} \sum_{p_1, p_2, \cdots, p_n} \sum_{q} s_q^{p_1 p_2 \cdots p_n} \{\hat{a}^\dagger_{p_1} \hat{a}^\dagger_{p_2} \cdots \hat{a}^\dagger_{p_n} \hat{a}_q\}. \tag{4.5}$$

The first transformation defines the singly transformed Hamiltonian of XVCCm

$$\begin{aligned}\bar{H} &= e^{-\hat{T}}\hat{H}e^{\hat{T}}, &(4.6)\\ &= \bar{h}_0 + \sum_p \bar{h}_p\{\hat{a}_p\} + \sum_p \bar{h}^p\{\hat{a}_p^\dagger\} + \frac{1}{2!}\sum_{p,q}\bar{h}_{pq}\{\hat{a}_p\hat{a}_q\} \\ &\quad + \sum_{p,q}\bar{h}_q^p\{\hat{a}_p^\dagger\hat{a}_q\} + \ldots, &(4.7)\end{aligned}$$

where the $\bar{h}$ amplitudes are connected products of the amplitudes of $\hat{T}$ and $\hat{H}$. The excitation amplitudes $\tau^{p_1p_2\cdots p_n}$ are determined such that the amplitudes of the pure excitation components of $\bar{H}$ are transformed to zero

$$\bar{h}^{p_1p_2\cdots p_n} = 0, \tag{4.8}$$

for all $p_1, p_2, \cdots p_n$ for $1 \leq n \leq m$. This is equivalent to the XVCCm amplitude equations in Eq. (2.41).

The doubly transformed Hamiltonian can also be formally written in a normal-ordered form as

$$\begin{aligned}\bar{\bar{H}} &= \{e^{-\hat{S}}\}^{-1}\bar{H}\{e^{\hat{S}}\}, \\ &= \bar{\bar{h}}_0 + \sum_p \bar{\bar{h}}_p\{\hat{a}_p\} + \sum_p \bar{\bar{h}}^p\{\hat{a}_p^\dagger\} + \frac{1}{2!}\sum_{p,q}\bar{\bar{h}}_{pq}\{\hat{a}_p\hat{a}_q\} \\ &\quad + \sum_{p,q}\bar{\bar{h}}_q^p\{\hat{a}_p^\dagger\hat{a}_q\} + \ldots, &(4.9)\end{aligned}$$

where the $\bar{\bar{h}}$ amplitudes are connected products of the amplitudes of $\bar{H}$ and $\hat{S}$. The amplitudes $s_q^{p_1p_2\cdots p_n}$ are determined such that the amplitudes of the net excitation components of $\bar{\bar{H}}$ which contain exactly one lowering operator are transformed to zero

$$\bar{\bar{h}}_q^{p_1p_2\cdots p_n} = 0, \tag{4.10}$$

for all $p_1, p_2, \cdots p_n$ for $2 \leq n \leq m$. This is equivalent to the STEOM-XVCCm amplitude equations in Eq. (3.46).

As shown in Sec. 3.3.2, the second similarity transformation preserves the decoupling achieved by the first transformation, so the pure excitation components of $\bar{\bar{H}}$ remain zero

$$\bar{\bar{h}}^{p_1p_2\cdots p_n} = 0, \tag{4.11}$$

for all $p_1, p_2, \cdots p_n$ for $1 \leq n \leq m$. Furthermore, the zero-mode component of the $\bar{\bar{H}}$ operator is simply the XVCCm energy for the ground state,

$$\bar{\bar{h}}_0 = \bar{E}_0^{(m)}. \tag{4.12}$$

.

Due to Eqs. (4.11) and (4.10), the zero-mode and one-mode excited Hartree products are exactly decoupled from more highly excited Hartree products and need not be included in the diagonalization space as illustrated in Fig. 4.1. Therefore, we define an two-mode to m-mode excitation operator

$$\hat{C}(\ell) = \hat{C}_2(\ell) + \hat{C}_3(\ell) + \cdots + \hat{C}_m(\ell), \tag{4.13}$$

with

$$\hat{C}_n(\ell) = \frac{1}{n!} \sum_{p_1,p_2,\ldots,p_n} c^{p_1 p_2 \cdots p_n}(\ell) \{\hat{a}^\dagger_{p_1} \hat{a}^\dagger_{p_2} \cdots \hat{a}^\dagger_{p_n}\}. \tag{4.14}$$

We require that

$$\langle \Phi_{p_1 p_2 \cdots p_n} | \bar{\bar{H}} \hat{C}(\ell) | \Phi_0 \rangle = \bar{\bar{E}}^{(m)}_\ell c^{p_1 p_2 \cdots p_n}(\ell), \tag{4.15}$$

be satisfied, where $\bar{\bar{E}}^{(m)}_\ell$ is the Ext-STEOM-XVCCm total energy of the ℓth excited state. Furthermore, Eqs. (4.8) and (4.12) imply

$$\langle \Phi_{p_1 p_2 \cdots p_n} | \hat{C}(\ell) \bar{\bar{H}} | \Phi_0 \rangle = E^{(m)}_0 c^{p_1 p_2 \cdots p_n}(\ell), \tag{4.16}$$

which, together with Eq. (4.15), leads to

$$\langle \Phi_{p_1 p_2 \cdots p_n} | \left(\bar{\bar{H}} \hat{C} \right)_{\mathrm{C}} | \Phi_0 \rangle = \bar{\bar{\omega}}^{(m)}_\ell c^{p_1 p_2 \cdots p_n}(\ell), \tag{4.17}$$

where $\bar{\bar{\omega}}^{(m)}_\ell = \bar{\bar{E}}^{(m)}_\ell - E^{(m)}_0$. We call this the $\hat{C}_n$ amplitude equation of Ext-STEOM-XVCC.

4.3 Approximations to Ext-STEOM-XVCC

As discussed in the previous section, both the ground state block and the block corresponding to one-mode excited products of $\bar{\bar{H}}$ are exactly decoupled from more highly excited blocks

$$\bar{\bar{h}}^{p_1 p_2 \cdots p_n} = 0, \tag{4.18}$$

$$\bar{\bar{h}}^{p_1 p_2 \cdots p_n}_q = 0. \tag{4.19}$$

While the matrix elements are not explicitly considered, the coupling between more highly excited products is also significantly reduced by the transformations. Consider the blocks of $\bar{\bar{H}}$ in Fig. 4.1 which are represented with "$\approx \mathbf{0}$". The only components of $\bar{\bar{H}}$ which are non-zero in those blocks are five- or higher-mode operators. Since the original Hamiltonian is only a four-body operator (in a QFF), it is expected that these terms are relatively small. Therefore, we

suggest approximations to the Ext-STEOM-XVCC method which neglect these blocks of $\bar{\bar{H}}$.

We construct a hierarchy of approximations to the Ext-STEOM-XVCCm method by considering all possible truncations of $\hat{C} = \hat{C}_2 + \cdots + \hat{C}_n$ for $n < m$. Using STEOM-XVCC4 as a concrete example, the lowest order approximation is to include only $\hat{C}_2$. This corresponds to diagonalization over the space of two-mode excited products only (the red dashed-box in Fig. 4.1). The next order approximation is to include up to $\hat{C}_3$ which is equivalent to diagonalizing over the space of two-mode and three-mode excited products (the green dashed-box in Fig. 4.1). We will refer to these methods as Ext-STEOM-XVCC-$\hat{C}_n$ where n represents the truncation rank of $\hat{C}$.

The approximations described here are quite analogous to a corresponding approximation in the electronic STEOM-CC formalism. As outlined in Fig. 1.1, the electronic STEOM-CC method obtains the energies of electronic excitations by diagonalization of the doubly transformed electronic Hamiltonian in the space of singly excited determinants. However, the electronic $\bar{\bar{H}}$ is not exactly block upper triangular. There are three-body terms which couple singly excited determinants and doubly excited determinants which are neglected. Since the electronic Hamiltonian is fundamentally a two-body operator, these three body terms are generally small, and STEOM-CC is an effective approximation. The extended electronic STEOM-CC method includes these previously neglected terms by diagonalizing $\bar{\bar{H}}$ in the full space.

4.4 Diagrammatic derivation

We now consider a diagrammatic representation of the Ext-STEOM-XVCC method. Since each amplitude of the doubly transformed Hamiltonian is connected it can be represented as

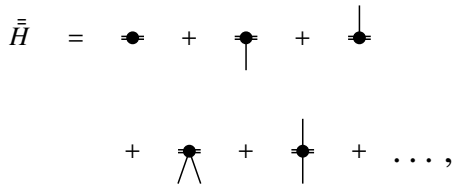

(4.20)

where there is a term-by-term correspondence with Eq. (4.9), and $\hat{C}$ [Eq. 4.13] is represented as

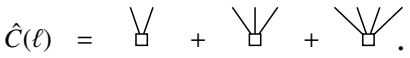

(4.21)

The $\hat{C}_n$ amplitude equations of Ext-STEOM-XVCC are obtained as a sum of all possible contractions of $\bar{\bar{H}}$ with

one vertex of $\hat{C}$ from below. Using Ext-STEOM-XVCC4 as an example, the $\hat{C}_2$, $\hat{C}_3$, and $\hat{C}_4$ equations are

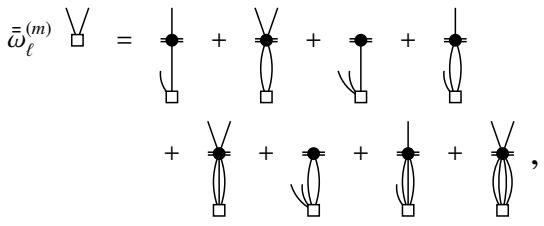

(4.22)

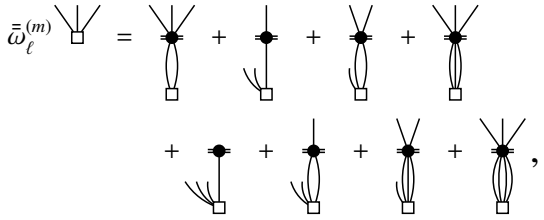

(4.23)

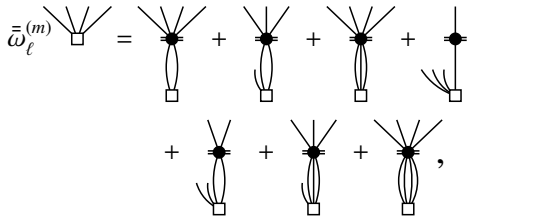

(4.24)

where we have used the fact that the net excitation components of $\bar{\bar{H}}$ with one lowering operator are zero

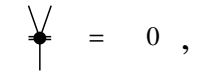

(4.25)

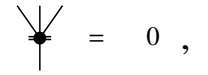

(4.26)

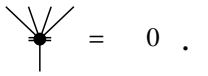

(4.27)

The expansion of $\bar{\bar{H}}$ in terms of the vertices of the singly transformed Hamiltonian $\bar{H}$ and $\hat{S}$ are discussed below.

4.4.1 Diagrammatic form of $\bar{\bar{H}}$

The connected form of the doubly transformed Hamiltonian does not simplify into the familiar form of the first transformation:

$$\bar{\bar{H}} \neq \left(\bar{H}\{e^{\hat{S}}\}\right)_{\mathrm{C}} . \tag{4.28}$$

Instead $\bar{\bar{H}}$ is obtained by solving the equation,

$$\{e^{\hat{S}}\}\bar{\bar{H}} = \bar{H}\{e^{\hat{S}}\}, \tag{4.29}$$

which can be achieved [110] by iteratively improving the left-hand side in the recursive and connected equation,

$$\bar{\bar{H}} = \left(\bar{H}\{e^{\hat{S}}\}\right)_{\mathrm{C}} - \left(\{e^{\hat{S}} - 1\}\bar{\bar{H}}\right)_{\mathrm{C}}, \tag{4.30}$$

Despite the recursive structure of the above equation, the components of $\bar{\bar{H}}$ can be easily obtained with the diagrammatic technique outlined in Table 4.1. [110]

Applying these rules to the one- to four-mode pure excitation operator of $\bar{\bar{H}}$ of STEOM-XVCC4 yields

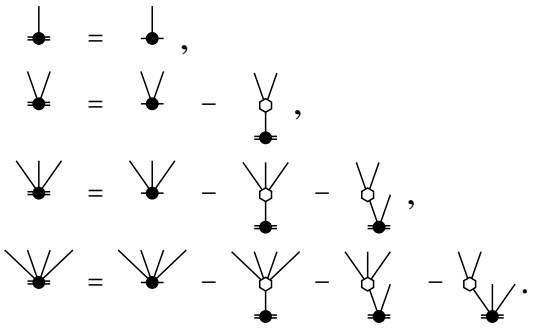

(4.31)

(4.32)

(4.33)

(4.34)

As illustrated in the above equations, because a $\hat{S}$ vertex connecting from above always raises the excitation level, each component of $\bar{\bar{H}}$ only depends on lower-order components of $\bar{\bar{H}}$. Therefore, a closed form expression may be obtained despite the recursive structure of Eq. (4.30). These equations also prove that the decoupling achieved by the first similarity transformation is preserved. Each term contains a pure excitation component of $\bar{H}$, which are zero to satisfy the XVCCm amplitude equations [Eqs. (3.11) - (3.14)], so

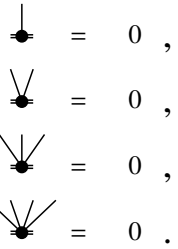

(4.35)

(4.36)

(4.37)

(4.38)

We may also use the rules of Table 4.1 to generate the STEOM-XVCC4 amplitude equations. Applying the rules to the one-mode net excitation component of $\bar{\bar{H}}$ with one lowering operator, we obtain the STEOM-XVCC4 $\hat{S}_{2,1}$

amplitude equation

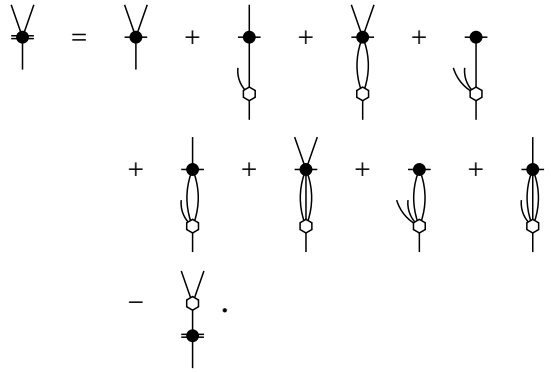

(4.39)

(4.40)

Likewise, applying the rules to the two- and three-mode net excitation components with one lowering operator, we obtain

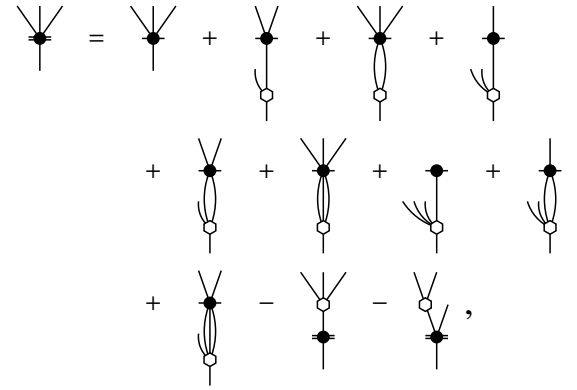

(4.41)

(4.42)

Using Eqs. (4.25) and (4.26), Eqs. (4.41) and (4.42) may be simplified to obtain the STEOM-XVCC4 $\hat{S}_{3,1}$ and $\hat{S}_{4,1}$

amplitude equations respectively

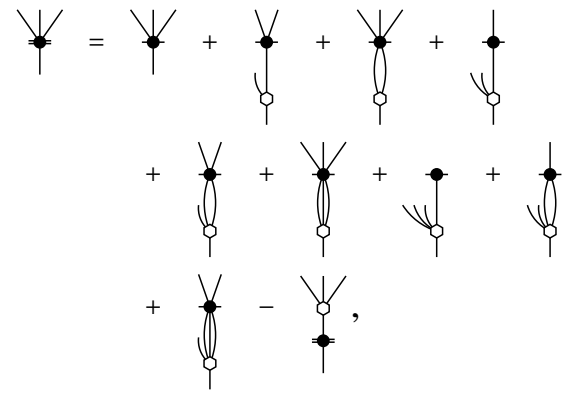

(4.43)

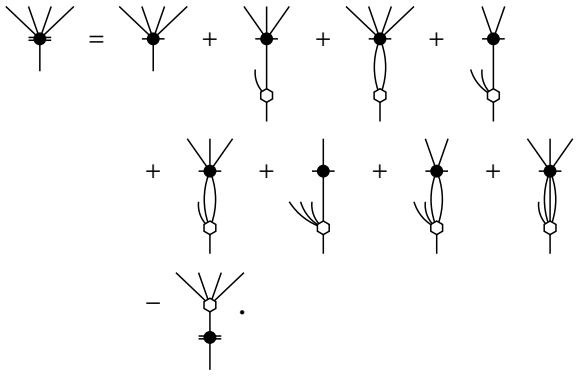

(4.44)

Each of these diagrams is then interpreted algebraically by using the previously established rules for the XVCC and EOM-XVCC diagrams in Table 2.2 with new types of vertices translated appropriately. The doubly similarity-transformed Hamiltonian amplitudes that become necessary in Ext-STEOM-XVCC4 are given in terms of the $\bar{H}$ amplitudes and $\hat{S}$ amplitudes in Appendix E, while the required $\bar{H}$ amplitudes are expanded in terms of the normal-ordered Hamiltonian $\hat{H}$ amplitudes and $\hat{T}$ amplitudes in Appendix C.

4.5 Comparision to EOM-XVCC

Here we compare the wave functions obtained by Ext-STEOM-XVCC and EOM-XVCC. The Ext-STEOM-XVCC wave function for the ℓth mode is

$$|\Psi_\ell\rangle = e^{\hat{T}}\{e^{\hat{S}}\}\hat{C}|\Phi_0\rangle, \tag{4.45}$$

while the EOM-XVCC excited state wave function is

$$|\Psi_\ell\rangle = e^{\hat{T}}\hat{R}|\Phi_0\rangle. \tag{4.46}$$

The two are equal in the exact limit

$$\{e^{\hat{S}}\}\hat{C}|\Phi_0\rangle = \hat{R}|\Phi_0\rangle,$$

where the common factor of $e^{\hat{T}}$ has been eliminated. We may expand $\{e^{\hat{S}}\}$ and compare the wave functions order by order

$$\begin{aligned}
\hat{C}_1 &= \hat{R}_1, \\
\hat{S}_{2,1}\hat{C}_1 + \hat{C}_2 &= \hat{R}_2, \\
\hat{S}_{3,1}\hat{C}_1 + \hat{S}_{2,1}\hat{C}_2 + \hat{C}_3 &= \hat{R}_3, \\
\hat{S}_{4,1}\hat{C}_1 + \hat{S}_{3,1}\hat{C}_2 + \frac{1}{2!}\{\hat{S}_{2,1}\}^2\hat{C}_2 + \hat{S}_{2,1}\hat{C}_3 + \hat{C}_4 &= \hat{R}_4, \\
&\vdots \quad . \qquad (4.47)
\end{aligned}$$

Using this logic, we can estimate the effect of the second similarity transformation. For example, the Ext-STEOM-XVCC4 excited state wave function includes $1/2\{\hat{S}_{2,1}\hat{S}_{4,1}\}\hat{C}_2$, $1/2\{\hat{S}_{2,1}\hat{S}_{4,1}\}\hat{C}_3$, and $1/2\{\hat{S}_{2,1}\hat{S}_{4,1}\}\hat{C}_4$ which approximate $\hat{R}_6$, $\hat{R}_7$, and $\hat{R}_8$ respectively. This further justifies the approximations introduced in Sec. 4.3. Although Ext-STEOM-XVCC4-$\hat{C}_2$ only includes up to $\hat{C}_2$, the wave function still approximately includes up to sixth-order excitations via $1/2\{\hat{S}_{2,1}\hat{S}_{4,1}\}\hat{C}_2$.

4.6 Numerical implementation

Ext-STEOM-XVCCm with $2 \leq m \leq 4$ were implemented for a XVSCF reference with a QFF, using our symbolic computing program [132] which automated derivation and code generation. To obtain optimal cost scaling, the $\hat{C}_n$ equations [Eqs. (4.22), (4.23), and (4.24)] are fully expanded in terms of the $\hat{H}$, $\hat{T}$, and $\hat{S}$ amplitudes (rather than of the $\bar{\hat{H}}$ amplitudes) by this program. They are transformed into an efficient computational sequence [126, 132, 145] and translated into c++ computer codes. The nonlinear $\hat{S}$-amplitude equations of STEOM-XVCC were solved iteratively with a Newton–Krylov algorithm, available from SCIPY. The $\hat{C}_n$ amplitude equations of Ext-STEOM-XVCCm were solved with the iterative Arnoldi method, a non-Hermitian generalization of the Lanczos method, [122–124] available in ARPACK. [125]

The peak cost scaling of the Ext-STEOM-XVCCm method ($2 \leq m \leq 4$) with respect to the number of modes N is illustrated in Table 4.2. The cost scaling of EOM-XVCCm and STEOM-XVCCm are included for reference. Implementation of the Ext-STEOM-XVCC method first requires the calculation of the $\hat{S}$ amplitudes via STEOM-XVCC. Alternatively, one can calculate the frequencies of all N fundamentals via EOM-XVCCm and use Eq. (3.62) to obtain the $\hat{S}$ amplitudes. Assuming an efficient root homing algorithm in conjunction with a subspace diagonalization

routine, the calculation of all N fundamentals by EOM-XVCCm has the same cost scaling as STEOM-XVCCm. Since the fundamental frequencies have special significance in a vibrational analysis and are likely to be routinely calculated, the applicability of the Ext-STEOM-XVCCm method will be greatly enhanced if the cost scaling does not exceed the preceding STEOM-XVCCm calculation. This is the case for Ext-STEOM-XVCC2 and Ext-STEOM-XVCC3; however, Ext-STEOM-XVCC4 increases the cost scaling by one rank relative to STEOM-XVCC4. Analysis of the Ext-STEOM-XVCC4 equations reveals that only one term, which is illustrated in Fig. 4.2, is responsible for the $O(N^8)$ cost scaling. This term involves the product of four $\hat{S}$ amplitudes and partially accounts for eighth-order excitations which should be very small for most modes of interest. Therefore, we propose neglecting this term as an approximation to Ext-STEOM-XVCC4 which generates an algorithm with the same cost scaling as the preceding STEOM-XVCC4 calculation.

While the peak cost scaling of Ext-STEOM-XVCCm described above is relevant for analyzing the relative accuracy of Ext-STEOM-XVCCm to other methods, the cost of the diagonalization step of Ext-STEOM-XVCCm is relevant for practical matters. The cost scaling of the $\hat{C}_n$ amplitude equations are the dominate cost of an iterative subspace diagonalization routine applied to $\bar{\bar{H}}$ for a few low lying roots. We report the cost scaling of the $\hat{C}_n$ amplitude equations of Ext-STEOM-XVCCm and its approximations in Table 4.3. Of particular note, the diagonalization step of Ext-STEOM-XVCC2 has the same cost scaling as EOM-XVCC2. Likewise the diagonalization step of the Ext-STEOM-XVCC4-$\hat{C}_3$ approximation has the same cost scaling as EOM-XVCC4. The peak cost scaling of both of these method is determined by the preceding STEOM-XVCC calculation. Therefore, if one has already calculated all the fundamental modes (either via STEOM-XVCC or EOM-XVCC), overtones and combinations can then be calculated at the same cost scaling as EOM-XVCC. This is not the case for Ext-STEOM-XVCC3 or Ext-STEOM-XVCC4 where the diagonalization step is the same as the peak cost scaling and one rank higher than the corresponding EOM-XVCC method.

4.7 Numerical tests

The vibrational frequencies of the water and formaldehyde molecules were calculated with Ext-STEOM-XVCC and its approximations. Their equilibrium structures, normal coordinates, and QFF's were calculated at the MP2/aug-cc-pVTZ level using NWCHEM [128] and SINDO. [129] The reference wave function was furnished by the XVSCF[4] method. [10]

4.7.1 Water

Table 4.4 lists the errors in the frequencies of overtones and combinations of the water molecule relative to the EOM-XVCC8 benchmark. The rigorous Ext-STEOM-XVCCm methods (truncation of $\hat{C}$ is equal to m) consistently outperform the corresponding EOM-XVCCm methods with drastically better results for certain overtones and combinations. Neglecting the product of four $\hat{S}$ amplitudes in Ext-STEOM-XVCC4 has a negligible effect on the accuracy of the method.

The average errors of the Ext-STEOM-XVCC3 and Ext-STEOM-XVCC4 methods including only $\hat{C}_2$ are roughly on par with EOM-XVCC3 and EOM-XVCC4 respectively, but they perform relatively poorly for highly anharmonic overtones and combinations. These modes are better described by EOM-XVCC3 and EOM-XVCC4 which include up to 3-mode and 4-mode excited products in the diagonalization space.

The results obtained with Ext-STEOM-XVCC4 including $\hat{C}_3$ for overtones and combinations with a quantum number of two are on the same order of accuracy as rigorous Ext-STEOM-XVCC4. The modes with a quantum number of three are mixed in accuracy. This method would seem to be a very effective choice if one is interested only in overtones and combinations with a quantum number of two. This would often be the case for overtones and combinations which are in resonance with the fundamentals. Assuming one has already paid the cost to obtain all the fundamental modes (whether by EOM-XVCC4 or STEOM-XVCC4), the final diagonalization step has the same cost scaling as EOM-XVCC4.

4.7.2 Formaldehyde

The ν_5 fundamental of formaldehyde is known to undergo a Fermi resonance with combinations (001001) and (010001). In the case of Fermi resonance, alternate solutions to the $\hat{S}$ amplitude equations can be found. Diagonalization of the singles block of $\bar{\bar{H}}$ (STEOM-XVCC) defined by these alternate $\hat{S}$ amplitudes yields an overtone or combination mode in place of one of the fundamental modes. This situation can usually be identified by the presence of a large (> 1) $\hat{S}$ amplitude. For example, the amplitude $s_5^{2,6}$ has a magnitude of over 1.5 for the alternate solution of the STEOM-XVCC equations for formaldehyde corresponding to the overtone (010001). Here we used the formaldehyde molecule to investigate the effect of these alternate $\hat{S}$ amplitudes on the accuracy of Ext-STEOM-XVCC.

Table 4.4 lists the errors in the frequencies (from the EOM-XVCC8 benchmark) of fundamental ν_5 along with selected combination modes of the formaldehyde molecule calculated by Ext-STEOM-XVCC3 with two sets of $\hat{S}$ amplitudes. The first set corresponds to the normal solution where the fundamental ν_5 is obtained from the preceding STEOM-XVCC3 calculation. The second set corresponds to an alternate solution in which the combination mode (010001) is obtained from STEOM-XVCC3 in place of ν_5. The frequencies obtained with each set of $\hat{S}$ amplitudes are

relatively similar and both outperform EOM-XVCC3. Despite the similar accuracy, the eigenvectors of the overtones and combinations obtained by Ext-STEOM-XVCC which involve the modes affected by resonance become muddled. For example, the amplitude $c^{2,6}$ becomes very large for the fundamental mode ν_5 when obtained by Ext-STEOM-XVCC3 with the alternate $\hat{S}$ amplitudes. Likewise, the amplitude $c^{2,4,6}$ becomes large for the overtone (000110) obtained with the alternate $\hat{S}$ amplitudes.

4.8 Conclusion

We have introduced Ext-STEOM-XVCCm (with m being the truncation rank of the $\hat{T}$ and $\hat{S}$ operators), for calculation of anharmonic vibrational frequencies of overtones and combinations. We have presented the diagrammatic working equations of Ext-STEOM-XVCCm in a QFF ($2 \leq m \leq 4$). They have been implemented into efficient computer codes with the aid of a symbolic algebra program and have been applied to two molecules with varied degrees of anharmonicity in their PES's. The Ext-STEOM-XVCCm method outperforms the corresponding EOM-XVCCm method at an increased cost scaling, but are equivalent in cost scaling to STEOM-XVCCm for $m = 2$ and $m = 3$. By invoking an approximation that has a negligible effect on the accuracy, Ext-STEOM-XVCC4 can be implemented at the same cost scaling as STEOM-XVCC4 as well. We have also investigated approximate Ext-STEOM-XVCC methods which we refer to as Ext-STEOM-XVCCm-$\hat{C}_n$ where $n < m$. The Ext-STEOM-XVCC4-$\hat{C}_3$ method proves to be an especially effective method for calculation of overtones and combinations whose character are predominantly two-mode excited products.

4.9 Figures

$$
\bar{\bar{H}} \;=\;
\begin{array}{c}
\\
\langle\Phi_0| \\
\langle\Phi_v| \\
\langle\Phi_{vv}| \\
\langle\Phi_{vvv}| \\
\langle\Phi_{vvvv}|
\end{array}
\begin{array}{c}
\begin{array}{ccccc}
|\Phi_0\rangle & |\Phi_v\rangle & |\Phi_{vv}\rangle & |\Phi_{vvv}\rangle & |\Phi_{vvvv}\rangle
\end{array} \\
\begin{bmatrix}
E_{\mathrm{XVCC}} & \mathbf{X} & \mathbf{X} & \mathbf{X} & \mathbf{X} \\
\mathbf{0} & \mathbf{X} & \mathbf{X} & \mathbf{X} & \mathbf{X} \\
\mathbf{0} & \mathbf{0} & \mathbf{X} & \mathbf{X} & \mathbf{X} \\
\mathbf{0} & \mathbf{0} & \approx \mathbf{0} & \mathbf{X} & \mathbf{X} \\
\mathbf{0} & \mathbf{0} & \approx \mathbf{0} & \approx \mathbf{0} & \mathbf{X}
\end{bmatrix}
\end{array}
$$

Figure 4.1: Structure of the doubly ($\bar{\bar{H}}$) similarity-transformed Hamiltonian of STEOM-XVCC4 in the basis of Hartree products of XVSCF modals. The blocks whose elements are zero or expected to be close to zero are represented by $\mathbf{0}$ and $\approx \mathbf{0}$, respectively, while the others by $\bar{\bar{\mathbf{X}}}$. E_{XVCC} denotes the XVCC4 energy for the ground state. The black dashed-boxed area is the formal diagonalization space of STEOM-XVCC4, while the blue dashed-box represents Ext-STEOM-XVCC4. The red and green dashed-box areas are approximations to the rigorous Ext-STEOM-XVCC4 method.

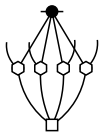

Figure 4.2: A diagram of the $\hat{C}_4$ amplitude equation of Ext-STEOM-XVCC4 in a QFF which contains a product of four $\hat{S}$ amplitudes. Neglecting this term reduces the cost scaling of the $\hat{C}_4$ amplitude equation Ext-STEOM-XVCC4 from $O(N^8)$ to $O(N^7)$.

4.10 Tables

Table 4.1: Rules to draw a component of the doubly similarity transformed Hamiltonian lines of STEOM-XVCCm in a nth-order Taylor-series PES with k upward lines and l downward lines.

(1)	Draw a $\bar{H}$ vertex with up to $n(m-1)$ lines. A $\bar{H}$ vertex with h downward lines can have at most $(n-h)(m-1)$ upward lines.
(2)	Connect zero to l $\hat{S}$ vertices from beneath the $\bar{H}$ vertex leaving k upward external lines and l downward external lines.
(3)	If $k > 1$, connect a $\hat{S}_{h,1}$ vertex (for $2 \leq h \leq k$) from the top to a $\bar{\bar{H}}$ vertex with $k-h+1$ upward lines and l downward lines. Associate a negative sign with these terms.

Table 4.2: The cost scaling of the EOM-XVCCm, STEOM-XVCCm, and Ext-STEOM-XVCCm methods for $2 \leq m \leq 4$. The cost scaling reported for EOM-XVCCm and Ext-STEOM-XVCCm corresponds to the calculation of a few low lying roots using a subspace diagonalization routine, while the STEOM-XVCCm cost is for the calculation of all N fundamentals.

m	EOM-XVCCm	STEOM-XVCCm	Ext-STEOM-XVCCm
2	$O(N^4)$	$O(N^5)$	$O(N^5)$
3	$O(N^5)$	$O(N^6)$	$O(N^6)$
4	$O(N^6)$	$O(N^7)$	$O(N^8)$[1]

[1] The scaling may be reduced to $O(N^7)$ by neglecting $\hat{S}^4$.

Table 4.3: The cost scaling of the $\hat{C}_n$ amplitude equations, which dominate the cost of an iterative subspace diagonalization for a few low lying roots, applied to $\bar{\bar{H}}$ for Ext-STEOM-XVCCm and its approximations. In cases where the cost scaling is lower than the preceding STEOM-XVCCm calculation, the overall cost scaling of the method is determined by the STEOM-XVCCm calculation.

	Ext-STEOM-XVCCm		
m	$\hat{C}_2$	$\hat{C}_3$	$\hat{C}_4$
2	$O(N^4)$	$\cdots$	$\cdots$
3	$O(N^4)$	$O(N^6)$	$\cdots$
4	$O(N^4)$	$O(N^6)$	$O(N^8)$[1]

[1] The scaling may be reduced to $O(N^7)$ by neglecting $\hat{S}^4$.

Table 4.4: The calculated frequencies of overtones and combinations (in cm^{-1}) of the water molecule with a quantum number up to three. Except for EOM-XVCC8, the errors from EOM-XVCC8 are shown.

	Ext-STEOM-XVCCm							EOM-XVCCm					
	2	3		4				2	3	4	5	6	8
Mode		$\hat{C}_2$	$\hat{C}_3$	$\hat{C}_2$	$\hat{C}_3$	$\hat{C}_4$	$\hat{C}_4$[1]						
(020)	23	9	8	4	2	1	1	46	14	5	1	0	3079
(110)	44	8	3	5	0	1	1	86	8	2	1	0	5193
(011)	47	7	2	6	0	0	0	110	12	3	1	0	5274
(200)	51	−19	−4	−13	1	0	0	321	11	−3	−1	1	7331
(101)	42	−36	−8	−27	−1	−1	−1	544	15	−6	−4	0	7431
(002)	50	−17	−5	−12	−0	−0	−0	465	11	−4	−2	0	7553
(030)	$\cdots$	$\cdots$	33	$\cdots$	21	9	9	$\cdots$	109	39	17	6	4553
(120)	$\cdots$	$\cdots$	14	$\cdots$	5	2	2	$\cdots$	38	20	9	3	6681
(021)	$\cdots$	$\cdots$	15	$\cdots$	8	3	3	$\cdots$	76	29	9	3	6730
(210)	$\cdots$	$\cdots$	20	$\cdots$	21	3	3	$\cdots$	215	38	11	4	8766
(111)	$\cdots$	$\cdots$	10	$\cdots$	13	2	2	$\cdots$	422	49	11	2	8832
(012)	$\cdots$	$\cdots$	10	$\cdots$	8	1	1	$\cdots$	361	38	9	2	8951
(300)	$\cdots$	$\cdots$	−82	$\cdots$	−64	4	4	$\cdots$	688	56	3	−5	10973
(201)	$\cdots$	$\cdots$	−152	$\cdots$	−129	4	4	$\cdots$	1322	72	−7	−14	11099
(102)	$\cdots$	$\cdots$	−130	$\cdots$	−113	5	5	$\cdots$	1210	82	−4	−14	11211
(003)	$\cdots$	$\cdots$	−64	$\cdots$	−54	3	3	$\cdots$	430	55	−6	−7	11302

[1] Neglecting $\hat{S}^4$.

Table 4.5: The calculated frequencies of the fundamental ν_5 and selected combination modes (in cm^{-1}) of the formaldehyde molecule. Except for EOM-XVCC8, the errors from EOM-XVCC8 are shown.

	Ext-STEOM-XVCCm		EOM-XVCCm	
Mode	$m = 3$	$m = 3$[1]	$m = 3$	$m = 8$
ν_5	1	−1	1	2873
(010001)	1	1	1	2989
(000101)	4	4	6	2400
(011000)	2	2	4	3213
(000110)	6	4	24	4001
(000011)	4	2	34	4082
(010002)	1	9	39	4226
(010010)	1	11	57	4555
(020001)	−5	4	67	4717

[1] Obtained with a different set of $\hat{S}$ amplitudes. The combination mode (010001) was obtained by the preceding STEOM-XVCC3 calculation and ν_5 was obtained by Ext-STEOM-XVCC3.

Chapter 5

XVMP2 for one-dimensional crystalline systems

5.1 Introduction

To date, the size-extensive vibrational methods of XVMP2 and XVCC have only been implemented on molecular systems. The rigorous size-consistency of these methods, along with their efficiency, make them ideal methods for anharmonic vibrational calculations on extended systems.

In this chapter, we present the first application of XVMP2 to calculate anharmonic phonon dispersion of one-dimensional periodic systems. Since XVMP2 was designed with ultimate applications to large molecules and solids in mind, there is no need to modify the formalism except to adapt it to periodic boundary conditions. However, the continuous nature of phonon dispersion seemingly leads to many divergent integrals in the XVMP2 equations. We demonstrate that this is only a technical challenge and successfully calculate finite corrections to the anharmonic phonon dispersion curves.

We first apply XVMP2 to a model solid with anharmonic nearest neighbor interactions. We demonstrate that the self-consistent solution of the XVMP2 equations allows us to obtain accurate results even in the presence of resonance between branches. We then apply XVMP2 to the optical phonon modes of polyethylene with a cubic force field. We obtain reasonable agreement with experiment and other theoretical calculations despite the relatively low accuracy PES. Furthermore, we also find examples of resonance between branches as predicted by experiment and previous VCI calculations.

5.2 XVMP2 for one-dimensional periodicity

The XVMPn method (where n is the perturbation order) is based on the vibrational Dyson equation, which reads

$$\mathbf{G}(\nu) = \mathbf{G}_0(\nu) + \mathbf{G}_0(\nu)\mathbf{\Sigma}(\nu)\mathbf{G}(\nu), \tag{5.1}$$

where $\mathbf{G}$ and $\mathbf{G}_0$ are the exact and zeroth-order single particle Green's functions respectively and $\mathbf{\Sigma}$ is the Dyson self-energy. The exact vibrational transition frequencies are given by the poles of $\mathbf{G}$. To find the poles of $\mathbf{G}$, we multiply

$\mathbf{G}^{-1}$ from the right and $\mathbf{G}_0^{-1}$ from the left to obtain the inverse Dyson equation

$$\mathbf{G}^{-1}(\nu) = \mathbf{G}_0^{-1} - \mathbf{\Sigma}(\nu). \tag{5.2}$$

The zeroth-order Green's function utilized in XVMP*n* (originally defined in Ref. 14) is given by

$$\{\mathbf{G}^{(0)}(\nu)\}_{q_{k_q}}^{p_{k_p}} = \frac{\delta_{pq}\Delta_{k_p+k_q}}{\nu - \omega_{p_{k_p}} + i\delta} + \frac{\delta_{pq}\Delta_{k_p+k_q}}{-\nu - \omega_{p_{k_p}} + i\delta} = \delta_{pq}\Delta_{k_p+k_q}\frac{2\omega_{p_{k_p}}}{\nu^2 - \omega_{p_{k_p}}^2 + i\delta}, \tag{5.3}$$

where we have modified the definition for periodic boundary conditions. The reference frequency of the pth phonon branch with quasimomentum k_p is given by $\omega_{p_{k_p}}$, $i\delta$ is a positive infinitesimal, and Δ_k enforces the momentum conservation condition. That is $\Delta_k = 1$ if $k = 2n\pi/a$ where n is an integer and Δk is zero. In the XVMP*n* formalism, the diagonal approximation to the self-energy was employed, so the inverse Dyson equation simplifies to

$$\{\mathbf{G}^{-1}(\nu)\}_{m_{-k_m}}^{m_{k_m}} = \frac{\nu^2 - \omega_{m_{k_m}}^2}{2\omega_{m_{k_m}}} - \Sigma_{m_{k_m}}(\nu), \tag{5.4}$$

where $\Sigma_{m_{k_m}}(\nu) = \{\mathbf{\Sigma}(\nu)\}_{m_{-k_m}}^{m_{k_m}}$. The off-diagonal elements of $\mathbf{\Sigma}(\nu)$ in the first-order perturbation approximation have been shown to be negligible. The off-diagonal elements of $\mathbf{\Sigma}$ for higher-orders are accounted for by the definition of the self-energy. [14] The XVMP*n* frequencies are then given by the poles of $\mathbf{G}(\nu)$ which occur at

$$\nu_{m_{k_m}} = \sqrt{\omega_{m_{k_m}}^2 + 2\omega_{m_{k_m}}\Sigma_{m_{k_m}}(\nu_{m_{k_m}})}. \tag{5.5}$$

The form of the self-energy utilized in our calculations will be defined in the next section.

5.2.1 Second-order Dyson self-energy

All possible second-order self-energy diagrams in a QFF were illustrated in Ref. 14. In this work we considered only up to cubic anharmonicity and utilized a harmonic reference. In this case, only the four self-energy diagrams illustrated in Fig. 5.1 are required. The corresponding algebraic interpretations of the diagrams are generated by the rules described in Ref. 14 with one modification for periodic boundary conditions: each line is labeled with a branch label and a quasimomentum. Applying these rules to the first two diagrams of Fig. 5.1 yields

$$\Sigma(\nu)_{m_{k_m}}^{(\mathbf{2a})} = \Sigma(\nu)_{m_{k_m}}^{(\mathbf{2b})} \tag{5.6}$$

$$= \frac{1}{2}\sum_{k_p,k_q}\sum_{p,q}\frac{\tilde{F}_{p_{k_p}m_{k_m}m_{-k_m}}\tilde{F}_{p_{k_p}q_{k_q}q_{-k_q}}}{-\omega_{p_{k_p}}}. \tag{5.7}$$

the $\tilde{F}$'s are scaled force constants

$$\tilde{F}_{p_{k_p} q_{k_q} r_{k_r}} = \frac{F_{p_{k_p} q_{k_q} r_{k_r}}}{(2\omega_{p_{k_p}})^{-1/2}(2\omega_{q_{k_q}})^{-1/2}(2\omega_{r_{k_r}})^{-1/2}}. \tag{5.8}$$

Enforcing conservation of momentum, the sum over k_p vanishes, so we obtain

$$\Sigma(\nu)^{(\mathbf{2a})}_{m_{k_m}} = \Sigma(\nu)^{(\mathbf{2b})}_{m_{k_m}} \tag{5.9}$$

$$= \frac{1}{2}\sum_{k_q}\sum_{p,q}\frac{\tilde{F}_{p_0 m_{k_m} m_{-k_m}}\tilde{F}_{p_0 q_{k_q} q_{-k_q}}}{-\omega_{p_0}}. \tag{5.10}$$

The contribution from this term is only non-zero when p does not label an acoustic branch. Otherwise, the term is zero because the numerator vanishes faster than the denominator. Likewise, the remaining diagrams are

$$\Sigma(\nu)^{(\mathbf{2e})}_{m_{k_m}} = \frac{1}{2}\sum_{k_p}\sum_{p,q}\frac{|\tilde{F}_{m_{-k_m} p_{k_p} q_{-(k_p-k_m)}}|^2}{\nu - \omega_{p_{k_p}} - \omega_{q_{-(k_p-k_m)}}}, \tag{5.11}$$

$$\Sigma(\nu)^{(\mathbf{2f})}_{m_{k_m}} = \frac{1}{2}\sum_{k_p}\sum_{p,q}\frac{|\tilde{F}_{m_{k_m} p_{k_p} q_{-(k_p+k_m)}}|^2}{-\nu - \omega_{p_{k_p}} - \omega_{q_{-(k_p+k_m)}}}, \tag{5.12}$$

where the sum over k_q vanishes due to momentum conservation.

Inspection of $\Sigma(\nu)^{(\mathbf{2e})}$ reveals a potential issue. Since the anharmonic and harmonic phonon dispersion curves are continuous, it would be expected that the integrals would be plagued with a large number of divergences. However, the term $\Sigma(\nu)^{(\mathbf{2e})}$ can also equivalently be written

$$\Sigma(\nu)^{(\mathbf{2e})}_{m_{k_m}} = \frac{1}{2}\frac{a}{2\pi}\sum_{p,q}\int_{-\pi/a}^{\pi/a}\frac{|\tilde{F}_{m_{-k_m} p_{k_p} q_{-(-k_m+k_p)}}|^2}{\nu - \omega_{p_{k_p}} - \omega_{q_{-(-k_m+k_p)}} + i\delta}dk_p \tag{5.13}$$

where a is the lattice constant which is equal to a volume element for a one-dimensional system. A well known relation from complex analysis [141] reads

$$\int_{-\infty}^{\infty}\frac{f(x)dx}{x - x_0 + i\epsilon} = \mathcal{P}\int_{-\infty}^{\infty}\frac{f(x)dx}{x - x_0} - i\pi f(x_0), \tag{5.14}$$

where $\mathcal{P}$ represents the principal value of the integral which is given by

$$\mathcal{P}\int_{a_1}^{a_3} f(x)dx = \lim_{\epsilon\to 0}\left[\int_{a_1}^{a_2-\epsilon} f(x)dx + \int_{a_2+\epsilon}^{a_3} f(x)dx\right], \tag{5.15}$$

where a_1 and a_3 are integration limits and a_2 is the location of a pole. Applying this relationship to $\Sigma(\nu)^{(\mathbf{2e})}$, the

correction to the anharmonic frequency is given by

$$\Sigma(\nu)^{(\mathbf{2e})}_{m_{k_m}} = \frac{1}{2}\frac{a}{2\pi}\sum_{p,q}\mathcal{P}\int_{-\pi/a}^{\pi/a}\frac{|\tilde{F}_{m_{-k_m}p_{k_p}q_{-(-k_m+k_p)}}|^2}{\nu-\omega_{p_{k_p}}-\omega_{q_{-(-k_m+k_p)}}}dk_p, \tag{5.16}$$

and the second term of Eq. (5.14) corresponds to a linewidth. Although the denominator of the integral may still go to zero, the principal value of the integral may remain finite and is calculated per Eq. (5.15). While the above analysis holds true for all four self-energy diagrams, only $\Sigma(\nu)^{(\mathbf{2e})}$ is affected by resonance. Therefore, the other terms may be accurately calculated on a grid using Eqs. (5.10) and (5.12).

5.3 Numerical tests

The XVMP2 method with a harmonic reference was used to calculate the phonon dispersion curves of a model two-mass solid and the optical modes of polyethylene.

Since ν appears on both sides, the solution of Eq. (5.5) requires a self-consistent solution. The frequency-dependence of the right-hand side arises from the presence of ν in the denominator of $\Sigma(\nu)^{(\mathbf{2e})}$ and $\Sigma(\nu)^{(\mathbf{2f})}$. The XVMP2 frequency of phonon branch m with quasimomentum k_m was found by locating the roots of $F(\nu)$ with the secant method available from SCIPY where

$$F(\nu) = \sqrt{\omega^2_{m_{k_m}} + 2\omega_{m_{k_m}}\Sigma_{m_{k_m}}(\nu)} - \nu. \tag{5.17}$$

In cases of resonance, multiple solutions of Eq. (5.17) may be found.

The principal value integrals required to calculate the contribution of $\Sigma(\nu)^{(\mathbf{2e})}$ were calculated as follows. First, the roots of the denominator $\nu - \omega_{p_{k_p}} - \omega_{q_{k_q}}$ were located in the range of $-\pi/a$ to π/a where a is the lattice constant. If no roots were found, the contribution of that term was simply calculated by Eq. (5.11). Otherwise, an interpolating spline was calculated separately for the numerator and denominator of $\Sigma(\nu)^{(\mathbf{2e})}$. Using the splines, an adaptive quadrature routine (available from SCIPY) was applied to each segment of the integral between the poles per Eq. (5.15).

The potential energy as a function of the Cartesian coordinates for the model system is

$$V(\mathbf{x}) = V_2(\mathbf{x}) + V_3(\mathbf{x}) \tag{5.18}$$

with

$$V_2(\mathbf{x}) = \frac{1}{2}k'\left(x_{2(0)} - x_{1(0)}\right)^2 + \frac{1}{2}k'\left(x_{1(1)} - x_{2(0)}\right)^2 + \frac{1}{2}k'\left(x_{1(0)} - x_{2(-1)}\right)^2 + \cdots, \tag{5.19}$$

$$V_3(\mathbf{x}) = \frac{1}{3!}k''\left(x_{2(0)} - x_{1(0)}\right)^3 + \frac{1}{3!}k''\left(x_{1(1)} - x_{2(0)}\right)^3 + \frac{1}{3!}k''\left(x_{1(0)} - x_{2(-1)}\right)^3 + \cdots, \tag{5.20}$$

where $x_{\mu(m)}$ is the displacement of the μth mass in the mth unit cell from its equilibrium position and k' and k'' are constants. The Cartesian force constants are then given by derivatives of the potential. For example, the non-zero harmonic force constants are given by

$$F_{\mu(0)\mu(0)} = \frac{2k'}{m_\mu} \tag{5.21}$$

$$F_{\mu(0)\nu(m)} = \frac{-k'}{m_\mu^{1/2} m_\nu^{1/2}} \tag{5.22}$$

for $\mu \neq \nu$ and m_μ is the mass associated with the μth coordinate. The constants k' and k'' were set to 0.5 for each calculation. The mass associated with the first coordinate m_1 was set to unity for each calculation, while we considered values of 3.5 and 5 for m_2. The third-order force constants are obtained in the same manner.

The polyethylene PES was approximated by a cubic force field generated by electronic structure calculations on long oligomers. Harmonic force constants were calculated for oligomers with 13 unit cells. Cubic force constants between atoms more than one unit cell apart were neglected. The equilibrium structure was determined by geometry optimizations of the oligomers at MP2 with the 6-31g(p,d) basis set using Gaussian. [149] The structural parameters utilized for all force constant calculations are listed in Table 5.1. The harmonic force constants were obtained via the analytic Hessian matrix available in the Gaussian program. The cubic force constants were obtained by finite difference of analytic gradients. Symmetry considerations were used to set force constants to zero when applicable.

The Cartesian force constants for each system were transformed into the normal-coordinates using Eqs. (1.36) and (1.37).

5.3.1 Two-mass system

The anharmonic and harmonic phonon dispersion of a two-mass system with $m_2 = 5$ are shown in Fig. 5.2. There are no major qualitative changes to the shapes of the curves, but there is a significant decrease in the frequency of both curves. This is expected since anharmonicity effectively softens the harmonic spring constant. It should be noted that despite the seemingly subtle anharmonic corrections, a self-consistent solution of Eq. (5.5) was required. A one-shot evaluation of Eq. (5.5) with $\nu_{m_{k_m}}$ equal to the reference frequency leads to divergent results for certain portions of the phonon dispersion curves.

The anharmonic and harmonic phonon dispersion of a two-mass system with $m_2 = 3.5$ are shown in Fig. 5.2. The effect of anharmonicity has a much larger effect on this system because of the smaller gap in energy between the two harmonic branches. There is coupling between the optical branch and branches which correspond to overtones and combinations of the acoustic branch (which are dark in the harmonic approximation). This gives rise to multiple solutions to Eq. (5.5) in certain regions of the dispersion curve. For example, a graphical representation of the solution of Eq. (5.5) is shown in Figs. 5.4 - 5.6. At the gamma point the self-energy is relatively weakly dependent on ν and there is only one root in the vicinity of the reference frequency. However, as seen in Fig. 5.5, at a phase difference of 0.5 the self-energy is more strongly dependent on ν and two roots are present. At a phase difference of 1.0, shown in Fig. 5.6, the self-energy is again more weakly dependent on ν and only one root is found in the vicinity of the reference frequency. Interestingly, there is no smooth curve connecting the frequencies obtained at the edges of the dispersion curves. The dispersion curve can be understood as follows. Near the gamma point, there is no strong coupling between the optical branch and overtones and combinations of the acoustic branch. However, as the phase difference approaches 0.5, the optical branch becomes close in frequency and couples with a branch corresponding to overtone and combination modes. The character of the branches is mixed in this region and assignment of one or the other to the optical branch is poorly defined. Moving towards the edge of the dispersion curve, the branches separate in frequency and the coupling weakens. However, the character of the branches flips. The higher frequency branch corresponds to the optical branch, while the dark branch has a lower frequency.

5.3.2 Optical modes of polyethylene

The anharmonic and harmonic phonon dispersion of the optical modes of polyethylene in the range of 700–1700 cm^{-1} are shown in Fig. 5.7. There is a modest correction (on the order of 10s of cm^{-1} for most of the branches. The magnitude of the corrections are similar to the anharmonic corrections obtained previously with VMP2 within the gamma approximation (only in phase vibrations are considered). [150] Since VMP2 is not rigorously size-consistent, the gamma approximation is required, so phonon dispersion cannot be calculated. The XVMP2 method can be equally applied to the entire phonon dispersion curve.

The XVMP2 calculations also successfully predict the presence of Fermi resonance. A Fermi doublet has been experimentally observed in Raman spectra [151–153], and VCI calculations within the gamma approximation revealed the presence of Fermi resonance between $\nu_2(0)$ (the second-highest frequency branch) and the first overtone of $\nu_8(\pi)$ (the lowest frequency branch). [150] (The naming convention for the modes is discussed in Ref. 154.) The experimentally observed frequencies are at approximately 1442 and 1468 cm^{-1}, while the VCI calculations predicted frequencies at 1498 and 1542 cm^{-1}. As illustrated in Fig. 5.8, XVMP2 also captures this resonance with roots at roughly 1482 and 1526 cm^{-1}. While the absolute frequencies are somewhat higher than the experimentally observed peaks, the split in

frequency is semi-qualitatively reproduced.

The results obtained here are still less accurate than harmonic frequencies scaled with a single empirical factor with a PES calculated by density functional theory. [154] Much of the error in our calculations can be attributed to the relatively inaccurate PES we utilized for these initial calculations. A PES obtained with a larger basis-set that includes up to quartic anharmonicity would be expected to significantly improve the accuracy. Furthermore, unlike XVMP2, the harmonic calculations are incapable of capturing the experimentally observed Fermi doublet.

5.4 Conclusion

We applied periodic boundary conditions to the XVMP2 formalism and reported the first application of XVMP2 to a system with one-dimensional periodicity. We demonstrated that finite results could be obtained by direct calculation of the principal value integrals which contribute to the Dyson self-energy. We applied XVMP2 to a model solid with varying degrees of coupling between branches. We demonstrated that XVMP2 could successfully describe Fermi resonance between branches which correspond to overtones and combinations and the fundamental branches. We successfully applied XVMP2 to polyethylene in a cubic force field. We obtained results which are on the same order of accuracy as similar VMP2 calculations obtained in the gamma approximation. However, unlike the VMP2 calculations, XVMP2 is rigorously size-consistent and can be applied to the entire phonon dispersion curve.

5.5 Figures

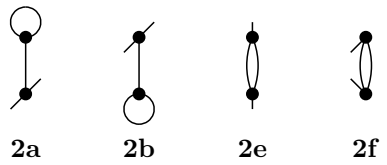

Figure 5.1: Required self-energy diagrams of XVMP2 with a harmonic reference in a 3rd-order Taylor-series PES.

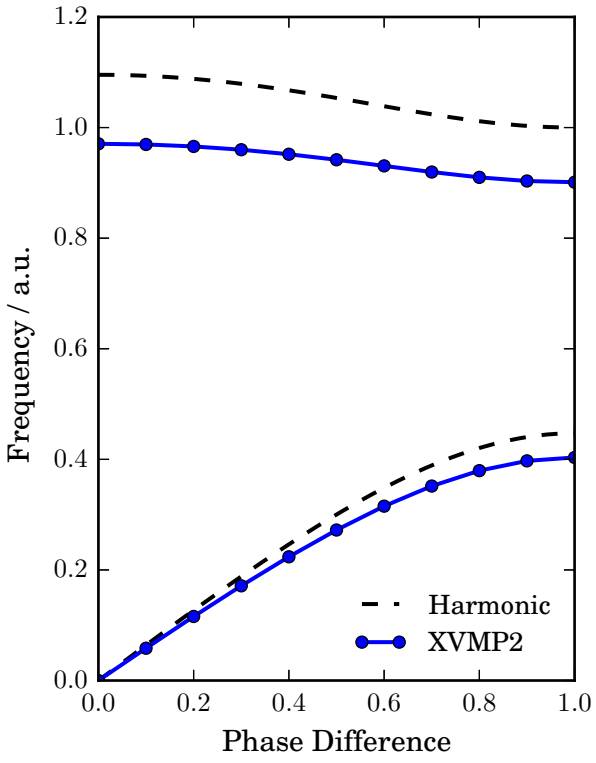

Figure 5.2: Calculated anharmonic phonon dispersion of two-mass sytem with $m_1 = 1$ and $m_2 = 5$ using XVMP2 with a harmonic reference. The harmonic approximation is shown for comparison.

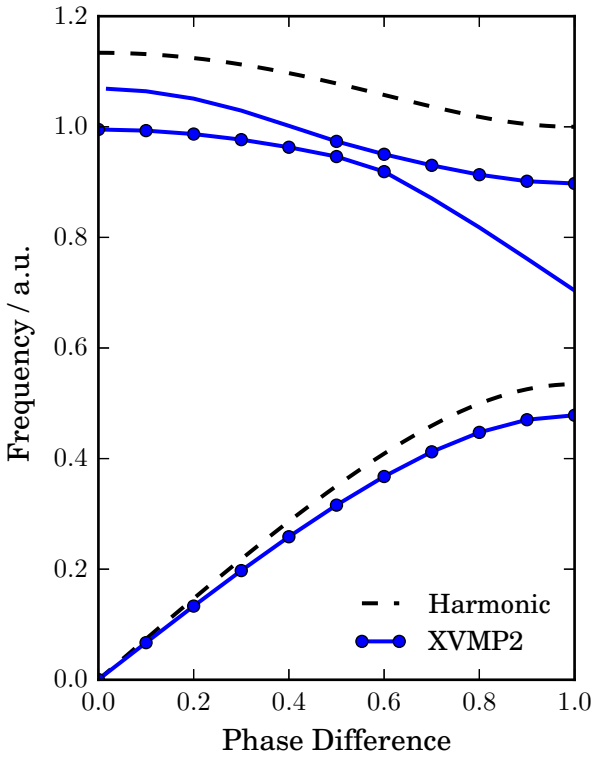

Figure 5.3: Calculated anharmonic phonon dispersion of two-mass sytem with $m_1 = 1$ and $m_2 = 3.5$ using XVMP2 with a harmonic reference. The harmonic approximation is shown for comparison. The portions of the dispersion curves labeled with points and lines were obtained as the fundamental solutions of the XVMP2 equations and correspond to the original optical branch obtained in the harmonic approximation. The absence of points indicates the frequencies were obtained as alternate solutions to the XVMP2 equations and correspond to weaker intensity modes which involve excitation of multiple quanta.

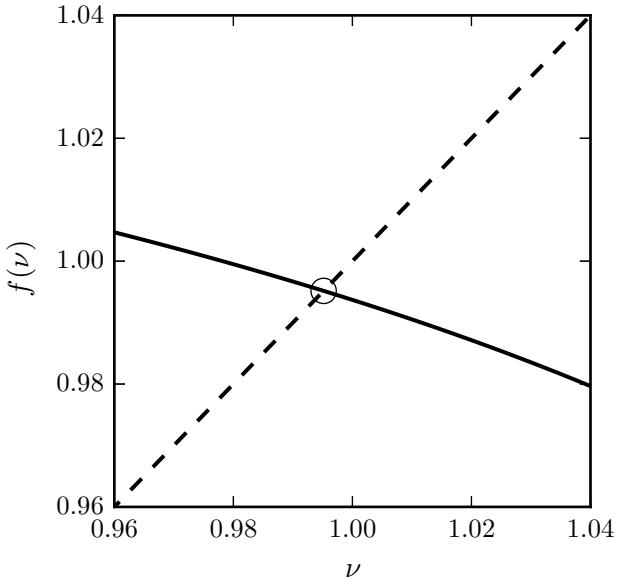

Figure 5.4: A graphical representation of the self-consistent solution of the XVMP2 equation at the gamma point for the two-mass system with $m_2 = 3.5$ where $f(\nu) = \sqrt{\omega_{m_{k_m}} + 2\omega_{m_{k_m}}\Sigma(\nu)_{m_{k_m}}}$. The intersection of the two lines (marked by a circle) is the XVMP2 frequency.

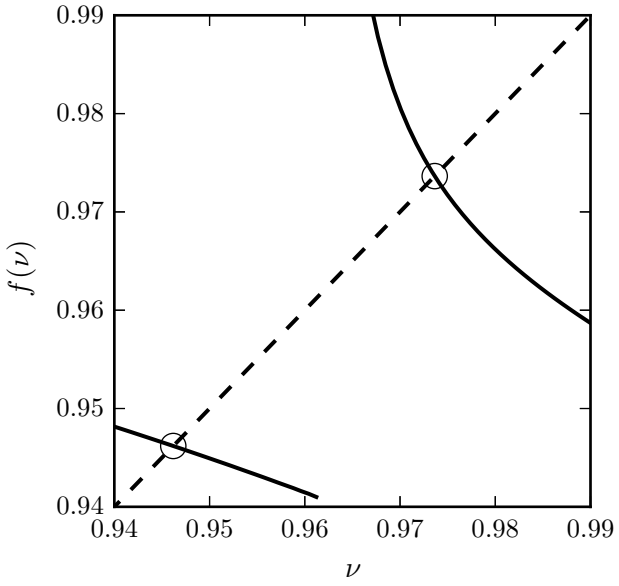

Figure 5.5: Same as Fig. 5.4 except the calculation corresponds to a phase difference of 0.5.

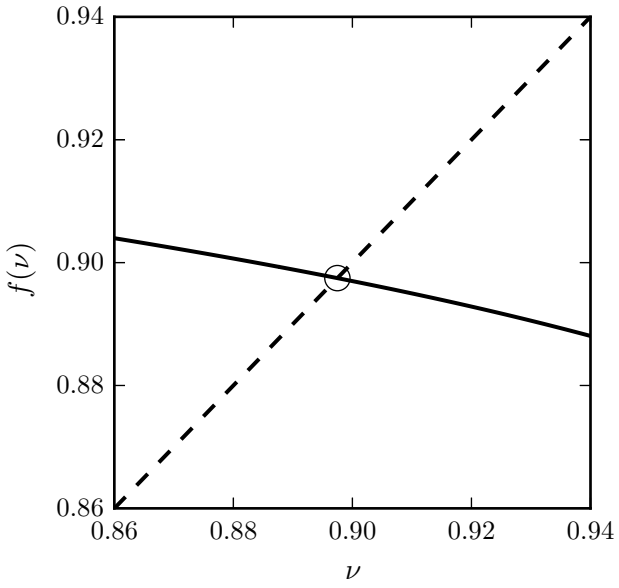

Figure 5.6: Same as Fig. 5.4 except the calculation corresponds to a phase difference of 1.0.

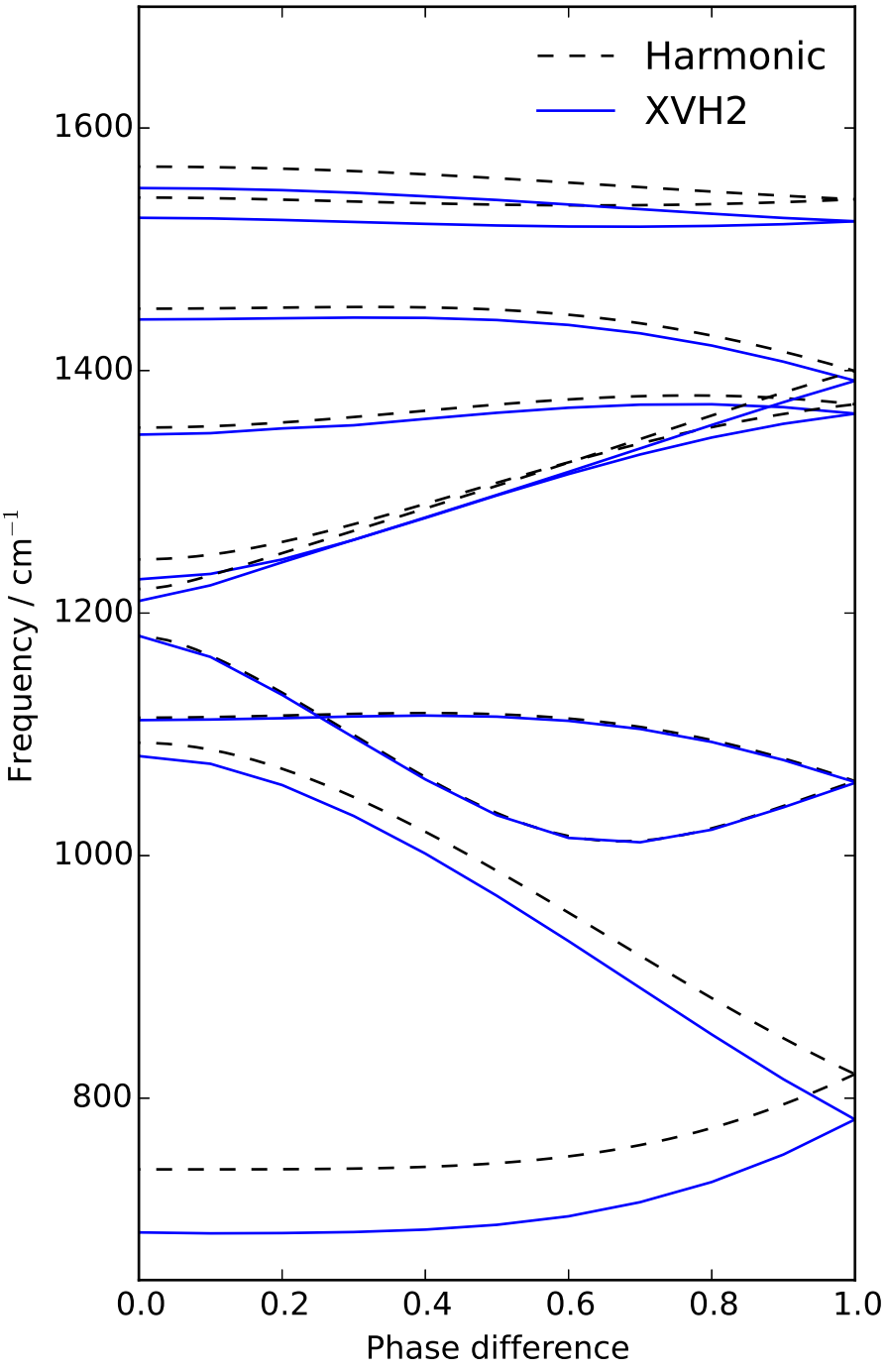

Figure 5.7: Phonon dispersion of the optical modes of polyethylene in the range of 650 cm^{-1} to 1700 cm^{-1}.

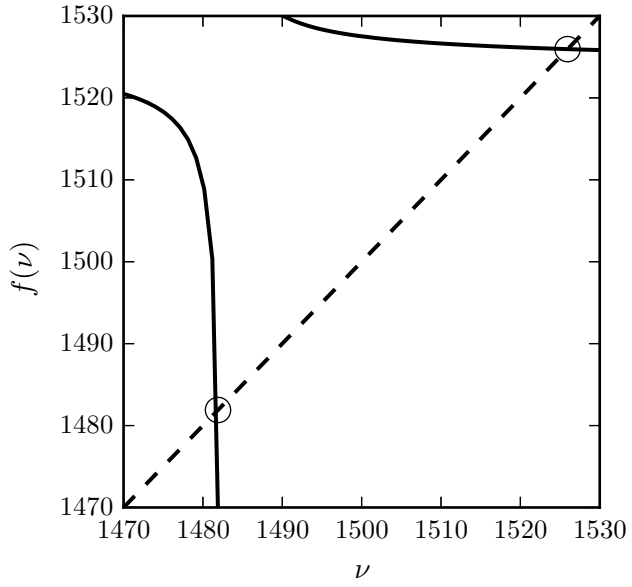

Figure 5.8: A graphical representation of the self-consistent solution of the XVMP2 equation at the gamma point for the phonon branch $\nu_2(0)$ of polyethylene where $f(\nu) = \sqrt{\omega_{m_{k_m}} + 2\omega_{m_{k_m}}\Sigma(\nu)_{m_{k_m}}}$. The intersection of the two lines (marked by a circle) is the XVMP2 frequency.

5.6 Table

Table 5.1: The structural parameters (in Å and degrees) of polyethylene obtained with MP2/6-31g(d,p).

$r_{C–C}$	$r_{C–H}$	a_{CCC}	a_{HCH}
1.526	1.095	113.3	106.3

Chapter 6

Conclusion

In Chapter 2, we presented the XVCC and EOM-XVCC methods for the calculation of zero-point energies and transition frequencies. The methods were built upon the diagrammatically size-consistent vibrational self-consistent field method XVSCF, and they inherit the underlying efficiency of the reference method which requires no basis-sets, grids, or quadrature. We established the rules for the derivation and interpretation of their diagrammatic equations. We authored a symbolic algebra program which enabled derivation of arbitrarily high-order XVCCm and EOM-XVCCm and was utilized to derive and implement the equations up to $m = 8$. The initial numerical tests on small molecules show that these method smoothly and rapidly converge towards the exact results.

In Chapter 3, we formulated the STEOM-XVCC method for the simultaneous calculation of all fundamental frequencies of a molecule. We proved the equivalence between the STEOM-XVCC and EOM-XVCC approach for the fundamentals. Therefore, STEOM-XVCC may be viewed as a particularly convenient root-homing implementation of the EOM-XVCC method. We clarified the relationship between the STEOM approach in the electronic and vibrational contexts and also highlighted the relationship between STEOM-XVCC and vibrational MBGF. We presented the diagrammatic and algebraic equations of STEOM-XVCC4 in a QFF and implemented the method on molecular systems.

In Chapter 4, we further investigated the effectiveness of similarity transformations for the vibrational correlation problem with the development of Ext-STEOM-XVCC for the calculation of the frequencies of overtones and combinations. Unlike STEOM-XVCC, Ext-STEOM-XVCC is not equivalent to EOM-XVCC. The frequencies obtained are higher in accuracy than those of the corresponding EOM-XVCC method but at a higher cost. We identified approximate Ext-STEOM-XVCC methods that give more accurate results than EOM-XVCC at the same cost for certain classes of overtones and combinations. The diagrammatic equations of Ext-STEOM-XVCC4 and the doubly transformed vibrational Hamiltonian in a QFF were documented.

In Chapter 5, we presented the first application of the XVMP2 formalism to a one-dimensional periodic system. We demonstrated that the continuous nature of phonon dispersion curves leads to a technical challenge in the implementation of XVMP2. We directly calculated the required principal value integrals which arise in the XVMP2 formalism under periodic boundary conditions to obtain finite anharmonic corrections. We demonstrated, in anal-

ogy with the molecular implementation, that a self-consistent solution of the XVMP2 equations allows the accurate description of phonon branches in resonance.

Appendix A

XVCC energy and amplitude equations

Below we document the diagrammatic form of the energy and amplitude equations of XVCCm for $m \leq 8$ in a QFF. The equations of XVCCm for $m < 8$ are easily obtained by removing all terms which include a $\hat{T}_n$ vertex with $n > m$.

The diagrammatic form of the XVCCm energy equation ($m \geq 4$) is

$E_0^{(m)}$ =

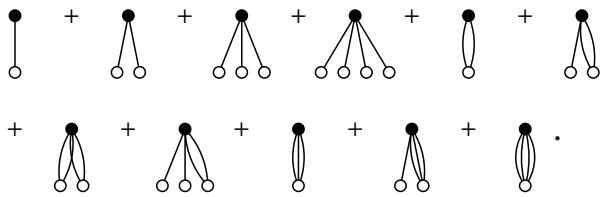

(A.1)

No new terms appear in the energy equation beyond $m = 4$ due to the truncation of the PES to a QFF. However, the numerical value of the energy changes since the $\hat{T}$ amplitudes which satisfy the XVCCm amplitude equations are different.

The $\hat{T}_n$ amplitude equations ($1 \leq n \leq 8$) of XVCC8 in a QFF are

0 =

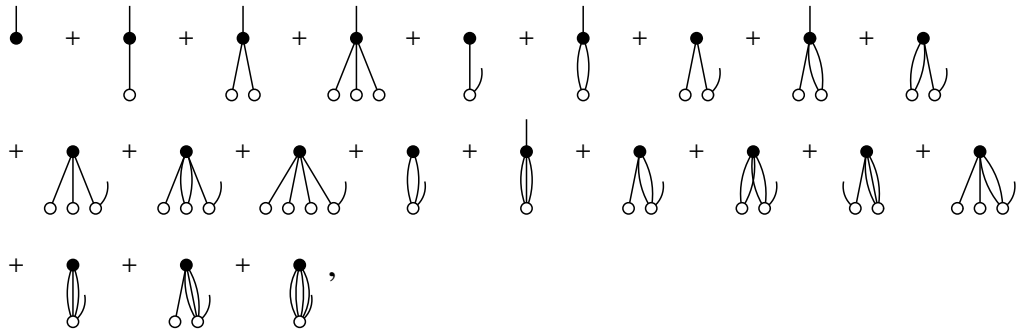

(A.2)

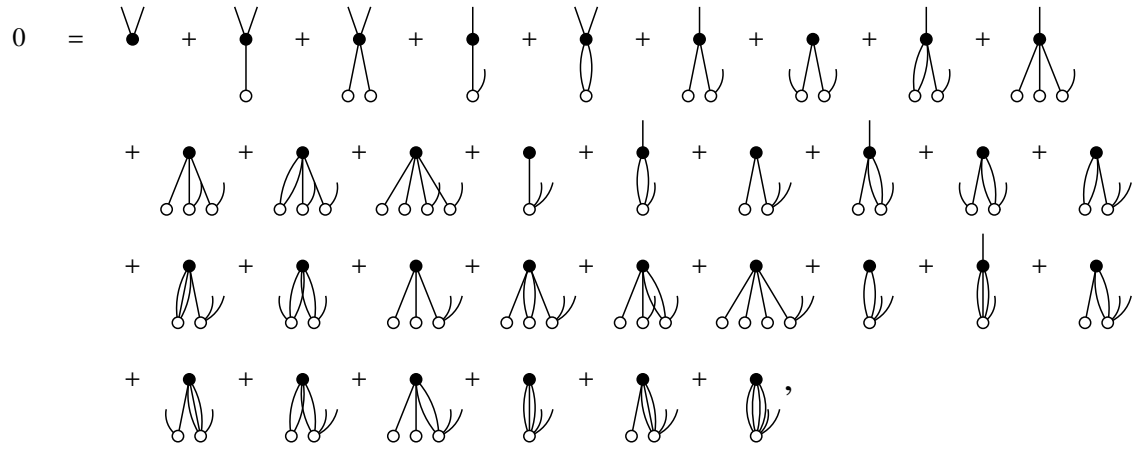

(A.3)

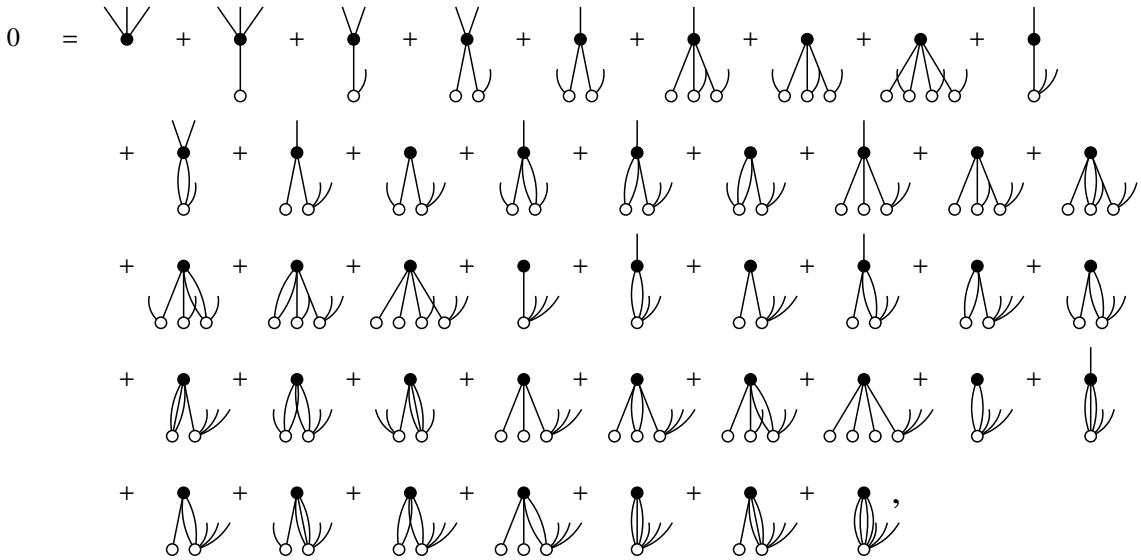

(A.4)

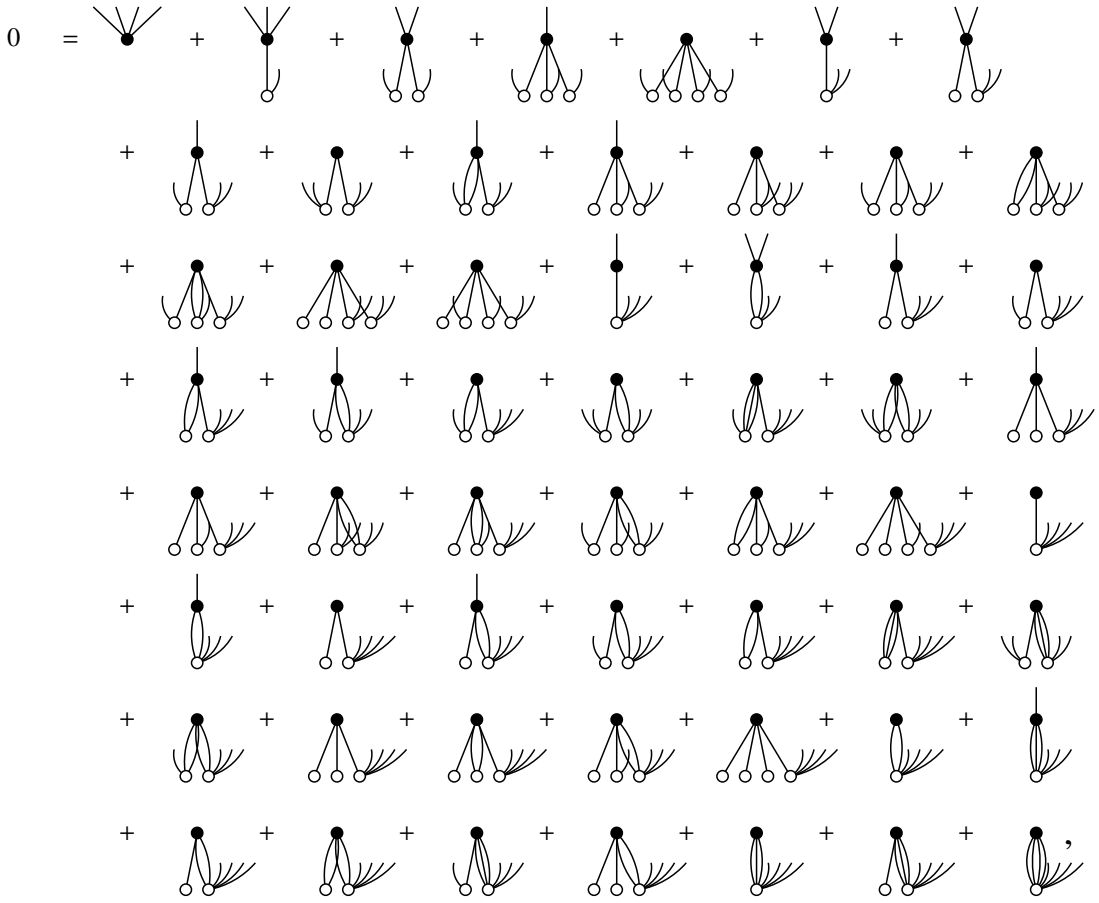

(A.5)

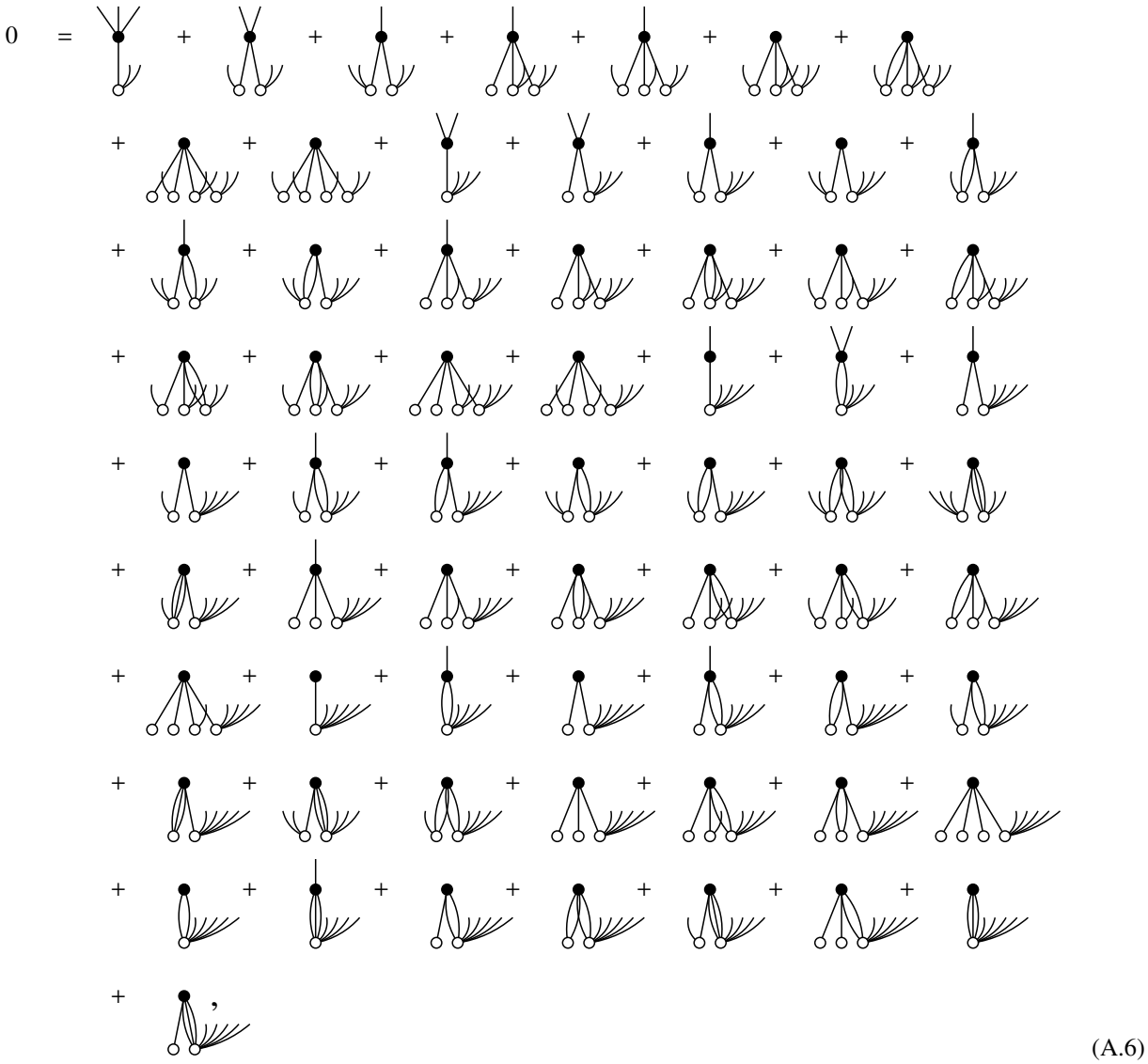

(A.6)

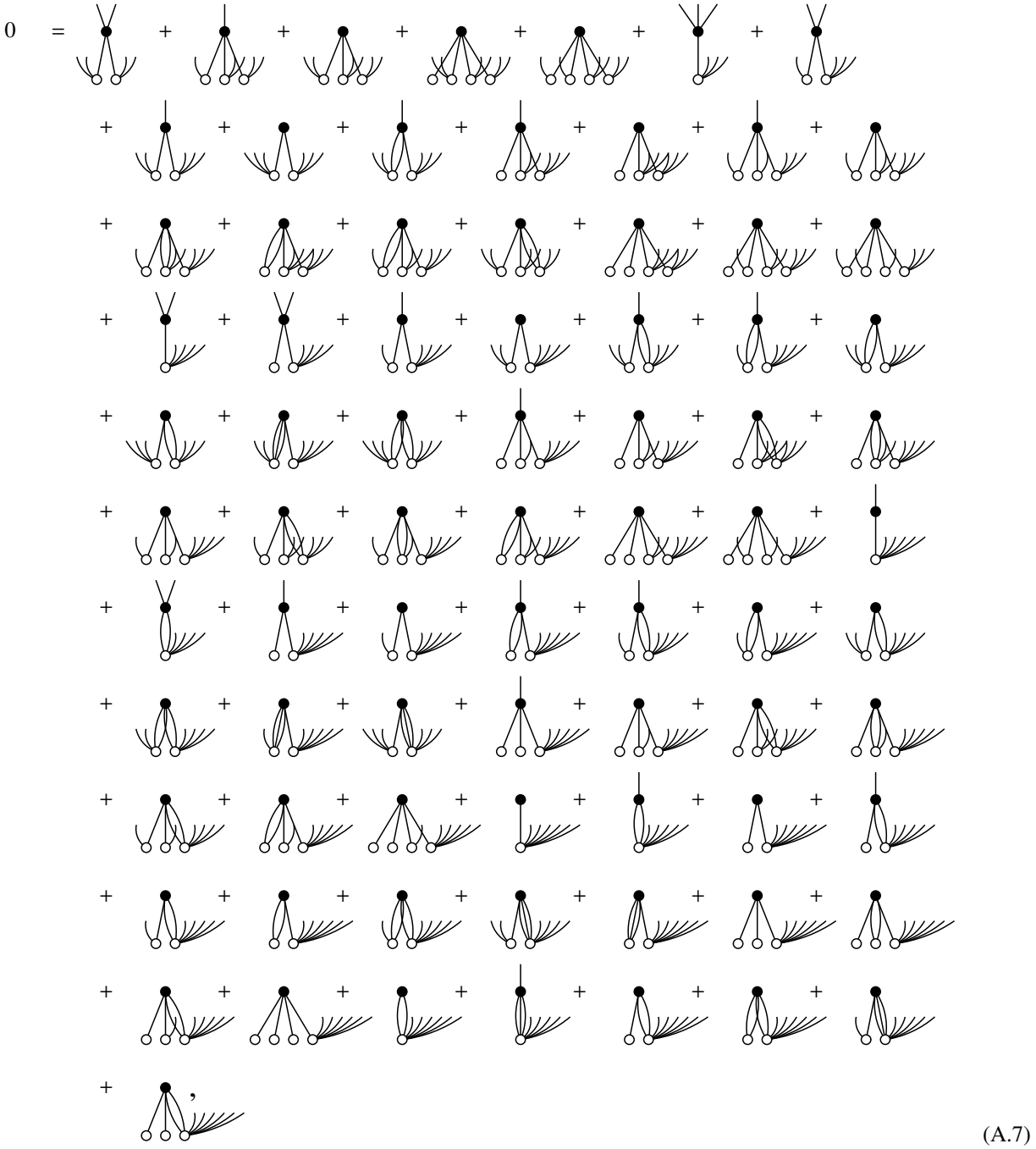

(A.7)

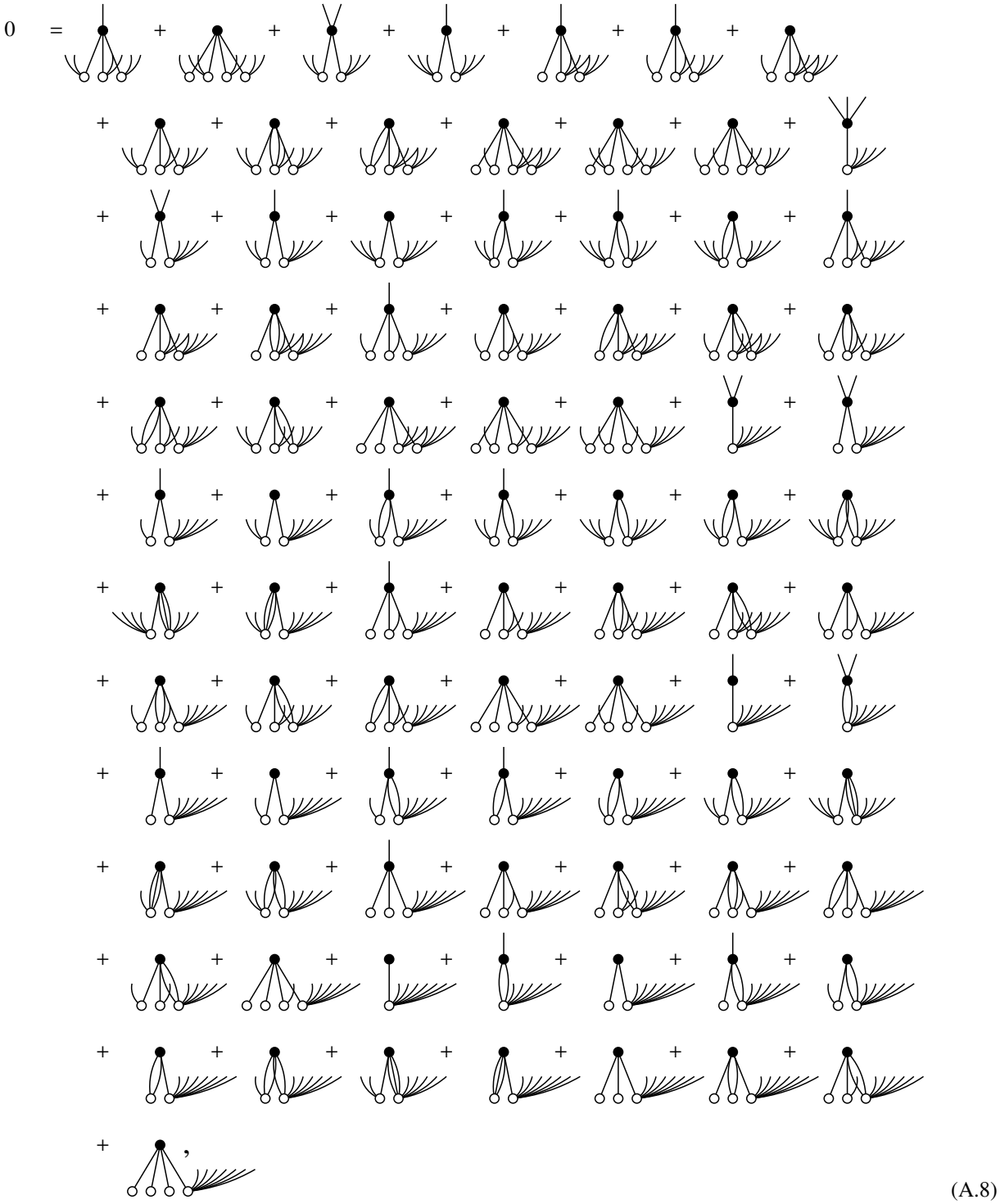

(A.8)

and

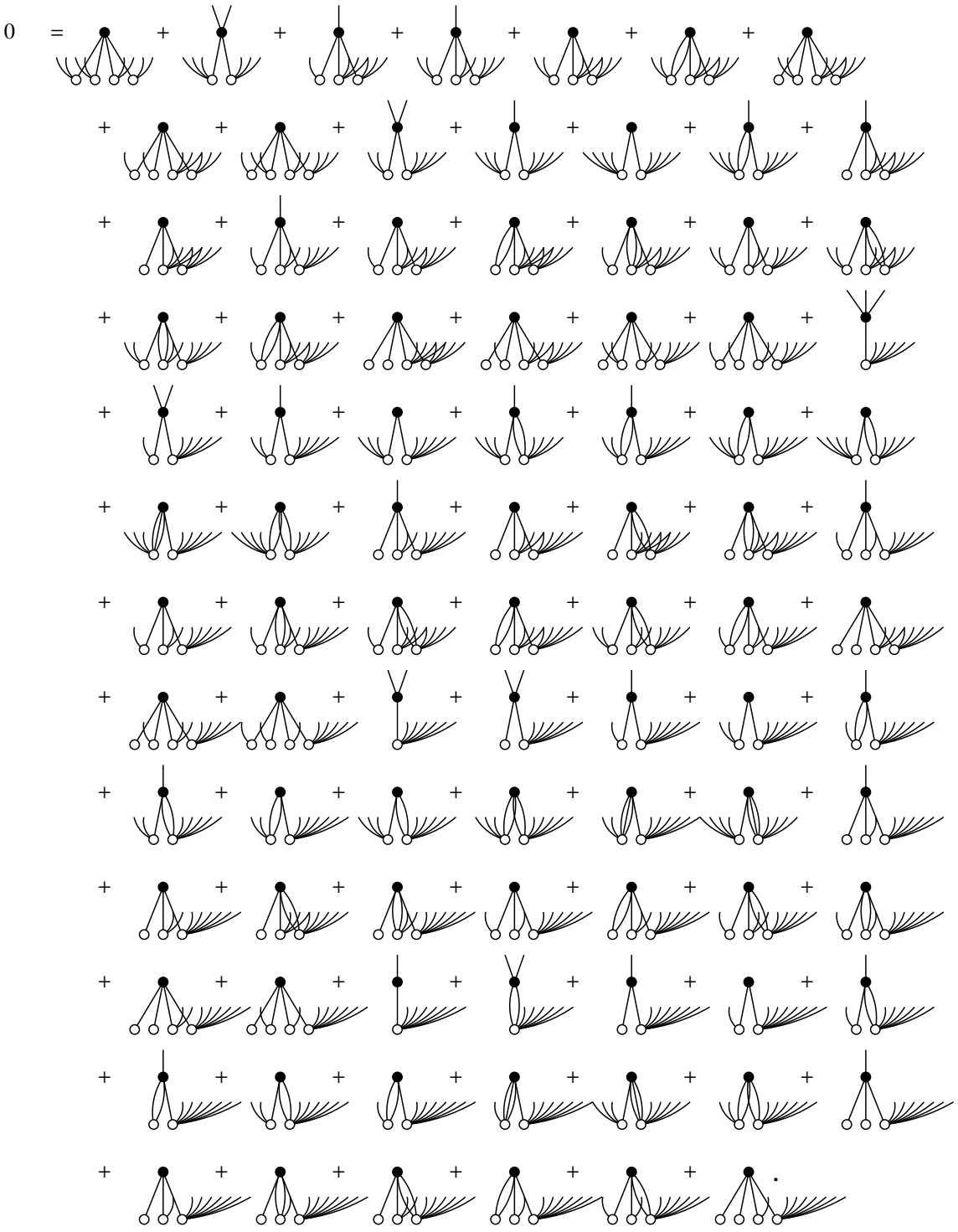

(A.9)

Appendix B

EOM-XVCC amplitude equations

Below we document the EOM-XVCCm amplitude equations for $m \leq 8$ in a QFF in terms of the vertices of the singly transformed Hamiltonian $\bar{H}$ and the vertices of $\hat{R}$. The formal definition of $\bar{H}$ and its diagrammatic representation are presented in Sec. 3.2. The required vertices of $\bar{H}$ in terms of the vertices of $\hat{H}$ and $\hat{T}$ are illustrated in Appendix C. The equations of EOM-XVCCm for $m < 8$ are easily obtained by removing all terms which include a $\hat{T}_n$ or $\hat{R}_n$ vertex with $n > m$.

The $\hat{R}_n$ amplitude equations ($1 \leq n \leq 8$) of EOM-XVCC8 are

$\bar{\omega}_\ell^{(m)}$ 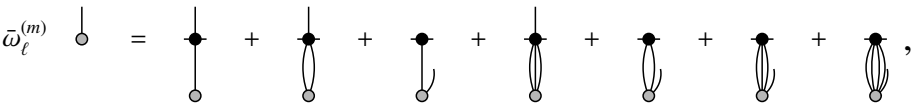 (B.1)

$\bar{\omega}_\ell^{(m)}$ 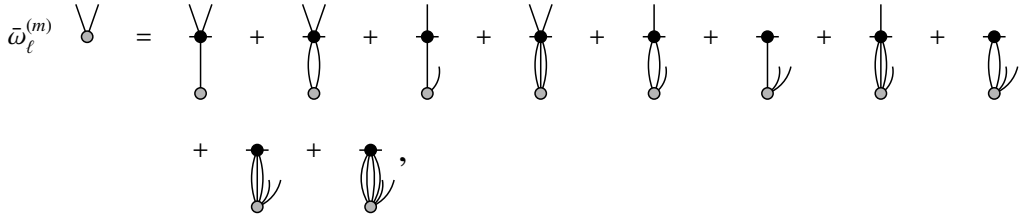 (B.2)

$\bar{\omega}_\ell^{(m)}$ 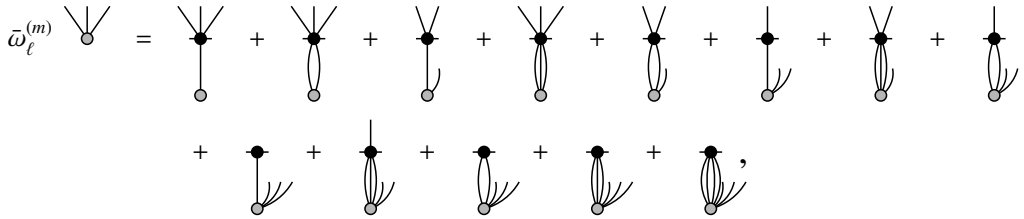 (B.3)

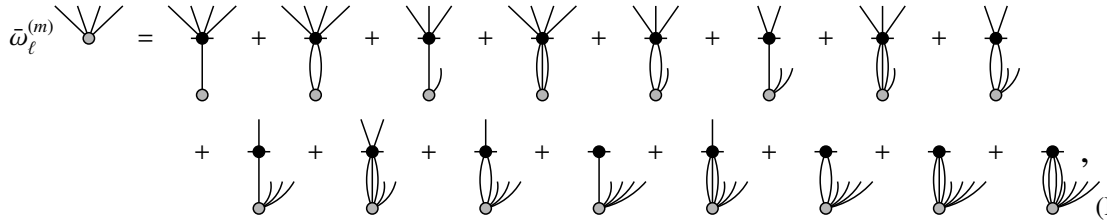

(B.4)

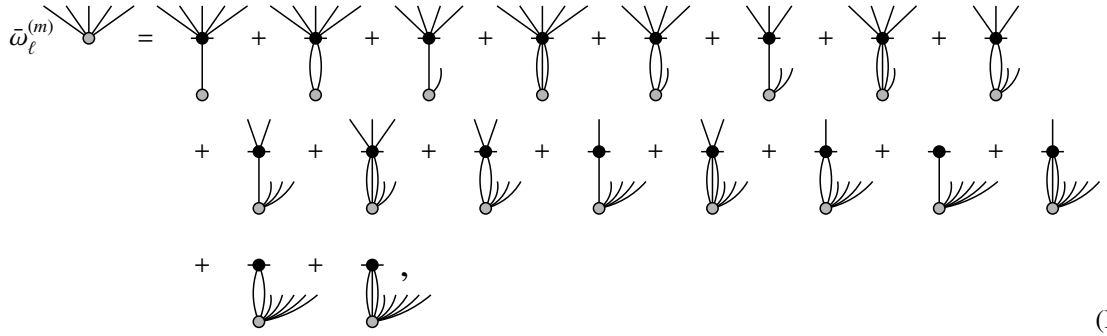

(B.5)

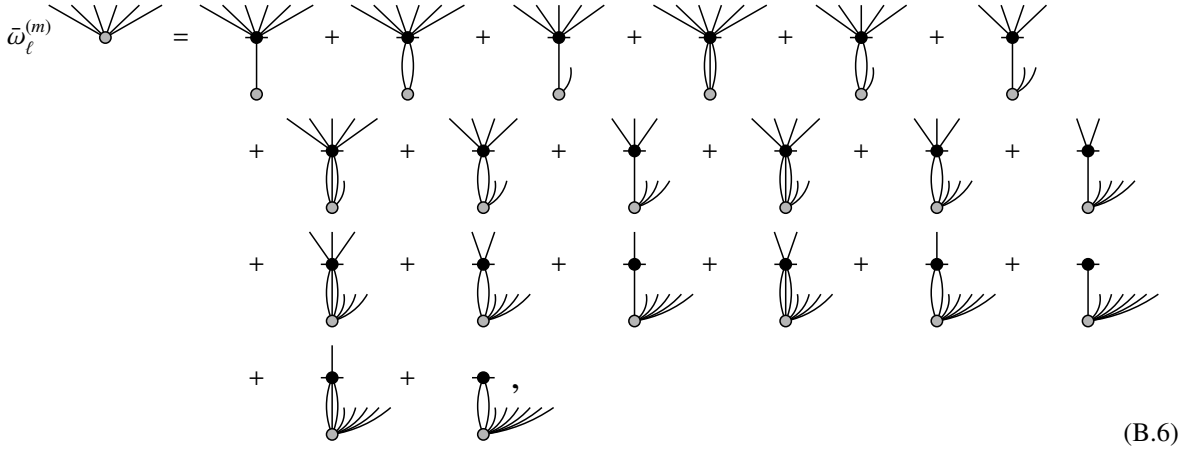

(B.6)

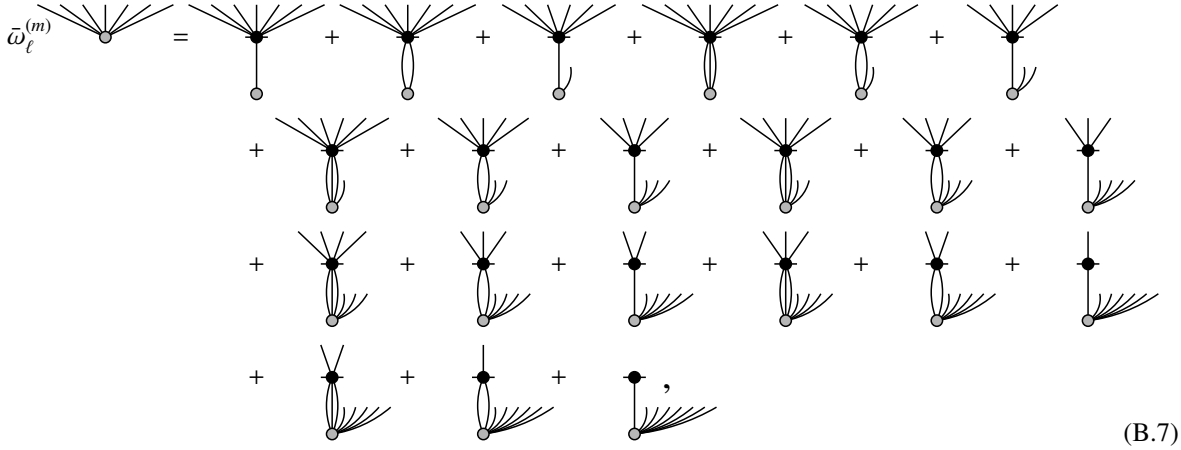

(B.7)

and

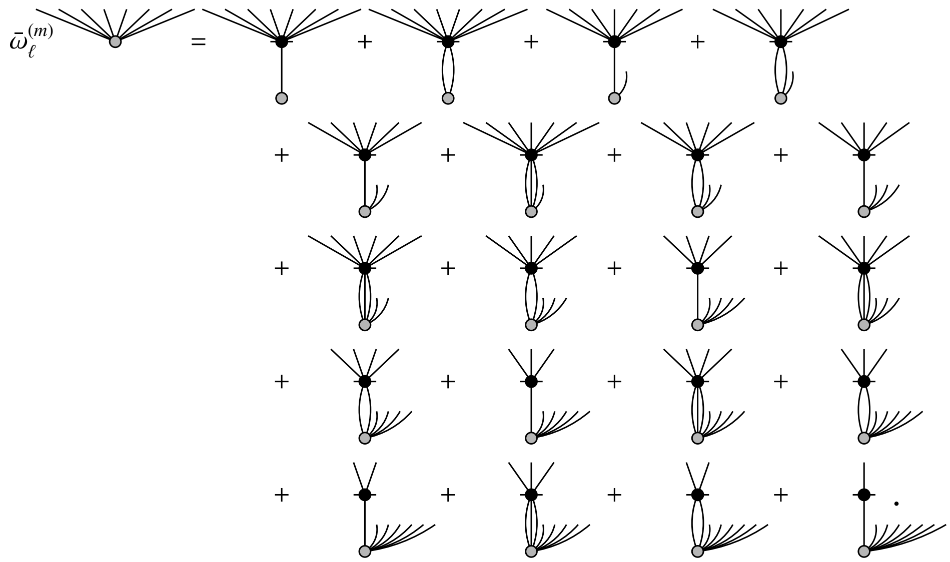

(B.8)

Appendix C

Singly transformed Hamiltonian

Below we document the diagrammatic expressions of the singly similarity-transformed Hamiltonian $\bar{H}$ in terms of the vertices of $\hat{H}$ and $\hat{T}$, which are necessary to define XVCCm, EOM-XVCCm, and STEOM-XVCCm in a QFF for $m \leq 8$.

The zero-mode component of $\bar{H}$ is equivalent to the XVCC energy equation and is illustrated in Eq. (A.1). The n-mode excitation components ($1 \leq n \leq 8$) of $\bar{H}$ are equivalent to the $\hat{T}_n$ amplitude equations of XVCC and are defined in Eqs. (A.2)-(A.9). The other net zero-mode parts of $\bar{H}$, which appear in the EOM-XVCC and STEOM-XVCC formalisms, are

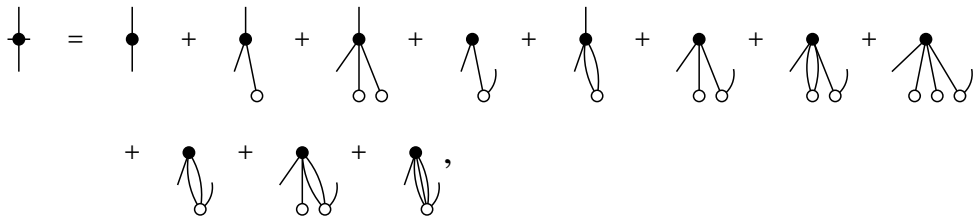

(C.1)

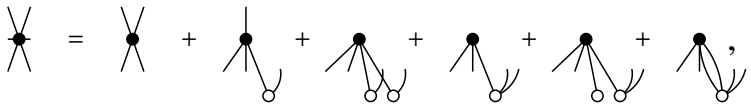

(C.2)

and

(C.3)

The net one-mode dexcitation components are given by

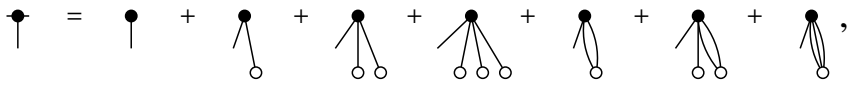

(C.4)

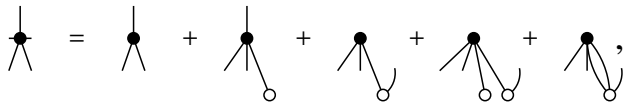

(C.5)

and

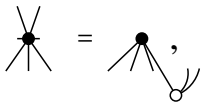

(C.6)

The net two-mode dexcitation components are

(C.7)

and

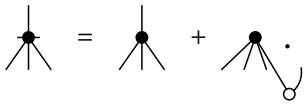

(C.8)

The three-mode dexcitation component is

(C.9)

while the four-mode dexcitation counterpart is simply

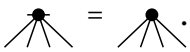

(C.10)

There are three pertinent net one-mode excitation components of $\bar{H}$, which are

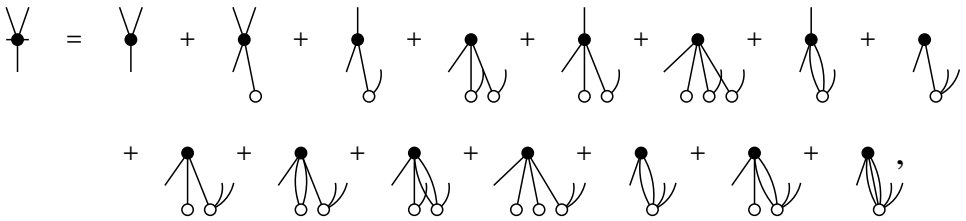

(C.11)

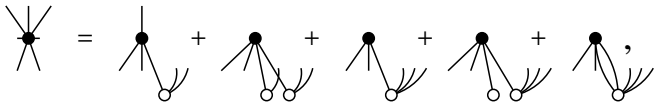

(C.12)

and

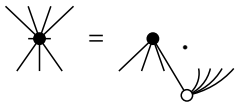

(C.13)

The net two-mode excitation components of $\bar{H}$ are

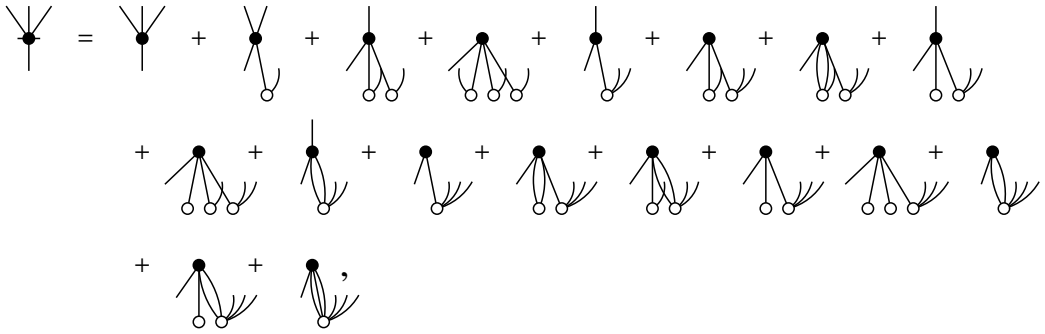

(C.14)

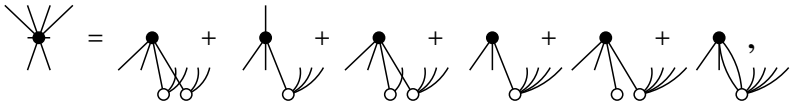

(C.15)

and

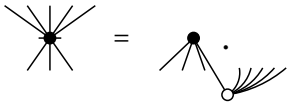

(C.16)

The net three-mode excitation component of $\bar{H}$ are

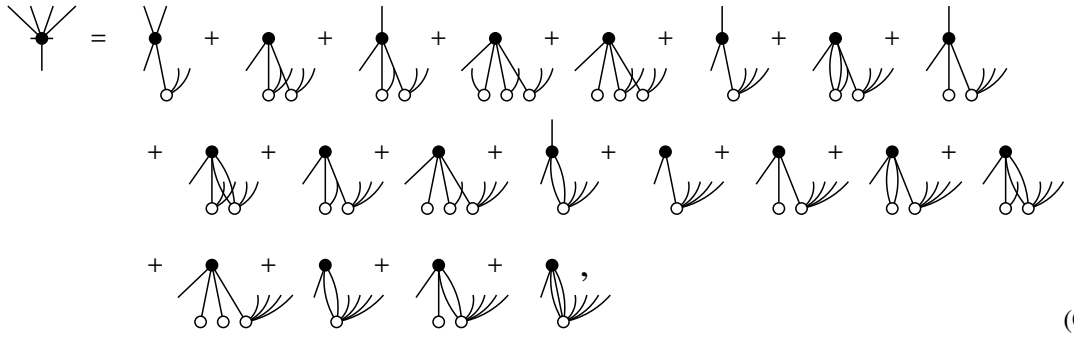

(C.17)

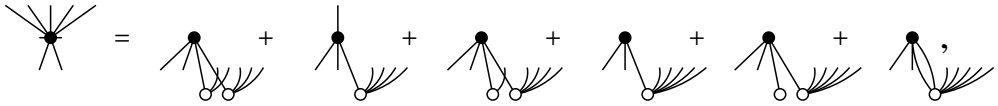

(C.18)

and

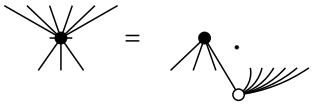

(C.19)

There are three pertinent net four-mode excitation components which are

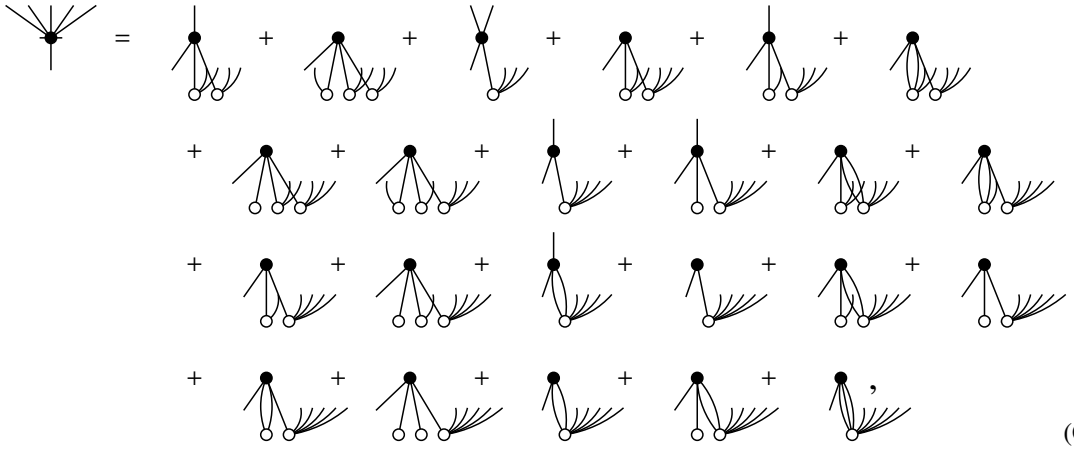

(C.20)

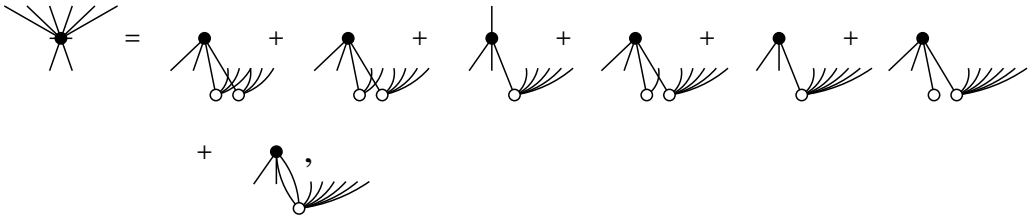

(C.21)

and

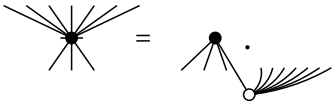

(C.22)

The net five-mode excitation components are

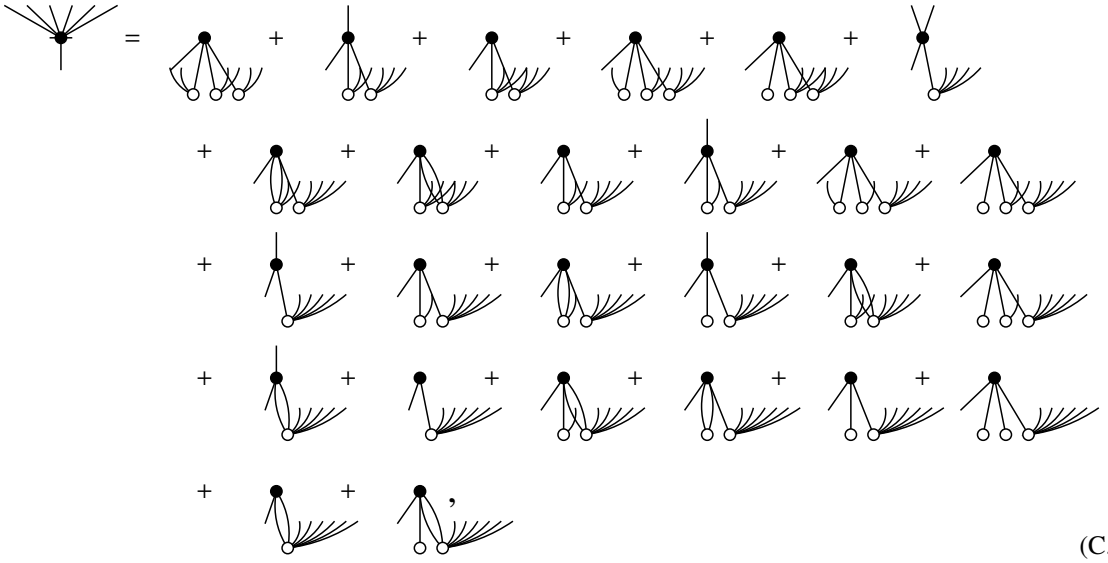

(C.23)

and

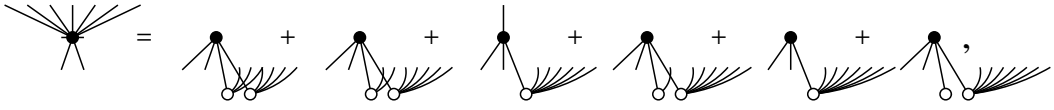

(C.24)

while the six-mode excitation components are

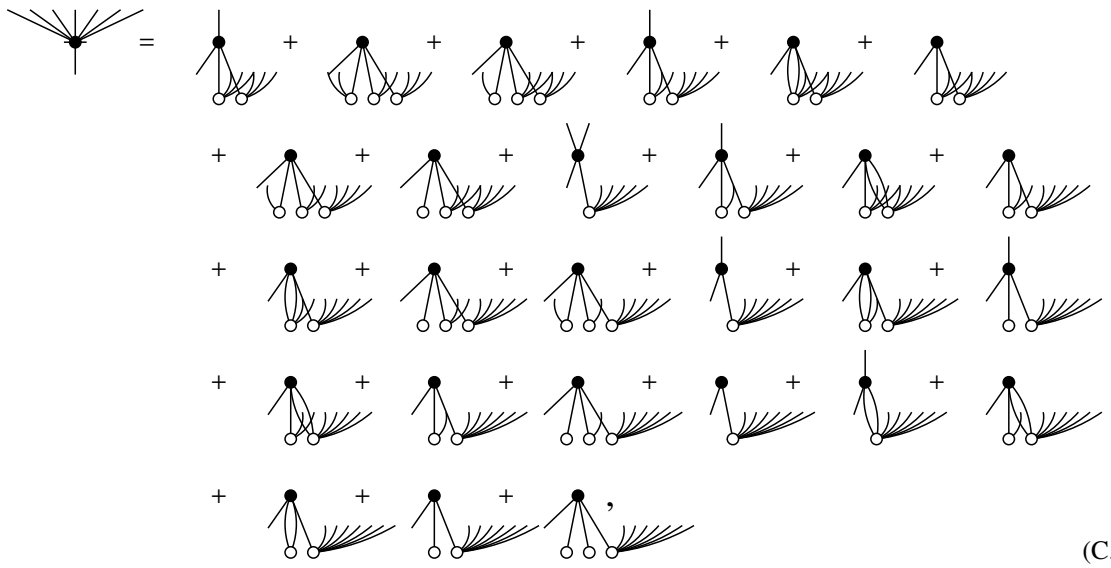

(C.25)

(C.26)

Finally, the seven-mode excitation component is

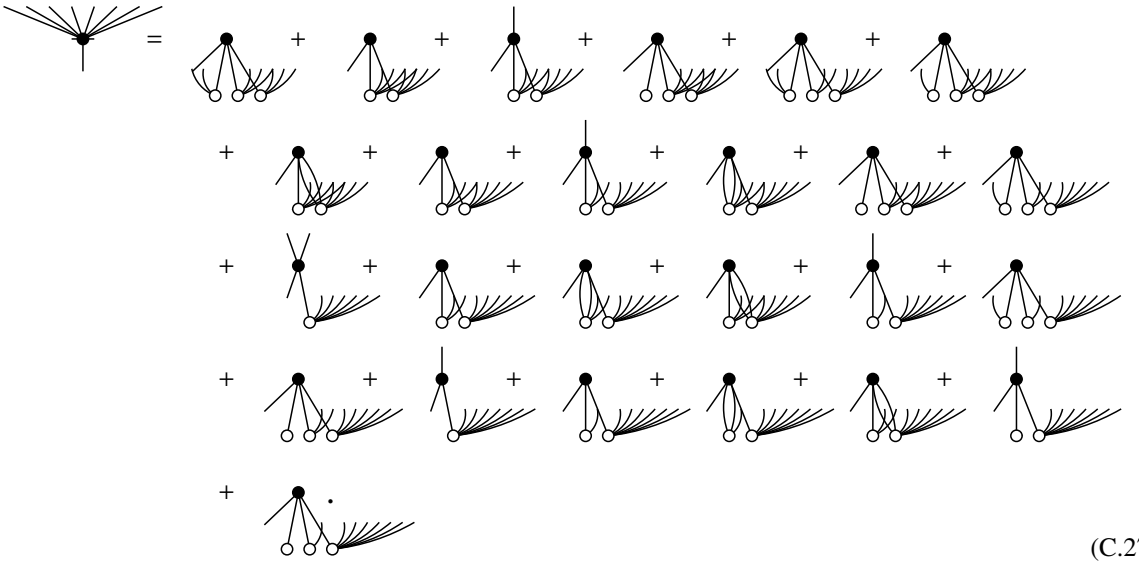

(C.27)

Appendix D

Cost scaling of XVCCm and EOM-XVCCm in an nth-order PES

Theorem. The peak operation cost of XVCCm or EOM-XVCCm in an nth-order PES can be expressed as $O(N^C)$ where N is the number of vibrational degrees of freedom and C is an integer. The lowest value of C ($C_{\min}$) is $m+\lfloor n/2 \rfloor$ for $m \geq n$ and is not greater than $n + \lfloor (m-1)/2 \rfloor$ for $m < n$.

Remark. The proof is given below separately for $m \geq n$ and for $m < n$. In both cases, we first show that the aforementioned values of C are an upper bound; for any matrix chain product appearing in XVCCm or EOM-XVCCm, there is at least one multiplication order whose cost function rank does not exceed the respective value. For $m \geq n$, we additionally show that the aforementioned value of C is also a lower bound; there is always one matrix chain product whose minimal cost function rank is exactly this value. Together they prove that the expression of C given above is minimal for $m \geq n$.

In what follows, we call an R amplitude of EOM-XVCC a T amplitude because they need not be distinguished in this context. We also only need to consider sequential multiplication orders in which the force-constant matrix is always multiplied first without losing rigor of the proof. Let $T^{(k)}$ be the kth T amplitude to be multiplied, having $T^{(k)}_{\text{ext}}$ external lines and $T^{(k)}_{\text{int}}$ internal lines. Let $I^{(k)}$ be the kth intermediate with $I^{(0)}$ being the force-constant matrix, i.e., $I^{(0)} = n$. The symbol $I^{(k)}$ also denotes its size, i.e., the total number of lines.

In the multiplication of $I^{(k-1)}$ with $T^{(k)}$, the number of summation indexes is $T^{(k)}_{\text{int}}$, because two T amplitudes never share common internal lines and, therefore, all internal lines of $T^{(k)}$ must connect with $I^{(k-1)}$. The size of the product, i.e., the kth intermediate, is $I^{(k-1)} + T^{(k)}_{\text{ext}} - T^{(k)}_{\text{int}}$ and the cost function rank of the multiplication is $I^{(k-1)} + T^{(k)}_{\text{ext}}$.

The argument should apply not only to XVCCm and EOM-XVCCm but also to other CC and EOM-CC methods for electrons and nucleons.

Lemma. Let h be the total number of T amplitudes in a matrix chain product. Given intermediate $I^{(i)}$ ($0 \leq i \leq h$), there is at least one multiplication order of remaining $(h-i)$ T amplitudes in which the size of any of the subsequent intermediates does not exceed $\max(I^{(i)}, I^{(h)})$.

Proof of the lemma. The size of the kth intermediate is given by

$$I^{(k)} = I^{(i)} + \sum_{l=i+1}^{k} \left(T^{(l)}_{\text{ext}} - T^{(l)}_{\text{int}} \right). \tag{D.1}$$

Let $T^{(k)}$ amplitudes be ordered as follows: $T^{(k)}$'s with negative values of the difference in the external and internal lines ($T^{(k)}_{\rm ext} - T^{(k)}_{\rm int}$) are multiplied first, next by $T^{(k)}$'s with zero difference, and lastly by $T^{(k)}$'s with positive values of the difference. Then, $I^{(k)}$ as a function of k for this multiplication order is a convex function and thus cannot exceed the greater of their values at the end points: $I^{(k)} \leq \max(I^{(i)}, I^{(h)})$.

Proof of the theorem for $m \geq n$. First, we show that $C = m + \lfloor n/2 \rfloor$ is an upper bound. We consider the following two cases: (1) there is at least one $T^{(k)}$ with $T^{(k)}_{\rm int} \geq \lceil n/2 \rceil$; (2) otherwise.

In case 1, the T amplitude with $T^{(1)}_{\rm int} \geq \lceil n/2 \rceil$ is multiplied first with the force-constant matrix. The cost function rank of this multiplication is given by

$$\begin{aligned} C &= n + T^{(1)}_{\rm ext} \leq n + m - T^{(1)}_{\rm int} \leq n + m - \lceil n/2 \rceil \\ &= m + \lfloor n/2 \rfloor, \end{aligned} \tag{D.2}$$

where we use $T^{(1)}_{\rm ext} + T^{(1)}_{\rm int} \leq m$ in the first inequality. The size of the resulting intermediate is

$$I^{(1)} = n + T^{(1)}_{\rm ext} - T^{(1)}_{\rm int} \leq m + \lfloor n/2 \rfloor - \lceil n/2 \rceil \leq m, \tag{D.3}$$

where Eq. (D.2) is used in the first inequality.

In case 2, $T^{(k)}_{\rm int} \leq \lfloor n/2 \rfloor$ for all k. In the second and subsequent multiplications in case 1, $T^{(k)}_{\rm int} \leq \lfloor n/2 \rfloor$ for all $k \geq 2$. Here, we multiply T amplitudes in one of the orders of the lemma. As per the lemma, this guarantees $I^{(k)} \leq m$ in both cases [see Eq. (D.3) in case 1]. The sizes of the kth and $(k-1)$th intermediates are related to each other by

$$I^{(k)} = I^{(k-1)} + T^{(k)}_{\rm ext} - T^{(k)}_{\rm int} \leq m. \tag{D.4}$$

Therefore, the cost function rank of the kth multiplication is

$$C = I^{(k-1)} + T^{(k)}_{\rm ext} \leq m + T^{(k)}_{\rm int} \leq m + \lfloor n/2 \rfloor. \tag{D.5}$$

Equations (D.3) and (D.5) prove $C_{\rm min} \leq m + \lfloor n/2 \rfloor$.

Second, we show that the same value of C is a lower bound. There is always a binary product of the force-constant matrix, $I^{(0)}$, and a T_m amplitude with $\lceil n/2 \rceil$ internal lines. Note that $\lceil n/2 \rceil$ cannot exceed n or m because $m \geq n \geq 1$. Furthermore, the number of external lines is $m + n - 2\lceil n/2 \rceil \leq m$. Hence, this is a valid matrix chain product. The cost function rank of this multiplication is

$$C = I^{(0)} + T^{(0)}_{\rm ext} = n + m - \lceil n/2 \rceil = m + \lfloor n/2 \rfloor, \tag{D.6}$$

which proves $C_{\min} \geq m + \lfloor n/2 \rfloor$.

Together, we obtain $C_{\min} = m + \lfloor n/2 \rfloor$ for $m \geq n$.

Proof of the theorem for $m < n$. We multiply T amplitudes in one of the orders of the lemma. As per the lemma, this ensures $I^{(k)} \leq n$. We consider the following three cases in each multiplication: (1) $T_{\text{ext}}^{(k)} < T_{\text{int}}^{(k)}$; (2) $T_{\text{ext}}^{(k)} > T_{\text{int}}^{(k)}$; (3) $T_{\text{ext}}^{(k)} = T_{\text{int}}^{(k)}$.

In case 1, since $T_{\text{ext}}^{(k)} + T_{\text{int}}^{(k)} \leq m$, we have $T_{\text{ext}}^{(k)} \leq \lfloor (m-1)/2 \rfloor$. The cost function rank of the kth multiplication is

$$C = I^{(k-1)} + T_{\text{ext}}^{(k)} \leq n + \lfloor (m-1)/2 \rfloor. \tag{D.7}$$

In case 2, similarly, $T_{\text{int}}^{(k)} \leq \lfloor (m-1)/2 \rfloor$ holds. The size of the kth intermediate is given by

$$I^{(k)} = I^{(k-1)} + T_{\text{ext}}^{(k)} - T_{\text{int}}^{(k)} \leq n, \tag{D.8}$$

which implies

$$C = I^{(k-1)} + T_{\text{ext}}^{(k)} \leq n + T_{\text{int}}^{(k)} \leq n + \lfloor (m-1)/2 \rfloor. \tag{D.9}$$

In case 3, m must be even and $T_{\text{ext}}^{(k)} = T_{\text{int}}^{(k)} = m/2$. The intermediate resulting from the multiplication of this T amplitude has the size:

$$I^{(k)} = I^{(k-1)} + T_{\text{ext}}^{(k)} - T_{\text{int}}^{(k)} \leq m < n. \tag{D.10}$$

The first inequality follows from the fact that $I^{(l)}$ is a convex function with its minimum occurring at $l = k$, where $T_{\text{ext}}^{(k)} - T_{\text{int}}^{(k)} = 0$. The cost function rank of this step is

$$C = I^{(k-1)} + T_{\text{ext}}^{(k)} \leq n + T_{\text{int}}^{(k)} - 1 \leq n + m/2 - 1. \tag{D.11}$$

Equations (D.7), (D.9), and (D.11) prove $C_{\min} \leq n + \lfloor (m-1)/2 \rfloor$ for $m < n$.

Remark. This upper-bound expression for $m < n$ happens to agree with the optimal cost function ranks for all cases of $m < n$ in Table 2.4. However, we have identified many other combinations of $m < n$ whose optimal ranks are lower.

Appendix E

Doubly transformed Hamiltonian

Below we document the doubly transformed Hamiltonian vertices required for Ext-STEOM-XVCCm ($2 \leq m \leq 4$) in terms of the vertices of $\bar{H}$, and $\hat{S}$.

The zero-mode component of the doubly transformed Hamiltonian is equivalent to the zero-mode component of the singly transformed Hamiltonian defined in Eq. (A.1). The pure excitation components up to four-mode excitations are shown in Eqs. (4.31) - (4.34) and are zero due to satisfaction of the XVCC amplitude equations. The net one-mode, two-mode, and three-mode excitation components of $\bar{\bar{H}}$ with one lowering operator are illustrated in Eqs. (4.39), (4.43), and (4.44). These components are also equal to zero and are identical to the STEOM-XVCC amplitude equations.

The other net zero-mode parts of $\bar{H}$, which appear in the Ext-STEOM-XVCC formalism, are

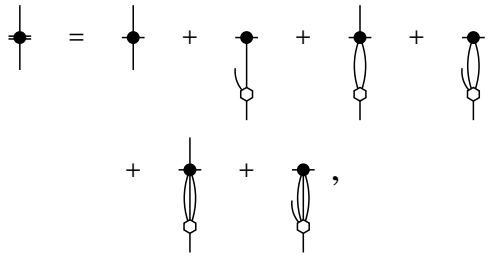

(E.1)

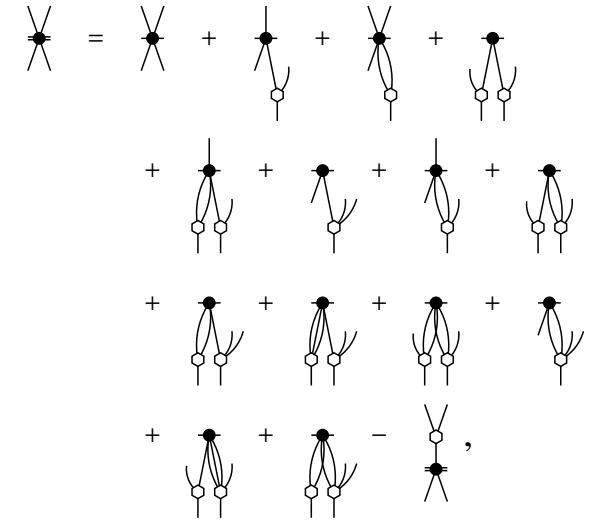

(E.2)

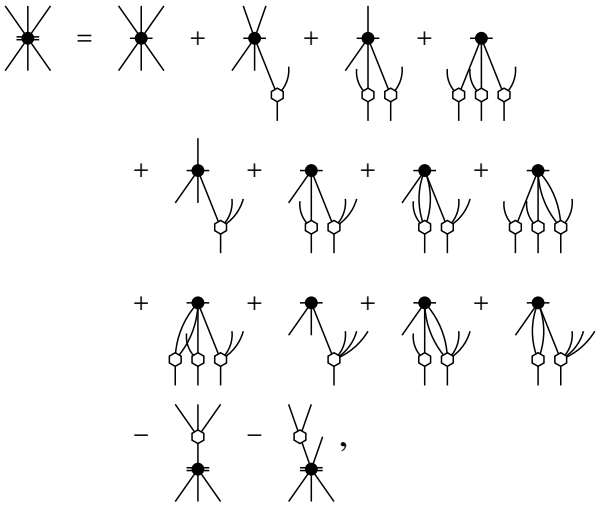

(E.3)

and

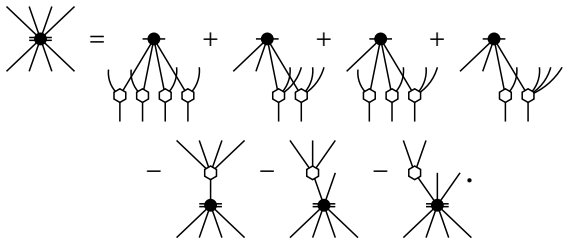

(E.4)

The required net one-mode dexcitation components of $\bar{\bar{H}}$ are

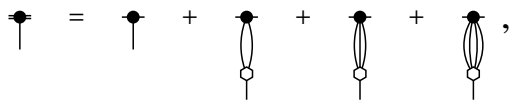

(E.5)

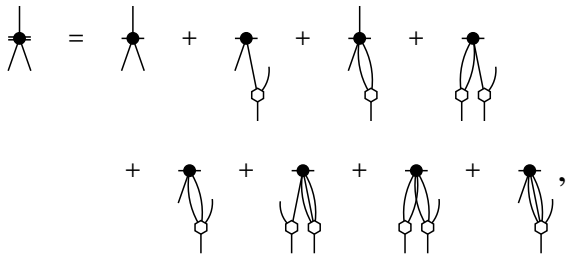

(E.6)

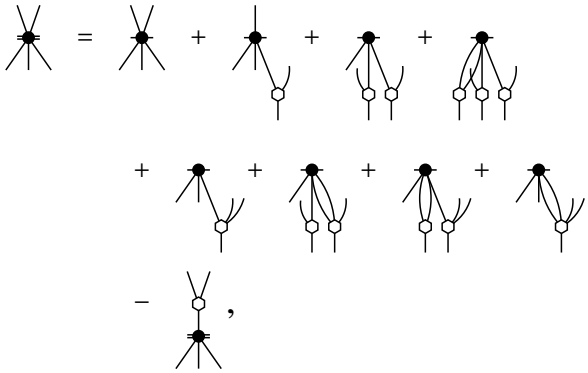

(E.7)

and

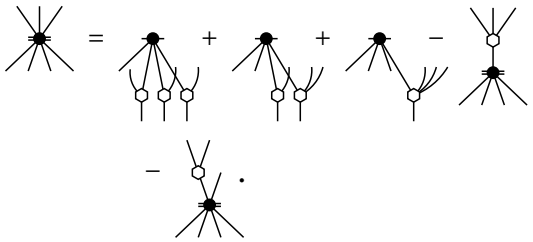

(E.8)

The net two-mode dexcitation components are

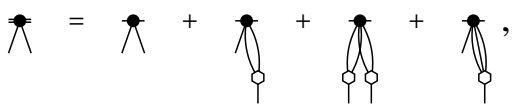

(E.9)

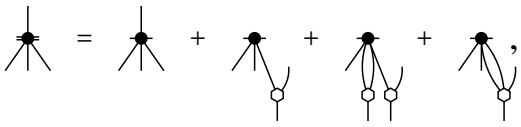

(E.10)

and

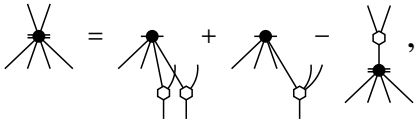

(E.11)

while the net three-mode dexcitation component is

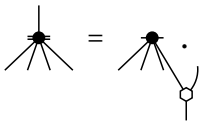

(E.12)

The required one-mode excitation components are given by

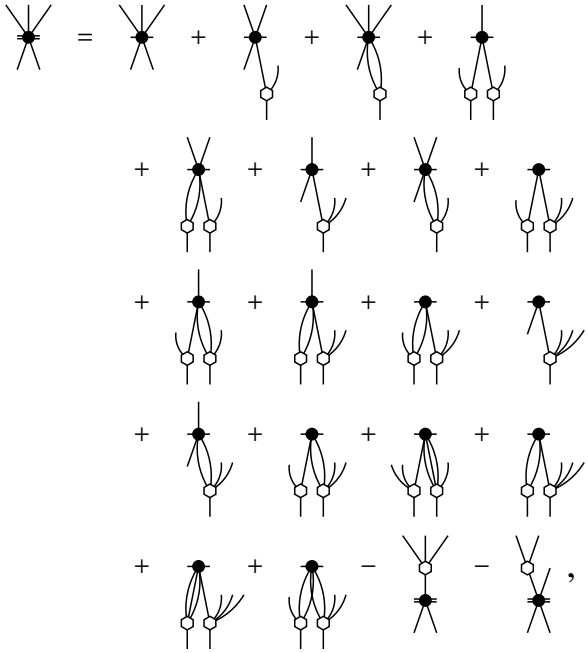

(E.13)

and

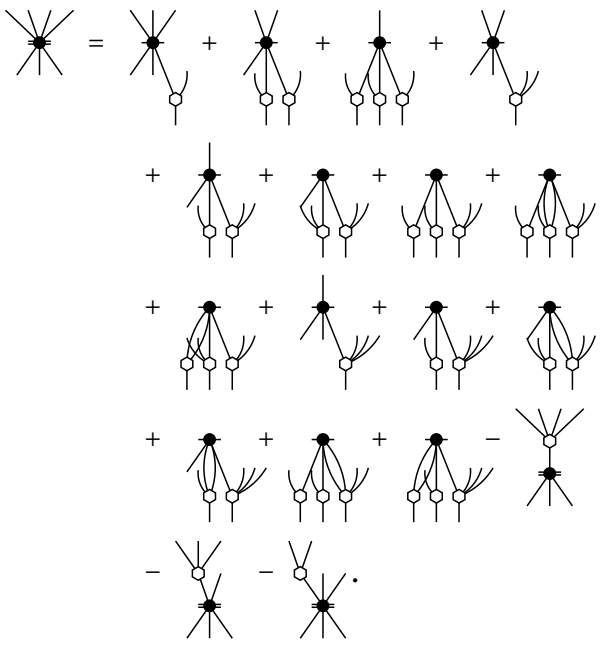

(E.14)

Finally, the required two-mode excitation component is

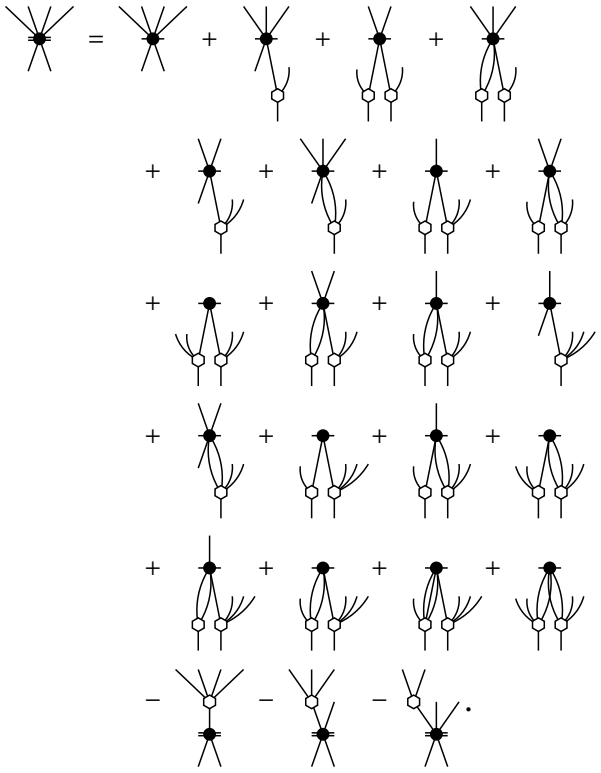

(E.15)

References

[1] D. M. Dennison. *Rev. Mod. Phys.* **3**, 280 (1931).

[2] A. Szabo and N. S. Ostlund. *Modern Quantum Chemistry Introduction to Advanced Electronic Structure Theory*. MacMillan, New York, 1989.

[3] M. Born and R. Oppenheimer. *Ann. Phys.* **84**, 457–484 (1927).

[4] J. K. G. Watson. *Mol. Phys.* **15**, 479 (1968).

[5] J. M. Bowman. *J. Chem. Phys.* **68**, 608 (1978).

[6] M. A. Ratner and R. B. Gerber. *J. Phys. Chem.* **90**, 20 (1986).

[7] J. M. Bowman. *Acc. Chem. Res.* **19**, 202 (1986).

[8] S. Hirata, M. Keçeli, and K. Yagi. *J. Chem. Phys.* **133**, 034109 (2010).

[9] M. Keçeli and S. Hirata. *J. Chem. Phys.* **135**, 134108 (2011).

[10] M. R. Hermes, M. Keçeli, and S. Hirata. *J. Chem. Phys.* **136**, 234109 (2012).

[11] M. R. Hermes and S. Hirata. *J. Phys. Chem. A* **117**, 7179–7189 (2013).

[12] N. Makri. *J. Phys. Chem. B* **103**, 2823 (1999).

[13] S. Hirata and M. R. Hermes. *J. Chem. Phys.* **141**, 184111 (2014).

[14] M. R. Hermes and S. Hirata. *J. Chem. Phys.* **139**, 034111 (2013).

[15] R. J. Bartlett and M. Musiał. *Rev. Mod. Phys.* **79**, 291 (2007).

[16] F. Coester. *Nucl. Phys.* **7**, 421 (1958).

[17] F. Coester and H. Kümmel. *Nucl. Phys.* **9**, 225 (1958).

[18] J. Čížek. *J. Chem. Phys.* **45**, 4256 (1966).

[19] J. Paldus, J. Čížek, and I. Shavitt. *Phys. Rev. A* **5**, 50 (1972).

[20] J. A. Pople, R. Krishnan, H. B. Schlegel, and J. S. Binkley. *Int. J. Quantum Chem.* **14**, 545 (1978).

[21] R. J. Bartlett and G. D. Purvis. *Int. J. Quantum Chem.* **14**, 561 (1978).

[22] G. D. Purvis III and R. J. Bartlett. *J. Chem. Phys.* **76**, 1910 (1982).

[23] S. Hirata. *Theor. Chem. Acc.* **129**, 727 (2011).

[24] S. Hirata, M. Keçeli, Y. Ohnishi, O. Sode, and K. Yagi. *Annu. Rev. Phys. Chem.* **63**, 131 (2012).

[25] R. F. Bishop. *Theor. Chim. Acta* **80**, 95 (1991).

[26] W. Förner. *Int. J. Quantum Chem.* **43**, 221 (1992).

[27] M. Yu, S. Kalvoda, and M. Dolg. *Chem. Phys.* **224**, 121 (1997).

[28] P. Reinhardt. *Theor. Chem. Acc.* **104**, 426 (2000).

[29] S. Hirata, I. Grabowski, M. Tobita, and R. J. Bartlett. *Chem. Phys. Lett.* **345**, 475 (2001).

[30] S. Hirata, R. Podeszwa, M. Tobita, and R. J. Bartlett. *J. Chem. Phys.* **120**, 2581 (2004).

[31] J. J. Shepherd, T. M. Henderson, and G. E. Scuseria. *J. Chem. Phys.* **140**, 124102 (2014).

[32] D. J. Dean, J. R. Gour, G. Hagen, M. Hjorth-Jensen, K. Kowalski, T. Papenbrock, P. Piecuch, and M. Wloch. *Nucl. Phys. A* **752**, 299C (2005).

[33] P. Piecuch, M. Wloch, J. R. Gour, D. J. Dean, M. Hjorth-Jensen, and T. Papenbrock. *Nucl. Mesosc. Phys.* **777**, 28 (2005).

[34] O. Christiansen. *Phys. Chem. Chem. Phys.* **9**, 2942 (2007).

[35] M. R. Hermes and S. Hirata. *Int. Rev. Phys. Chem.* **34**, 71 (2015).

[36] U. B. Kaulfuss and M. Altenbokum. *Phys. Rev. D* **33**, 3658 (1986).

[37] R. F. Bishop and M. F. Flynn. *Phys. Rev. A* **38**, 2211 (1988).

[38] R. F. Bishop, M. C. Bosca, and M. F. Flynn. *Phys. Rev. A* **40**, 3484 (1989).

[39] M. D. Prasad. *J. Chem. Phys.* **88**, 7005 (1988).

[40] V. Nagalakshmi, V. Lakshminarayana, G. Sumithra, and M. D. Prasad. *Chem. Phys. Lett.* **217**, 279–282 (1994).

[41] G. M. Sastry and M. D. Prasad. *Chem. Phys. Lett.* **228**, 213 (1994).

[42] G. Latha and M. D. Prasad. *Chem. Phys. Lett.* **241**, 215 (1995).

[43] G. S. Latha and M. D. Prasad. *J. Chem. Phys.* **105**, 2972 (1996).

[44] M. D. Prasad. *Int. J. Mol. Sci.* **3**, 447 (2002).

[45] S. Banik, S. Pal, and M. D. Prasad. *J. Chem. Phys.* **129**, 134111 (2008).

[46] S. Banik, S. Pal, and M. D. Prasad. *J. Chem. Theory Comput.* **6**, 3198 (2010).

[47] S. Banik, S. Pal, and M. D. Prasad. *J. Chem. Phys.* **137**, 114108 (2012).

[48] O. Christiansen. *J. Chem. Phys.* **120**, 2149 (2004).

[49] O. Christiansen. *J. Chem. Phys.* **122**, 194105 (2005).

[50] P. Seidler and O. Christiansen. *J. Chem. Phys.* **126**, 204101 (2007).

[51] P. Seidler, M. B. Hansen, and O. Christiansen. *J. Chem. Phys.* **128**, 154113 (2008).

[52] P. Seidler, E. Matito, and O. Christiansen. *J. Chem. Phys.* **131**, 034115 (2009).

[53] P. Seidler and O. Christiansen. *J. Chem. Phys.* **131**, 234109 (2009).

[54] P. Seidler, M. Sparta, and O. Christiansen. *J. Chem. Phys.* **134**, 054119 (2011).

[55] K. M. Christoffel and J. M. Bowman. *Chem. Phys. Lett.* **85**, 220 (1982).

[56] L. S. Norris, M. A. Ratner, A. E. Roitberg, and R. B. Gerber. *J. Chem. Phys.* **105**, 11261 (1996).

[57] J. Paldus, J. Čížek, and I. Shavitt. *Phys. Rev. A* **5**, 50–67 (1972).

[58] J. A. Pople, R. Krishnan, H. B. Schlegel, and J. S. Binkley. *Int. J. Quantum Chem.* **14**, 545–560 (1978).

[59] R. J. Bartlett and G. D. Purvis III. *Int. J. Quantum Chem.* **14**, 561–581 (1978).

[60] G. D. Purvis III and R. J. Bartlett. *J. Chem. Phys.* **76**, 1910–1918 (1982).

[61] R. J. Bartlett and M. Musiał. *Rev. Mod. Phys.* **79**, 291–352 (2007).

[62] C. Bloch. *Nucl. Phys.* **6**, 329 (1958).

[63] K. F. Freed. *J. Chem. Phys.* **60**, 1765 (1974).

[64] W. Kutzelnigg. *J. Chem. Phys.* **77**, 3081–3097 (1982).

[65] W. Kutzelnigg and S. Koch. *J. Chem. Phys.* **79**, 4315–4335 (1983).

[66] W. Kutzelnigg. *J. Chem. Phys.* **80**, 822–830 (1984).

[67] F. A. Evangelista. *J. Chem. Phys.* **141**, 054109 (2014).

[68] I. Lindgren and J. Morrison. *Atomic Many-Body Theory, Second Edition*. Springer-Verlag, 1986.

[69] S. F. Boys and N. C. Handy. *Proc. Roy. Soc. A.* **310**, 43–61 (1969).

[70] S. F. Boys and N. C. Handy. *Proc. Roy. Soc. A.* **310**, 63–78 (1969).

[71] I. Shavitt and R. J. Bartlett. *Many-Body Methods in Chemistry and Physics: MBPT and Coupled-Cluster Theory*. Cambridge University Press, 2009.

[72] S. Hirata. *Theor. Chem. Acc.* **129**, 727–746 (2011).

[73] K. Emrich. *Nucl. Phys. A* **351**, 379 (1981).

[74] K. Emrich. *Nucl. Phys. A* **351**, 397 (1981).

[75] H. Sekino and R. J. Bartlett. *Int. J. Quantum Chem.* **S18**, 255 (1984).

[76] J. Geertsen, M. Rittby, and R. J. Bartlett. *Chem. Phys. Lett.* **164**, 57 (1989).

[77] D. C. Comeau and R. J. Bartlett. *Chem. Phys. Lett.* **207**, 414 (1993).

[78] H. J. Monkhorst. *Int. J. Quantum Chem.* **S11**, 421 (1977).

[79] S. Ghosh, D. Mukherjee, and S. Bhattacharyya. *Mol. Phys.* **43**, 173 (1981).

[80] M. Takahashi and J. Paldus. *J. Chem. Phys.* **85**, 1486 (1986).

[81] J. F. Stanton and R. J. Bartlett. *J. Chem. Phys.* **98**, 7029-7039 (1993).

[82] J. F. Stanton and J. Gauss. *J. Chem. Phys.* **101**, 8938-8944 (1994).

[83] J. F. Stanton and J. Gauss. *J. Chem. Phys.* **111**, 8785-8788 (1999).

[84] M. Musiał, S. A. Kucharski, and R. J. Bartlett. *J. Chem. Phys.* **118**, 1128-1136 (2003).

[85] M. Kamiya and S. Hirata. *J. Chem. Phys.* **125**, 074111 (2006).

[86] M. Nooijen and R. J. Bartlett. *J. Chem. Phys.* **102**, 3629-3647 (1995).

[87] M. Nooijen and R. J. Bartlett. *J. Chem. Phys.* **102**, 6735-6756 (1995).

[88] M. Musiał and R. J. Bartlett. *J. Chem. Phys.* **119**, 1901-1908 (2003).

[89] M. Kamiya and S. Hirata. *J. Chem. Phys.* **126**, 134112 (2007).

[90] H. Koch and P. Jørgensen. *J. Chem. Phys.* **93**, 3333 (1990).

[91] H. Koch, H. J. A. Jensen, P. Jørgensen, and T. Helgaker. *J. Chem. Phys.* **93**, 3345 (1990).

[92] R. J. Rico and M. Head-Gordon. *Chem. Phys. Lett.* **213**, 224 (1993).

[93] L. Z. Stolarczyk and H. J. Monkhorst. *Phys. Rev. A* **32**, 725–742 (1985).

[94] L. Z. Stolarczyk and H. J. Monkhorst. *Phys. Rev. A* **32**, 743–747 (1985).

[95] L. Z. Stolarczyk and H. J. Monkhorst. *Phys. Rev. A* **37**, 1908–1925 (1988).

[96] L. Z. Stolarczyk and H. J. Monkhorst. *Phys. Rev. A* **37**, 1926–1933 (1988).

[97] M. Nooijen and R. J. Bartlett. *J. Chem. Phys.* **106**, 6441 (1997).

[98] M. Nooijen and R. J. Bartlett. *J. Chem. Phys.* **106**, 6449 (1997).

[99] M. Nooijen and R. J. Bartlett. *J. Chem. Phys.* **107**, 6812 (1997).

[100] M. Nooijen. *Spectrochim. Acta Part A Mol. Biomol. Spectrosc.* **55**, 539–559 (1999).

[101] M. Nooijen and V. Lotrich. *J. Chem. Phys.* **113**, 494 (2000).

[102] J. Sous, P. Goel, and M. Nooijen. *Mol. Phys.* **112**, 616-638 (2014).

[103] S. R. Gwaltney, R. J. Bartlett, and M. Nooijen. *J. Chem. Phys.* **111**, 58 (1999).

[104] D. Mukherjee, R. K. Moitra, and A. Mukhopadhyay. *Mol. Phys.* **33**, 955–969 (1977).

[105] I. Lindgren. *Int. J. Quantum Chem.* **14**, 33–58 (1978).

[106] M. A. Haque and D. Mukherjee. *J. Chem. Phys.* **80**, 5058 (1984).

[107] D. Mukherjee. *Chem. Phys. Lett.* **125**, 207–212 (1986).

[108] I. Lindgren and D. Mukherjee. *Phys. Rep.* **151**, 93–127 (1987).

[109] B. Jeziorski and J. Paldus. *J. Chem. Phys.* **90**, 2714 (1989).

[110] M. Nooijen. *J. Chem. Phys.* **104**, 2638 (1996).

[111] L. Meissner and R. J. Bartlett. *J. Chem. Phys.* **102**, 7490 (1995).

[112] D. J. Hooton. *Phil. Mag.* **3**, 49 (1958).

[113] T. R. Koehler. *Phys. Rev. Lett.* **17**, 89–91 (1966).

[114] P. Choquard. *The Anharmonic Crystal*. Benjamin, 1967.

[115] N. S. Gillis, N. R. Werthamer, and T. R. Koehler. *Phys. Rev.* **165**, 951–959 (1968).

[116] T. Luty, A. van der Avoird, R. M. Berns, and T. Wasiutynski. *J. Chem. Phys.* **75**, 1451 (1981).

[117] K. Yagi, K. Hirao, T. Taketsugu, M. W. Schmidt, and M. S. Gordon. *J. Chem. Phys.* **121**, 1383 (2004).

[118] G. C. Wick. *Phys. Rev.* **80**, 268 (1950).

[119] M. R. Hermes and S. Hirata. *J. Chem. Phys.* **141**, 084105 (2014).

[120] J. Goldstone. *Proc. Roy. Soc. London A* **239**, 267 (1957).

[121] D. Knoll and D. Keyes. *J. Comput. Phys.* **193**, 357 (2004).

[122] C. Lanczos. *J. Res. Nat. Bur. Stand.* **45**, 255 (1950).

[123] E. R. Davidson. *J. Comput. Phys.* **17**, 87–94 (1975).

[124] K. Hirao and H. Nakatsuji. *J. Comput. Phys.* **45**, 246–254 (1982).

[125] D. Sorensen, R. Lehoucq, C. Yang, and K. Maschhoff. *ARPACK*, Rice University, 1996-2008.

[126] S. Hirata. *J. Phys. Chem. A* **107**, 9887 (2003).

[127] T. Shiozaki, M. Kamiya, S. Hirata, and E. F. Valeev. *Phys. Chem. Chem. Phys.* **10**, 3358 (2008).

[128] M. Valiev, E. Bylaska, N. Govind, K. Kowalski, T. Straatsma, H. Van Dam, D. Wang, J. Nieplocha, E. Apra, T. Windus, and W. de Jong. *Comput. Phys. Commun.* **181**, 1477–1489 (2010).

[129] K. Yagi. SINDO, The University of Tokyo, 2006.

[130] M. Keçeli. MAVI, University of Illinois at Urbana-Champaign, 2011.

[131] S. Hirata, M. Nooijen, and R. J. Bartlett. *Chem. Phys. Lett.* **326**, 255 (2000).

[132] J. A. Faucheaux and S. Hirata. *J. Chem. Phys.* **143**, 134105 (2015).

[133] C. Lanczos. *J. Res. Natl. Bur. Stand.* **45**, 255 (1950).

[134] S. Hirata, A. E. Doran, P. J. Knowles, and J. V. Ortiz. *J. Chem. Phys.* **147**, 044108 (2017).

[135] M. Born and K. Huang. *Dynamical Theory of Crystal Lattices*. Oxford University Press, 1954.

[136] J. A. Reissland. *The Physics of Phonons*. Wiley, 1973.

[137] O. Christiansen. *J. Chem. Phys.* **120**, 2140–8 (2004).

[138] M. R. Hermes and S. Hirata. *Int. Rev. Phys. Chem.* **34**, 71–97 (2015).

[139] D. Mukherjee and S. Pal. *Adv. Quantum Chem.* **20**, 291-373 (1989).

[140] D. Sinha, S. K. Mukhopadhyay, R. Chaudhuri, and D. Mukherjee. *Chem. Phys. Lett.* **154**, 544–549 (1989).

[141] R. D. Mattuck. *A Guide to Feynman Diagrams in the Many-Body Problem*. Dover,New York, 1992.

[142] J. V. Ortiz. *Adv. Quantum Chem.* **35**, 33–52 (1999).

[143] J. V. Ortiz. *Wiley Interdiscip. Rev.: Comput. Mol. Sci.* **3**, 123–142 (2013).

[144] S. Hirata, M. R. Hermes, J. Simons, and J. V. Ortiz. *J. Chem. Theory Comput.* **11**, 1595-1606 (2015).

[145] T. Shiozaki, M. Kamiya, S. Hirata, and E. F. Valeev. *Phys. Chem. Chem. Phys.* **10**, 3358-3370 (2008).

[146] D. Knoll and D. Keyes. *J. Comp. Phys.* **193**, 357 (2004).

[147] A. Baker, E. Jessup, and T. Manteuffel. *SIAM J. Matrix Anal. Appl.* **26**, 962 (2005).

[148] J. J. More, B. S. Garbow, and K. E. Hillstrom. MINPACK, University of Chicago, 1999.

[149] M. J. Frisch, G. W. Trucks, H. B. Schlegel, and et. al. GAUSSIAN 09, Gaussian, Inc. Wallingford, CT 2016.

[150] M. Keçeli, S. Hirata, Y. Ohnishi, and K. Yagi. *J. Chem. Phys* **133**, 034110 (2010).

[151] Y. Takahasi. *Macromolecules* **34**, 7836 (2001).

[152] R. G. Snyder, S. L. Hsu, and S. Krimm. *Spectrochim. Acta, Part A* **34**, 395 (1978).

[153] S. Abbate, G. Zerbi, and S. L. Wunder. *J. Phys. Chem.* **86**, 3140 (1982).

[154] S. Hirata and S. Iwata. *J. Phys. Chem. A* **102**, 8426 (1998).